METHOD FOR QUANTIFYING THE SPECTRAL BASED ERROR IN LUMINANCE MEASUREMENTS

by

KATHERINE LOUISE TEMAN

B.S., University of Colorado Boulder, 2017

A thesis submitted to the

Faculty of the Graduate School of the

University of Colorado in partial fulfillment

Of the requirement for the degree of

Master of Science

Department of Civil, Environmental, and Architectural Engineering

2017

This thesis entitled:
Method for Quantifying the Error Inherent in HDRI Luminance Measurements of Colored Light Sources
written by Katherine Louise Teman
has been approved for the Department of Civil, Environmental, and Architectural Engineering

C. Walter Beamer IV, Ph.D.

Gregor Henze, Ph.D., P.E.

Mark Jongewaard, M.S.

Date_____

The final copy of this thesis has been examined by the signatories, and we find that both the content and the form meet acceptable presentation standards of scholarly work in the above mentioned discipline.

IRB protocol # _____N/A_____

IACUC protocol # _____N/A_____

ABSTRACT

Teman, Katherine Louise

Method for Quantifying the Spectral Based Error in Luminance Measurements

Thesis Directed by Professor C. Walter Beamer IV, Ph.D.

The accuracy of luminance measurements throughout the visible spectrum was investigated by breaking down a broadband source into narrow bandwidth sections. Measurements from a standard luminance meter were then compared to a derived luminance found with an illuminance spectrophotometer. High Dynamic Range Images (HDRI) of the narrow bandwidth sources were also taken in order to evaluate the spectrally dependent accuracy of HDRI as a luminance measurement tool. These results were evaluated for nine saturated color sources throughout the visible spectrum, as well as a white LED. The saturated sources were expected to produce errors in luminance measurements, based on previous studies. However, results of the white LED condition raised additional concerns about the accuracy of photometric measurements for LED sources. Additional research on how the spectral characteristics of a source affect the accuracy of standard illuminance and luminance meters is also presented in this report.

DEDICATION

To my Mom for her constant love, encouragement, and friendship.

To my Dad for always being just as excited about my dreams as I am.

And to my friend, Josie, for being by my side throughout this whole adventure.

TABLE OF CONTENTS

LIST OF FIGURES

LIST OF TABLES

Chapter 1: Introduction

1.1 Motivation

The initial motivation behind this work was to better understand and quantify the errors involved in high dynamic range images (HDRI) used for luminance analysis. While the potential of HDRI for the lighting industry is exciting, previous experiments have exposed shortcomings of the technology which lead to errors in the results. Vignetting effects were already tackled for the particular camera system discussed herein through previous research conducted at the University of Colorado Boulder, but other issues with the technique still require further investigation. The specific source of error targeted for this report was saturated color light sources. A broadband light source was broken down into small sections by means of narrow bandwidth filters in order to create many saturated sources throughout the human visible spectrum. This experiment was broken up into two main sections. First, the accuracy of a standard luminance meter throughout the visible spectrum was investigated by means of an illuminance spectrophotometer. Spectrally-based illuminance information was used to calculate luminance for comparison with a luminance meter. Second, these luminance values were compared to those obtained through calibrated HDRI of the narrow bandwidth light source.

Experimental results regarding the accuracy of the standard luminance meter introduced unanticipated concerns about lighting measurements of unique source types. Potential errors from the luminance meter for broadband light sources, other than incandescent, changed the focus of this experiment from HDRI based error, to spectral based error in common lighting measurements. Additional research was conducted to understand the reasons behind this error and typical results for an LED light source.

1.2 Report Overview

This report is broken into six chapters, with the first being this introduction. Chapter 2 consists of a literature search which provides background information on the lighting concepts referenced throughout the paper, as well as past research that informed the design of this experiment. Chapter 3 will introduce and explain the novel method that was used to determine spectral accuracy of luminance meters. This was achieved through illuminance measurements of various narrow bandwidth sources with an illuminance spectrophotometer. Chapter 4 will further the investigation of luminance measurement errors for broadband, white light sources. Then, Chapter 5 will explain the HDRI collection and analysis procedure used in conjunction with the narrow bandwidth sources. Finally, Chapter 6 will conclude the document by recapping the most substantial findings of this experiment.

Chapter 2: Literature Search

This section will introduce relevant concepts and definitions pertaining to light and color that will be referenced throughout the rest of this paper. This is not an extensive list of all lighting metrics in use today; however, more information on these concepts may be found in the IES Lighting Handbook (1).

2.1 Relevant Definitions

Light is defined as visually evaluated radiant energy. Radiometry is the measurement of optical radiation, while photometry is a specific branch of this area of science that accounts for the human visual response to radiation (1).

2.1.1 Photometric Quantities

Luminous flux, Φ, is defined as the time rate of flow of light and is measured in lumens (2). This may be thought of as the amount of light that is leaving a source and is independent of direction.

$$\phi \equiv 683 \int_0^\infty \phi_{e\lambda}(\lambda) v(\lambda)\, d\lambda$$

CIE Photopic Luminous Efficiency Curve, V(λ), is a function that was defined by the CIE based on standard observers which tested the sensitivity of the human eye to wavelengths throughout the visible spectrum. This normalized, bell-shaped curve demonstrates that sources of equal intensity will be perceived as brighter in the green regions of the spectrum than the red and blue ends of the spectrum. The peak sensitivity wavelength occurs at 555 nm. The red curve shown in Figure 1 below represents the photopic response, while the blue curve represents the scotopic vision response. Photopic vision is categorized to function for light levels over 10 cd/m^2 and scotopic vision includes

light levels below 0.001 cd/m² (1). The range between these values is a transitional stage referred to as mesopic vision, which utilizes both cones and rod photoreceptors. The light levels in this experiment will only focus on the photopic vision response shown in the red curve of Figure 1.

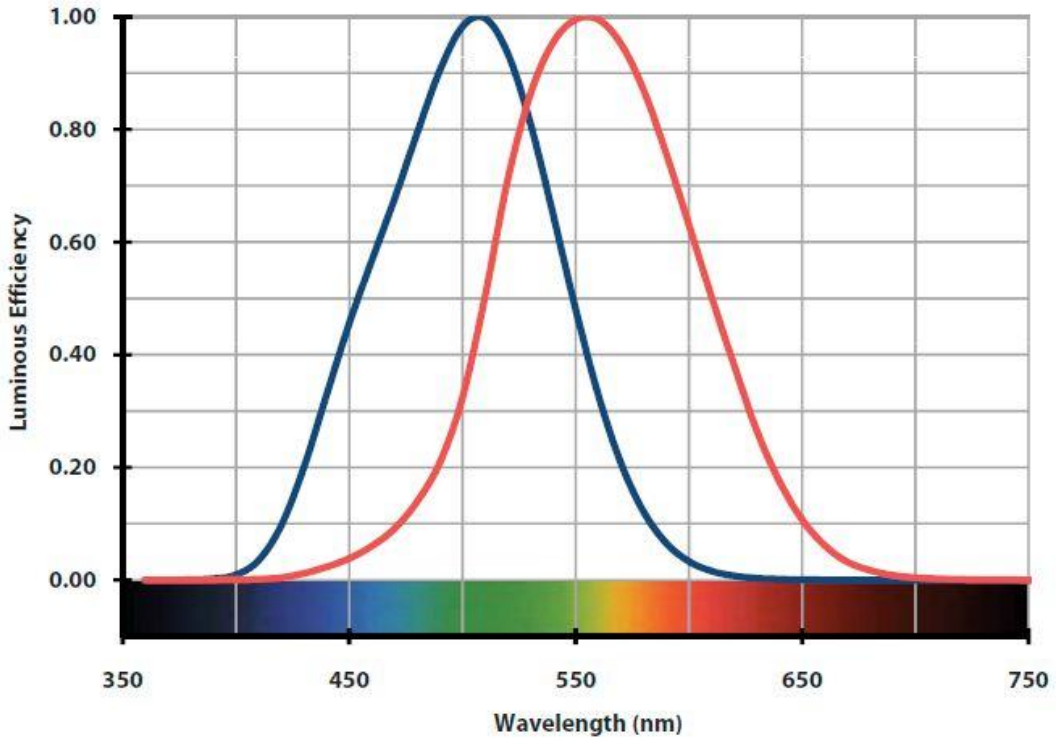

Figure 1: Photopic Luminous Efficiency Curve, V(λ) (5)

Solid angle, ω, is a spatial extent and is measured in steradians (1). This spatial quantity is used to characterize the distribution and density of light in space.

$$d\omega \equiv \frac{dA\,cos(\theta)}{D^2}$$

Luminous intensity, I, is the spatial density of luminous flux from a point and is measured in candelas (1). The unit candela is also defined as lumens per steradian.

$$I(\theta, \Psi) \equiv \frac{d\phi(\theta, \Psi)}{d\omega}$$

Illuminance, E, is the luminous flux density per unit area onto a surface. The SI unit is based on lumens per square meter, but and given the name lux. The common Imperial unit of measurement for illuminance is footcandle, or lumens per square foot (1).

$$E \equiv \frac{d\phi_{on}}{dA}$$

Irradiance, E_e, is the density of radiometric flux per unit area arriving at a surface and does not depend on the human visual system sensitivity to the radiant energy. The unit of irradiance is watts per unit area, either square meter or square foot. While this is not used as commonly in the lighting industry as illuminance, certain meters discussed in this paper measure irradiance in addition to illuminance (1).

Luminance, L, is the luminous intensity over the projected area and is measured in candelas per square meter. Unlike illuminance, this unit is never simplified to lux or footcandle as a way to differentiate between the two systems SI and English units. The key difference between these metrics is that luminance is a characteristic of the light emitting source, while illuminance is a measurement of how much light arrives at a surface. Luminance is often equated to source brightness; however, these two terms are not interchangeable. Brightness is subjective and depends on human perception, while luminance is a measurable quantity (3).

$$L(\theta, \Psi) \equiv \frac{dI(\theta, \Psi)}{dA\,cos(\theta)} = \frac{d^2\phi}{d\omega dA\,cos(\theta)}$$

2.1.2 Color Related Definitions

Colorimetry is the science of measuring color and is governed by the International Commission on Illumination (CIE) (1).

Hue is the relative perception of how closely a stimulus identifies as red, green, blue, or yellow (1). On a three-dimensional color wheel this is depicted by the angle around the circle on which the stimulus falls.

Value is also synonymous with the term lightness, more commonly used by engineers and color scientists. This characteristic identifies how much gray is in the stimulus ranging between the two extremes of black and white (1). In a three-dimensional color space this parameter is up and down the z-axis.

Chroma is the degree to which a color departs from gray within the same lightness (1). In a three-dimensional color space this would be represented by how far radially a sample is from the center of the circle.

Spectral power distribution (SPD) is a graph of relative radiant energy output by a source at each wavelength throughout the visible spectrum. An example of common source SPDs is shown in Figure 2.

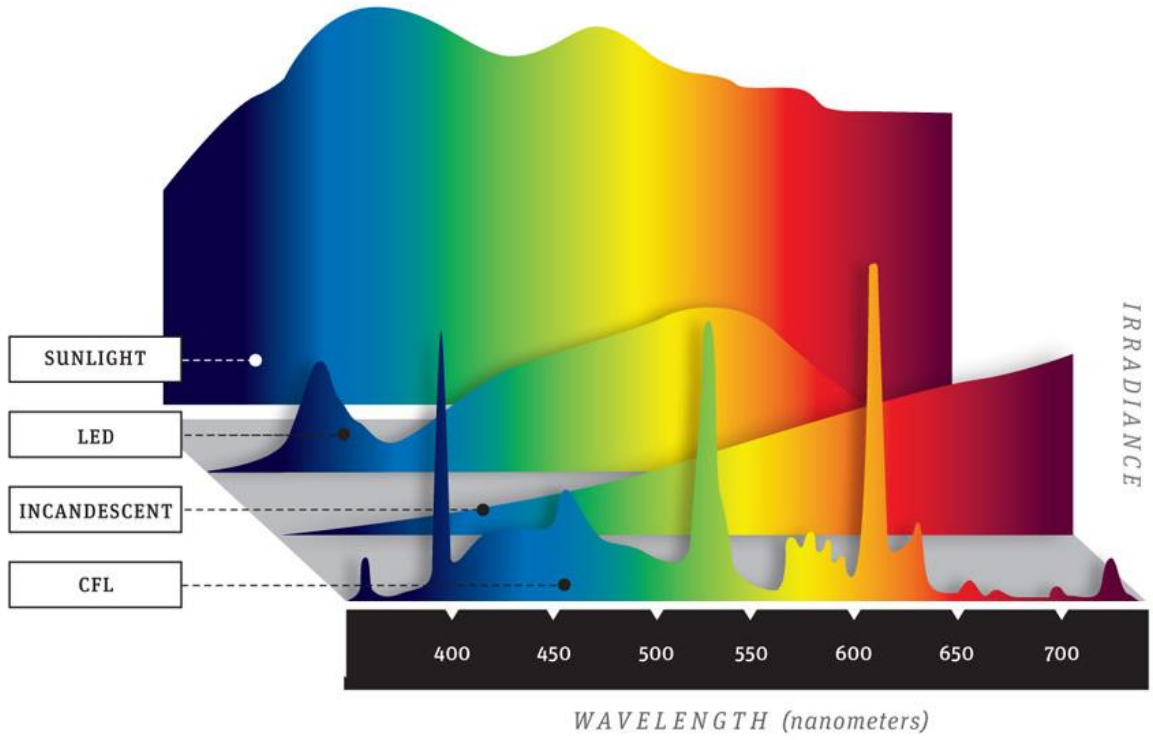

Figure 2: SPD Example of Common Source Types (4)

Spectral reflectance is a property of objects that are not acting as a light source. Opaque objects either reflect or absorb radiation at each wavelength and may do so in varying amounts. The spectral reflectance of an object determines what color the object appears because the wavelengths that are reflected are registered by the eye, while the wavelengths that are absorbed are not seen.

2.2 Color Luminance Measurement Error

2.2.1 Colorimetry

Isaac Newton defined his color theory in 1671 which explained that white light is composed of multiple colors (6). In 1760, Johann Heinrich Lambert defined the theory of additive color mixing which described that all colors of light together produce white light (6). Human color perception is a complex subject because it depends on three unique components: optical radiation, object properties, and human vision (1). While all three components are critical in order to understand how colors will be seen, the experiment in this paper will focus on characteristics pertaining to the optical radiation component. The three primary colors of light differ from primary colors of pigments that are commonly taught in art classes. The primaries of light are red, green, and blue. These may sound familiar from typical 'RGB' diodes used for many LED luminaires to produce white light. The specific wavelengths, which would be considered the true primary value of each, are 700.0 nm wavelength for red, 546.1 nm for green, and 435.8 nm for blue (6). These values may be attributed to color perception rather than a quality of light itself.

Any color produced by a wavelength in the visible spectrum may be matched with a particular combination of the three primary colors of light (6) (7). These two unique spectral

combinations which produce the same perceptual experience of a color are called metamers (6). Similarly, multiple unique combinations of radiance throughout the visible spectrum may produce the same luminance (7). In the human visual system, there exists an achromatic channel which responds to luminance separately from other color channels (6). Therefore, luminance and perceived color are not exclusively related to one another.

2.2.2 Human Photopic Vision Response

While most of this research focuses on the accuracy of various measurement processes and tools, it is important to remember that these metrics are desirable for better design and applications of lighting in environments occupied by humans. Perception of light is more complex than the spectrum and intensities of a source, or reflective properties of materials. The human visual system is controlled by chemical, electrical, and physical processes which create a nonlinear response to colors (8). The retina of the eye is covered by rods and cones which control scotopic and photopic vision, respectively. Scotopic vision is activated at low light levels and is mostly in use after dark. Photopic vision is triggered at daytime light levels and is responsible for color vision. Each of these two visual systems have their own responsivity curve to wavelengths in the visible spectrum. Three types of cones exist, long, medium, and short wavelength cones, and these each also have their own unique sensitivities to certain wavelengths. The combined response of the three types of cones results in the CIE photopic luminous efficiency curve, V(λ) (6). As can be seen in the V(λ) curve, the average peak sensitivity for photopic vision is to the 555 nm wavelength which most would describe as a bright green. The sensitivity to wavelengths on either side of this central point decrease exponentially which makes certain parts of the visible spectrum appear stronger than others. Humans are typically able to detect a difference

between wavelengths that vary just 1 nm, but require up to a 10 nm difference in other less sensitive parts of the spectrum (9).

The human eye is extremely adaptive and is able to respond to between a 12 to 14 order of magnitude change in intensity over time (10). Within one particular scene, the eye has a 10,000 to 1 adaptation range which means details in both very dark and light subjects are able to be observed at the same time (10). In comparison, standard digital cameras are only able to capture an average range of 1,000 to 1 which means that a photograph of the same scene will be missing details in either light or dark areas that would have been observed by a person (10).

2.2.3 V(λ) Function Assumptions and Errors

Incandescent was the primary light source technology when the V(λ) function was determined. Since the adoption of this standard, colors have proven to be an issue, especially blue. Research has suggested that the values provided for the blue-violet region of the spectrum may be too low (11). It is also important to remember that there are two different luminous efficiency curves, one for photopic vision, or high light levels, and one for scotopic vision, or low light levels. V(λ) is based on the average photopic vision response of the eye, while the unique response of scotopic vision is represented by V'(λ). Therefore, the light levels in an environment are important to consider when evaluating metrics based on the V(λ) response such as illuminance and luminance. Both V(λ) and V'(λ) were shown in Figure 1, which illustrates that the peak sensitivity occurs roughly 50 nm towards the blue end of the spectrum for scotopic vision, or low light levels.

Lamp spectra is known to have an effect on the visual perception of brightness. This has been tested with multiple subjective, perception based experiments (12). The experiments included side-by-side visual matching, brightness ranking, and subjective ranking. These were used to relate perceived brightness to illuminance conditions for sources with various CCTs and of saturated colors. The tests confirmed that illuminance does not correspond to perceived brightness when chromatic subjects are involved. In fact, the correlation between illuminance values from a meter and "perceived brightness can be off by 100% and more" (12). The same study also suggested that CCT, CRI, gamut area, or chromaticity information do not produce good predictions on their own of the perceived brightness. Only illuminance was investigated in this case, but it was noted that the same conclusion would apply to any V(λ) based quantity, such as luminance, as well. If the V(λ) curve is correct, then different sources of equal luminance should have equal perceived brightness, but they do not (11).

2.2.4 Chromatic Based Errors in Lighting Metrics

Standard illuminance and luminance meters consist of a sensor with one type of photoreceptive cell, which responds to the entire visible spectrum. A correction filter then covers this sensor to limit each wavelength to the proportions specified by V(λ). The resulting response must meet specified lab standard tolerances. The meter classification determines how well the correction filter correlates to the V(λ) curve. Meter specifications often acknowledge that the error may increase slightly "for sources of irregular spectral distribution such as low pressure sodium" (12). The subtle implication here is that the accuracy of the correction filter is spectrally dependent. CIE Standard Illuminant A is the light source basis of calibration for most photometric meters. Differences between the

incandescent spectrum of illuminant A and the actual source measured with the meter introduce errors. Manufacturers often downplay this subject by noting something along the lines of a "slight deviation of the relative spectral response" for spectra that are considerably different from the standard calibration source (13). Research studies which mention this fact often overlook the potential severity of this error as well (14). However, the degree of error introduced by the V(λ) correction filter depends on the particular source spectrum. One article suggests that errors may even reach "several tens of percent" for colored sources (15).

While both blackbody radiators, daylight has a significantly different spectrum than the incandescent source of CIE Standard Illuminant A. The incandescent of illuminant A is specified at a CCT of 2856 K (16). Standard Illuminant D65 is the most common model for average daylight with a CCT specified as 6504 K (16). Another standard daylight model is classified as Standard Illuminant C which does not include the ultraviolet wavelength region, and has a cooler CCT at 6774 K. The drastic difference between these models is shown in Figure 3. In general, blue wavelengths will be underestimated by standard lighting meters and reds will be overestimated in the case of average daylight measurements (17).

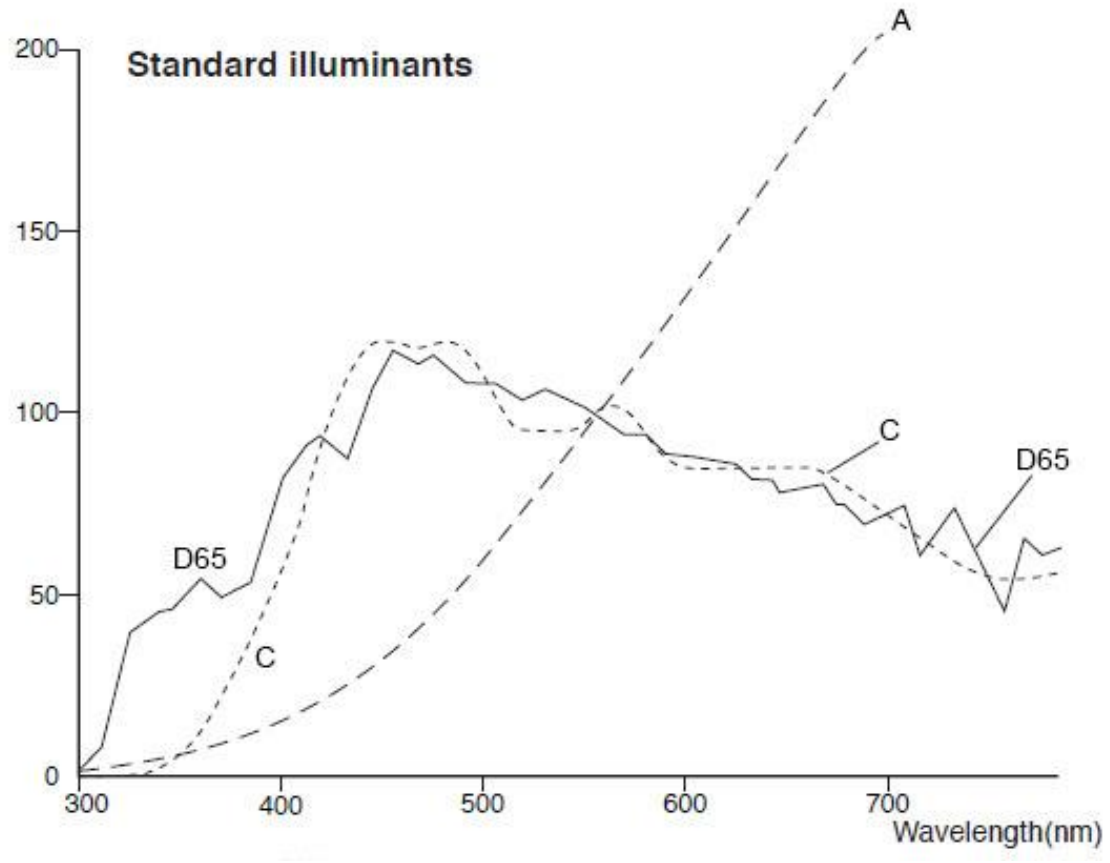

Figure 3: Standard Illuminant Spectra (16)

It is important to remember that the spectrum of daylight is dependent on time of day, geographic location, weather, and various other factors. Thus, a calculated daylight error may vary drastically depending on the specific measurement conditions. Similarly, modern LED light sources come in a wide range of spectra, which each have their own unique degree of error.

2.2.5 Lighting Meter Errors

Now that it is understood that there are spectrally based errors in many measurements, some simple studies of meter accuracy under different source spectra have been completed. One manufacturer published a comparison of different classifications of

V(λ) correction filters among their own meters (18). Two classification types were compared, A, and C, which are determined by the quality of the filter. An error percentage was calculated as the sum of the deviation from V(λ) relative to the total area underneath V(λ) (18). The classification A filter was stated to have less than a 3% error relative to V(λ), while the classification C filter was less than 6.5% (18). What remains unclear from this report is how the given error percentages of each filter type were initially tested. A warm white LED tested with both filter types did not produce significant differences in V(λ) matching error when compared to the error found for measurements of CIE Standard Illuminant A. Additionally, a typical chip on board (COB) LED with a large blue peak resulted in an insignificant error difference compared to the standard illuminant error. RGB white light LED sources for both warm and cool white resulted in increased V(λ) deviation errors, but the differences were still determined to be insignificant. Lastly, red, orange, green, and blue-green colored LEDs did not result in a significant error difference. However, the blue colored LED tested resulted in drastic differences of deviation from V(λ) when compared to CIE Standard Illuminant A (18).

There is a difference in the way a typical illuminance or luminance meter measures light, versus a meter with spectral characteristics. As mentioned earlier, a typical illuminance meter contains one type of photoreceptive cell, covered by a V(λ) correction filter, and then a cosine correction filter. Typical luminance meters also consist of a single type of photoreceptive cell with a V(λ) correction filter, but no cosine correction is required for this measurement. Instead, optical systems that allow the user to focus on the subject are a unique component of luminance meters. There are multiple spectral meter options with unique applications such as radiometers, spectrophotometers, and spectroradiometers (19). Radiometers are used to measure certain energy outside of the visible spectrum, such

as ultraviolet or infrared. Spectrometers also focus on a particular range of wavelengths, but the energy is broken down into its wavelength components via an optical grating or prism. Spectroradiometers utilize a sensor with many unique photoreceptive cells, each with various responsivities to wavelengths throughout the visible spectrum (19). The photopic conversion then occurs via internal software, avoiding the issues discussed due to physical V(λ) correction filters in typical light meters. The intended application for a meter should be discussed with the manufacturer before deciding between these technologies, in order to best understand its process and limitations.

A comparison between measurements from a spectroradiometer, which is believed to avoid spectrally-based errors, and a standard illuminance meter was conducted by Olino Renewable Energy (20). The two meters were expected to produce a maximum difference of 7.4% due to the combined effect of each of their uncertainty specifications. Any resultant error less than this may be attributed to the specified accuracy of the two meters. A 100 W incandescent lamp resulted in a difference of 5.4% which confirms that the illuminance meter was able to accurately measure an incandescent source, as would be expected. Comparison of a typical compact fluorescent (CFL) resulted in a much larger difference of -21%, with the higher illuminance measurement coming from the spectroradiometer. Four unique white light LEDs were compared as well including RGB, neutral white, warm white, and warm white plus red. These sources resulted in differences of 31%, -14%, 2%, and -15%, respectively. Not only did the range change drastically with different spectra, but whether the illuminance meter measured over or under the true illuminance also changed. The warm white condition resulted in only 2% error which appears to be acceptable, but this may have simply been a lucky match based on the extreme variation in other LED conditions.

Another experiment was conducted by a curious industry professional which compared illuminance meters from various manufacturers to each other under multiple source types (21). Again, the measured illuminance from an illuminance meter was compared to that of an illuminance spectrophotometer. Four illuminance meters of different quality were used and the sources measured were an LED, fluorescent, high pressure sodium (HPS), and incandescent. Two meters showed an acceptable difference for the LED condition at 1% and 2%, while the other meters resulted in 10% and 21% errors. The fluorescent condition resulted in the exact same differences for each meter as the LED scene. The HPS condition resulted in 4%, 0%, 22%, and 10% differences from the same illuminance meters. Finally, the incandescent condition resulted in 0% error for all meters, except for the model which consistently produced the largest errors. This meter resulted in a slight difference of only 1% for the incandescent condition. This study also discussed the differences in LED spectra and how that affects potential correction factors. When eight unique LED sources were measured with the same four meters, correction factors were drastically source dependent for the meters which consistently produced the largest differences. Thus, poor quality illuminance meters result in unreliable correction factors. While manufacturers often provide correction factors for general spectra, the process to determine these factors is not described. In fact, experimental results have shown that errors may far exceed the correction factors provided in many user manuals for certain source types. The errors found with illuminance meters are expected to be similar for standard luminance meters because they require the same sensor type and correction filter.

In the interest of better understanding inherent meter errors, other potential issues have often been overlooked as well. Cosine correction filters for illuminance meters are also

susceptible to imperfections, but this would not be an issue with luminance meters which do not require this correction (17). The maximum value limits are also important to consider for all meters, as these are commonly encountered during typical daylight conditions.

2.2.6 Color Accuracy of Meter Measurements for Luminance and Illuminance

The response of meters to colored surfaces and sources is also a potential source of error to be aware of for general luminance measurements. The Konica Minolta LS-110 luminance meter manual specifies that the meter uses a spectral response filter to relate the energy that the sensor receives to within 8% of the V(λ) curve, as shown in Figure 4 (22). Color correction factors (CCF) are able to be used with the LS-110 meter when measurements are taken of targets that differ greatly from the calibration test source. The test source and basis of the 1.000 CCF is the CIE standard illuminant A. CCFs are multipliers which may be automatically applied to the standard luminance measurements. A list of standard light sources and their corresponding CCF are listed in the manual, but the ones of most importance in this experiment are color CRT-red, color CRT-green, and color CRT-blue which are 0.995, 1.018, and 1.123, respectively (22). These values were determined by Konica Minolta based on spectrophotometer data.

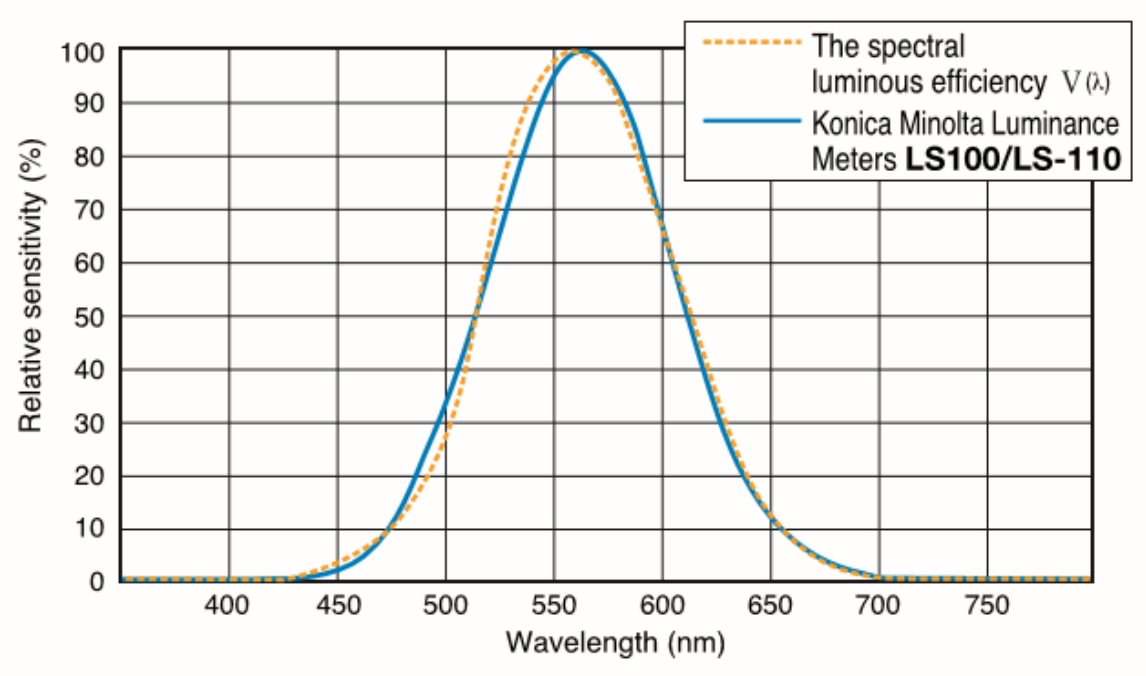

Figure 4: Konica Minolta LS-110 Luminance Meter Spectral Response (23)

The Konica Minolta CL-500A illuminance spectrophotometer produces data that is much more closely matched to the V(λ) curve. This device is classified by Japan Industrial Standards (JIS) with a rating of "general class AA." The responsivity throughout the visible spectrum is shown in better detail in Figure 5 (24). Measurements for the complete visible spectrum from 360 nm to 780 nm are attainable with a spectral bandwidth of 10 nm (24). The wavelength precision for this device is specified as ± 0.3 nm (24).

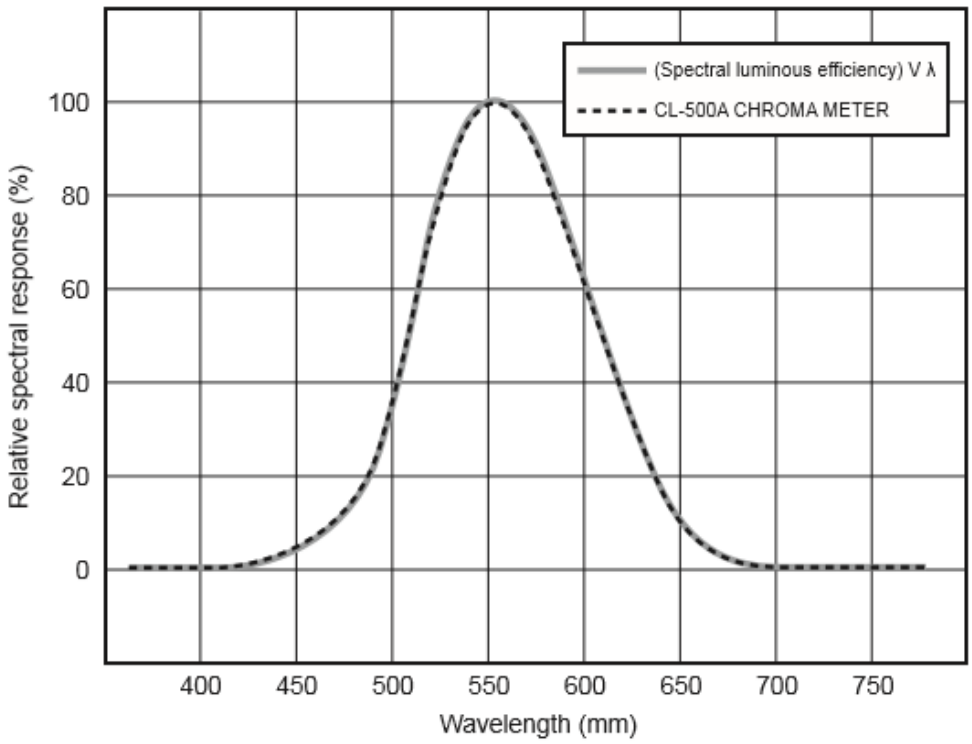

Figure 5: Konica Minolta CL-500A Illuminance Spectrophotometer Spectral Response (24)

The CIE provides standards and recommendations for testing the spectral responsivity of detectors, radiometers, and photometers (25). These guidelines were considered when defining the approach to this experiment for analyzing error inherent to both the luminance meter and CMOS digital camera sensor. The CIE suggests four unique techniques: laser beams for power mode measurements, a monochromator to control wavelength output and bandwidth, Fourier-transform infrared (FTIR), and narrow-bandwidth filters with a broadband source. Multiple light sources were specifically mentioned in this standard with importance placed on a smooth spectral output and broadband distribution. Sources that were specifically mentioned are tungsten halogen, xenon, and argon arc lamps (25). This standard is typically used for reference radiometers and also as a guide for equipment manufacturers.

2.3 High Dynamic Range Photography

2.3.1 Camera Sensor and Color Response

The camera image sensor detects photons that land on each pixel while the shutter is open (26). Different types of sensors have different patterns of pixel areas which are sensitive to certain wavelengths, typically categorized as red, green, and blue (RGB) channels. The RGB channels each have independent response curves which may vary even within products from the same manufacturer (27) (28). Cameras with complementary metal oxide semiconductor (CMOS) sensors have become the primary equipment used for HDR photography (26). The Nikon D5200 which was used by the University of Colorado Boulder for HDR luminance measurement studies, uses a CMOS sensor with 2.71 million pixels (3) (29).

Values collected by the camera sensor may be saved in a RAW file format which maintains the raw data measured by each sensor pixel. These files are generally very large and take up a lot of storage space on computers and require additional computation time. More commonly in photography, JPEG files or other compressed file formats, such as PNG, are used because they are quicker to work with. These smaller files are created by combining the information received by each sensor pixel into small clusters to decrease the quantity of data. The methodology and pattern for how RAW data is condensed into fewer packets of information is proprietary information unique to each manufacturer.

Color calibration of image sensors may be an issue when looking to derive accurate color information from an image (28). Color images may easily be able to contain up to 16.7 million colors by varying the relative levels of RGB values (7). Amazingly, this color range

is still an incomplete depiction of color spaces observed through human perception of the colors available in the world (6). Cameras automatically self-calibrate color mismatches based on dynamic programming methods to fit all of the information collected by the sensor into bins of the color ranges that are available for the technology (28).

2.3.2 Process and Theory of High Dynamic Range Photography

The amount of time between when a camera shutter opens and closes is referred to as the length of exposure. The exposure time controls how much light is able to enter the camera and fill the sensor with information from the scene. HDR photography is a process with digital images which combines multiple exposures of low dynamic range (LDR) to create a more accurate depiction of what the human eye is able to see (30). Over exposed images stay open for a longer shutter release and often appear washed out but provide details from areas which otherwise would appear very dark. Under exposed images are the result of short shutter speeds and collect more information from very bright subjects. All of the LDR images must be taken with the same subject and view angle in order to be combined seamlessly, so the use of a tripod and a still scene is highly recommended (7). The relevant information is extracted from each exposure and combined into one final HDRI with more information of the scene than would have been capable of being captured by the sensor in a single shot.

2.3.3 Potential Applications of HDRI Luminance Mapping

The lighting industry has found many potential uses for HDR photography besides simply creating a more accurate picture. Luminance measurements and glare metrics are now able to be derived through HDRI (10) (30). The major benefit of using HDRI for these

measurements, which are usually taken with existing lighting specific meters, is that many more measurements can be captured at one time. This provides abundant data for analysis in a very simple and straight forward process. Similarly, sky capture images are able to provide significant sky characteristic data for daylight modeling and analysis (10) (30). This information would provide more accuracy to daylight analysis than current average sky models.

Another potential application of the technology is for image-based lighting. This would use lighting measurements derived through HDRI of an actual scene to simulate how light would behave for a computer world, often referred to as photogrammetry (7) (3). Since the measurements would easily be transferred to the computer, this would make modeling light behave how it would in the real world more accurately. This process also makes it possible to capture 3D coordinates of subjects for modeling purposes (3). While there are additional steps and equipment to effectively use photogrammetry, HDRI with lighting measurements is a crucial tool in this process (3).

Near-field photometry could also benefit significantly from the use of HDRI luminance analysis. The main concept behind near-field photometry is that the luminous intensity distribution of a light source is not independent of distance when the distance is less than five times greater than the largest dimension of the source (3). At large distances, far-field photometry is used which includes many assumptions that essentially treat a larger light source as if it were a point source. These simplifications help with calculations and work very well for certain applications. However, some lighting applications, such as coves, indirect lighting, wall washing, or other wall mounted fixtures, simply do not fit into these distance guidelines (3). Near-field photometry is still rarely used in the industry

because methods for producing, communicating, and using this detailed information have yet to be widely accepted.

2.3.4 Accuracy of Using HDRI for Lighting Measurements

HDRI contains luminance information automatically, but these values are simply relative to each other rather than absolute measurements. When HDRI is to be used for absolute luminance analysis, the scene requires a known luminance value for calibration (31). The luminance of a point in the scene should be measured at approximately the same time the photos are taken, and then that same point in the final image will later be defined by the user via software. The calibration point or small area should be representative of the majority of the scene in terms of luminance in order to improve accuracy (32).

This technique was used by researchers in real architectural settings for glare analysis of spaces with daylight. In one specific experiment, a fisheye lens was used to create HDRI of a scene that was also recreated in multiple digital simulation software (30). Luminance measurements were taken with standard meters as well to compare the results from HDRI, digital simulations, and measured data of the same space. This experiment focused specifically on glare metrics which utilize luminance to characterize the perceptual experience of glare. Suk found that neither HDRI nor computer simulations produced consistent glare analysis results in this experiment (30).

Luminance data from HDRI has been investigated in contexts other than glare metrics as well, and particular sources of error have been identified. Vignetting is an inevitable characteristic of images that is due to the optical components of a camera lens at

a particular aperture. The result is a fall-off of brightness towards the edge of an image. Some lens aperture combinations produce obvious vignetting and others produce much less noticeable effects but they still affect luminance information in the image. This issue has been investigated and was thoroughly documented (3). This research performed at the University of Colorado Boulder resulted in various correction filters that may be applied to HDRI of certain lens and aperture combinations. Additional sources of error occur with high luminance sources, and areas with dramatic contrast, that produce lens flare in the images. Research is currently being performed on this topic as well to investigate the cause and potential correction for this phenomenon.

One of the main issues with using HDRI for absolute luminance analysis is the combination and analysis software currently available in this market. A thorough study of many different HDRI software packages available was conducted (3). The results of this study showed that most of the software investigated resulted in extremely high and unacceptable error of luminance values (3). The two best software options in terms of accuracy were determined to be hdrgen and raw2hdr, with negligible difference between the JPEG and RAW file formats for broadband light sources (3).

2.3.5 Color Related Error with HDRI

The errors associated with colorful subjects in HDRI luminance readings has been acknowledged in multiple previous experiments. A standard approach to this issue has been to photograph color sample cards with known reflectance and spectral characteristics. In 2005, Anaokar and Moeck tested six Munsell color cards with 14 chips of varying value and chroma per hue – with the exception of the gray card which included 16 chips (33). The

colors included red, yellow, green, blue, purple, and gray. HDR photographs and illuminance measurements were taken of the colored surfaces under multiple lighting conditions including high and low illuminance of florescent, metal halide, and mercury indirect light sources. Significant error was identified for cool colors (blue, green, and purple), while a lower magnitude of error was found with warm colors (red and yellow). The magnitude of error increased with saturation, and dark surfaces showed a tendency to be overestimated. These error results were found to be independent of illuminance level and light source spectrum.

A similar experiment was conducted by Inanici the following year using a Macbeth ColorChecker, Nikon camera, and Konica Minolta LS-110 luminance meter (34). HDR photographs of these color samples were taken under illumination from multiple light sources which included incandescent, 500W tungsten (projector), fluorescent (T12 – 6500K, T8 – 3500K, and T5 – 3000K), metal halide, and high pressure sodium. The error margin for gray and colored targets were found to be dependent on the source SPD. Colored targets resulted in an average error of 9.3% compared to 5.8% for grayscale targets. Darker targets and saturated colors resulted in increased error. Overestimation of luminance values from HDRI for dark surfaces or regions was concluded to be expected for most HDRI applications.

Color sample cards were used again for further experiments, but with daylight as the source by both Moeck and Chung (32) (35). Matte gray and colored sample cards of known reflectance were photographed in natural daylight on a rooftop in Arizona (32). Results showed that dark surfaces were overestimated, while light surfaces were underestimated. Error was also seen to increase with saturation. Cool colors produced the

largest error, with blue producing the maximum error observed, and yellow produced the minimum error. Similar results were observed in an interior space with natural daylighting as the source and HDRI luminance values compared to luminance meter measurements (35). The findings of these experiments suggested that a specific color with similar characteristics to the majority of the scene should be used for calibration when dominant colors appear in the HDRI (32) (35).

Colored subjects in HDRI have been thoroughly investigated and noticeable trends have been documented such as increased error with high saturation, as well as with dark and cool colors. However, object color is a product of both the spectral reflectance of the subject and the incident, illuminating power (6). Stanley broadened the investigation of color related error in HDRI luminance measurements by photographing saturated color sources rather than non-light emitting surfaces (3). An acrylic lens covered aperture of a small integrating sphere was illuminated from behind with a color changing LED. Red, green, blue, and white settings were evaluated with neutral density filters covering half of the lens to create both high and low luminance conditions. The dominant wavelength of the red, green, and blue outputs were 620 nm, 520 nm, and 450 nm, respectively. An HDRI of each scenario was analyzed and compared using seven different HDRI software; hdrgen, raw2hdr, bracket, picturenaut JPEG, picturenaut RAW, Luminance HDR JPEG, and Luminance HDR RAW. Similar to previous color based HDRI experiments, blue was found to produce the highest amount of error compared to the red and green conditions. The software that produced the most accurate luminance values with the blue LED was picturenaut RAW, while hdrgen was the least accurate. Both green and blue luminance accuracy was significantly improved by analyzing compiled RAW files rather than JPEG files. The red, high luminance LED measurement resulted in the lowest overall error of all

the color and luminance combinations tested. The lowest average error across all conditions was found to be 32% with picturenaut RAW, and raw2hdr was second best with an average of 68% error (3). Based on these findings with a RGBW LED, no color, luminance, and available software combinations resulted in an acceptable percentage of error for HDRI of saturated color sources. It is known that using JPEG images for HDRI will result in color issues because correction adjustments such as white balancing, tone curves, and color saturation are applied to the raw data during compression (36). To avoid color issues related to in-camera processing and compression, RAW file formats should be used when color accuracy is a concern.

Chapter 3: Spectral Luminance Measurement Error Detection

Luminance measurements of narrow band sources within the visible spectrum were evaluated in order to understand which range of wavelengths, if any, are most likely to result in significant error of luminance values with a traditional luminance meter. An LED source was illuminated inside of an integrating sphere, then the spectral output was broken down into sections via a collection of narrow bandwidth filters. Measurements from an illuminance spectrophotometer were used to compare values found with a traditional luminance meter. The following sections detail the characteristics of equipment used, experimental setup, and the process followed.

3.1 Equipment

3.1.1 Measurement Devices: Illuminance Spectrophotometer and Luminance Meter

The Konica Minolta LS-110 luminance meter was used for all luminance measurements and is shown in Figure 6: Konica Minolta LS-110 Luminance Meter Figure 6. The specified range of values that this meter is reliably able to measure spans from 0.01 cd/m^2 to 999,900 cd/m^2 (22). The accuracy of this meter is stated to be "±2% ±2 digits of measured value" for luminance levels between 0.01 cd/m^2 and 9.99 cd/m^2, and "±2% ±1 digits of measured value" for luminance levels greater than 10.00 cd/m^2. The short-term repeatability alludes to a higher accuracy of "±0.2% ±2 digits of measured value" for luminance levels between 0.01 cd/m^2 and 9.99 cd/m^2, and "±0.2% ±1 digits of measured value" for luminance levels greater than 10.00 cd/m^2 (22). The CCF feature explained in the Literature Search chapter was utilized for some measurements during the experiment. The red, green, blue, and white source CCF multipliers, and the filters that they were used in

conjunction with, are listed in Table 1. The filter and CCF pairing was chosen based on the closest apparent color of the filter when illuminated, either red, green, or blue.

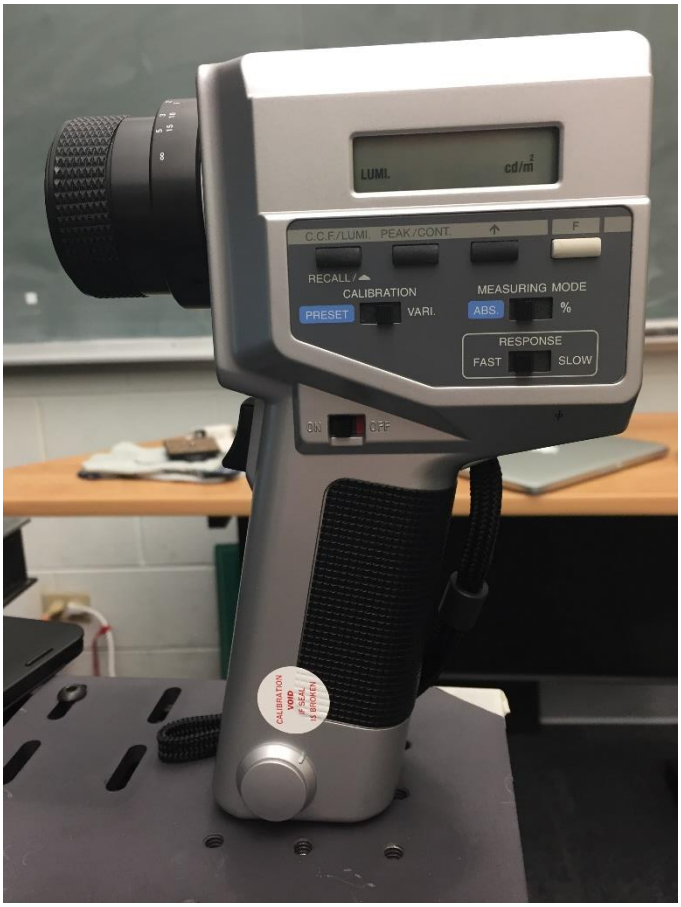

Figure 6: Konica Minolta LS-110 Luminance Meter

Table 1: Color Correction Factors for Each Condition

Illuminant Name	**CCF**	**Filters Tested**
Color CRT – white	1.023	No filter (acrylic)
Color CRT – blue	1.123	435 nm, 465 nm, 495 nm
Color CRT – green	1.018	525 nm, 555 nm, 585 nm
Color CRT – red	0.995	615 nm, 645 nm, 675 nm

The CL-500A illuminance spectrophotometer was used to measure both illuminance and spectral output, and is shown below in Figure 7. The illuminance measurements were used to calculate luminance in order to check the accuracy of the LS-110. More information on these calculations will be presented in later sections of this paper. Spectral information recorded by this meter was used to confirm the filter data provided and to understand which portions of the spectrum were present in each trial. A minimum of 5.0 lux was required for accuracy of saturated color measurements made by the CL-500A per specifications given in the manual (24). For typical broadband sources, the minimum illuminance the meter could accurately measure was 0.1 lux (24). The illuminance measurements from this meter are specified to have an accuracy of "±2% ±1 digit of displayed value" and a repeatability of "±0.5% ±1 digit" (24). There does not exist a minimum measurement distance between the light source in question and the sensor head of the meter. These restraints greatly impacted the design of the experimental setup, as certain filters required a very short distance between the source and meter to attain an illuminance measurement above 5.0 lux.

Figure 7: Konica Minolta CL-500A Illuminance Spectrophotometer

The accuracy of the CL-500A at each wavelength was evaluated by measuring an absolutely calibrated NIST test source with the meter and by comparing the measured spectrum to the known spectrum of this source. The data for both curves was normalized at 750 nm. The two SPDs of the NIST test source are shown in Figure 8.

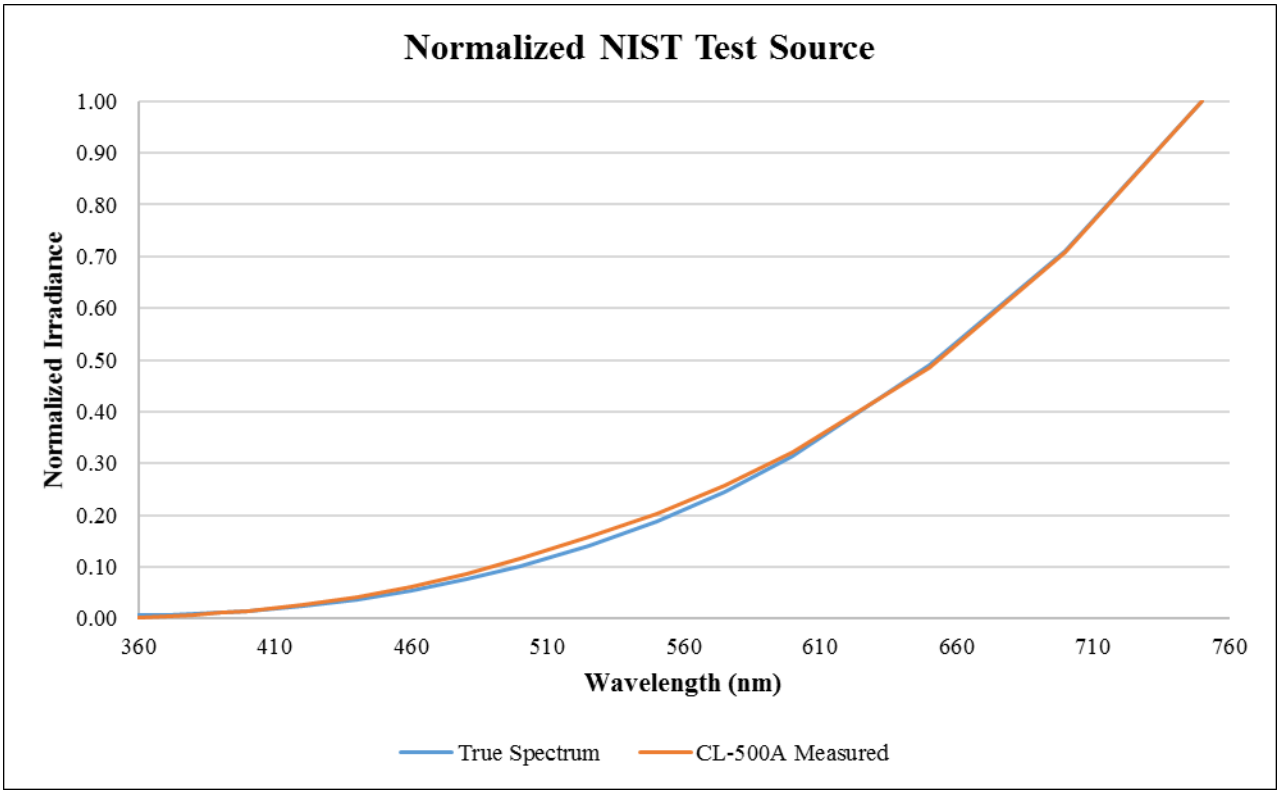

Figure 8: SPD of Calibration Source

The two SPDs follow a very similar curve but clearly separate from about 460 nm to 610 nm. The severity of this difference was investigated further and a graph of the difference at each wavelength is shown in Figure 9.

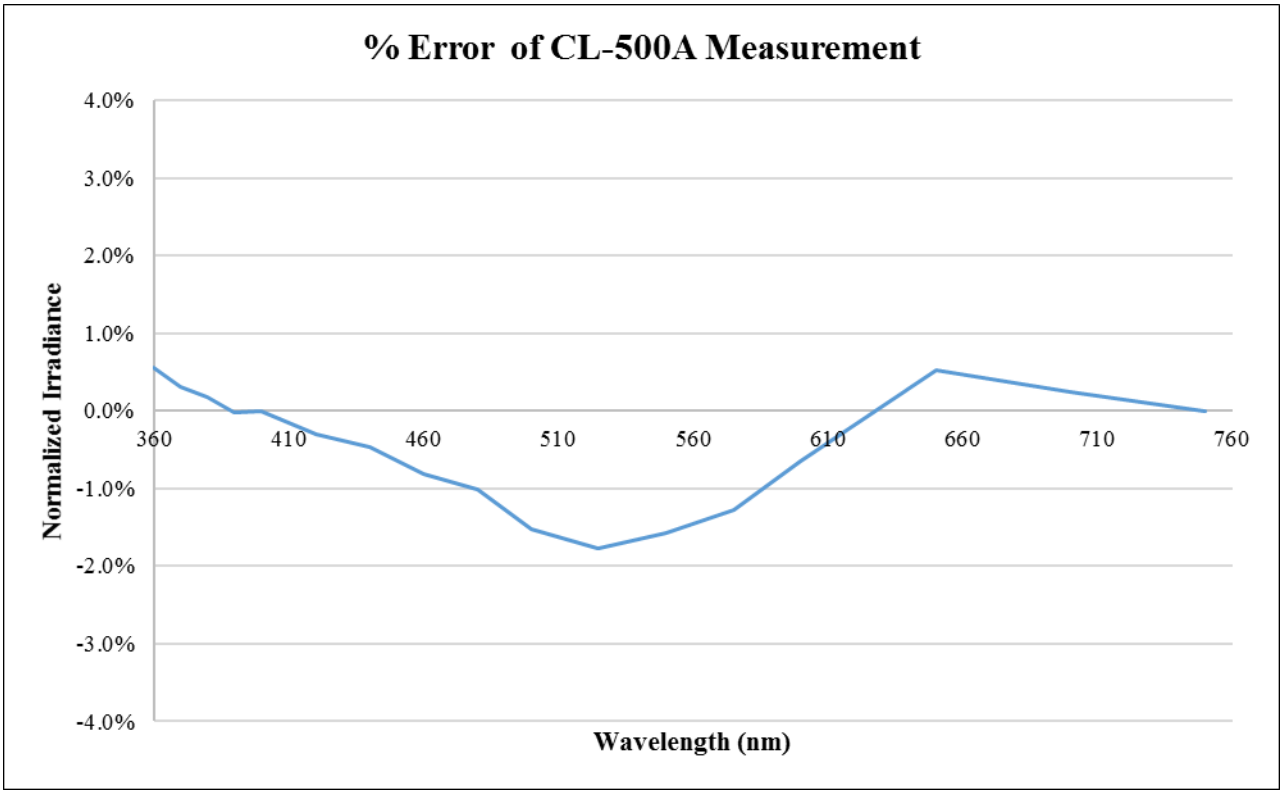

Figure 9: Difference in SPD of CL-500A Measurement and Known Spectrum of Calibration Source

Most measured wavelengths resulted in less than a 1% error, which is within the tolerance of the CL-500A meter, and all were below 2% error. The maximum difference of 1.8% occurs at 525 nm. These results confirm that the illuminance spectrophotometer measurements taken will be accurate to within 2% as specified. It should be noted that the spectrum of the NIST test source appears to be a typical incandescent spectrum. As previously mentioned, most light meters are calibrated with an incandescent spectrum to determine the specified tolerance. Therefore, this accuracy could be susceptible to change under different source types. The illuminance spectrophotometer should be reliable throughout the visible spectrum based on the nature of the sensor design, however this was not confirmed under standardized test sources with unique spectra.

A custom baffle was designed for the illuminance spectrophotometer in order to relate the measurements made with this device to those from the luminance meter. More information on these calculations will be presented in later sections of this paper. The viewing angle of the baffle was slightly oversized compared to the light source because the goal was to mitigate reflected light in the room, rather than to isolate a section of the illuminated surface, which is possible to do with luminance meters. The design was modeled in SolidWorks and 3D printed by Shane Lillya. The interior was spray painted with matte black chalkboard paint to minimize internal light reflections. This baffle was attached to the CL-500A meter for certain measurements in this experiment. More information regarding which measurements utilized the baffle will be specified in later sections. The design and final product of the baffle is shown in more detail in Figure 10 and Figure 11.

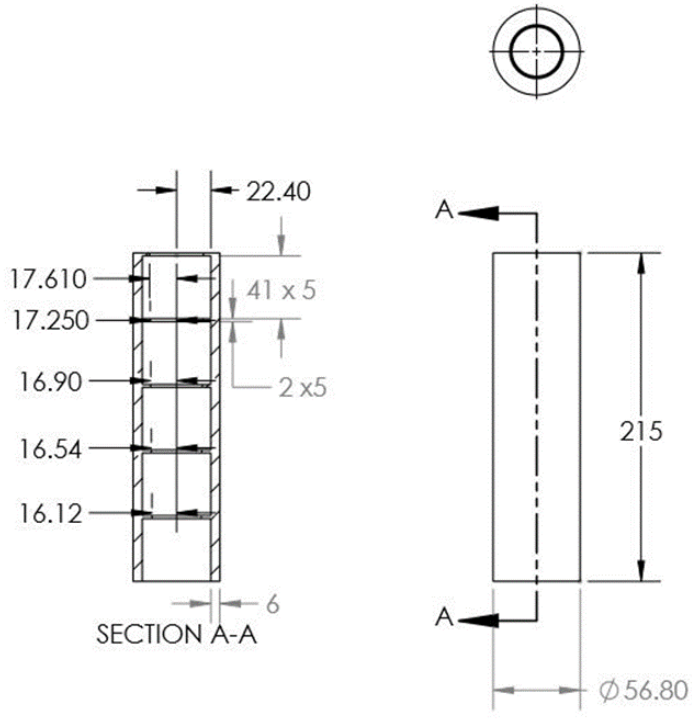

Figure 10: Dimensioned Baffle Design (all units are mm)

Figure 11: Spray Painted Baffle Interior

3.1.2 Software: Tethering Program for CL-500A

The CL-500A illuminance spectrophotometer came with CL-S10w software to tether the meter to a computer. This software allowed direct transfer of data to an Excel spreadsheet format which made data review and analysis simple. Data recorded includes illuminance, peak wavelength, and irradiance at each wavelength in the visible spectrum, among others. Measurements were initiated from the computer which allowed for hands-free use of the device to minimize misalignment, as well as other human error factors during the measurement process.

3.1.3 Integrating Sphere

A perfectly diffuse source is defined as one that emits light in a Lambertian distribution. By definition, the luminance of a Lambertian source is constant regardless of viewing angle, while the luminous intensity decreases by the cosine of the viewing angle

(3). An integrating sphere was designed and constructed by Mark Jongewaard for a previous experiment at the University of Colorado Boulder (3). This same integrating sphere was also used for this research. The sphere is painted with a diffuse white paint on the interior and has a diameter of 6 inches. A round port on one side was designed for light source access. A 1-inch port directly opposite of the light source was filled with an acrylic lens to create a diffuse light emitting surface. A small, white mask was secured inside of the sphere to block the direct view of the source from the acrylic port. Figure 12 shows the interior of the integrating sphere used in this experiment.

Figure 12: Integrating Sphere Interior

3.1.4 Broadband Light Source Selection

The complete extent of the visible spectrum spans from 360 nm to 830 nm (37). A light source was desired that would emit sufficient radiant energy across the entire visible spectrum to be measured by the meters. Many unique light sources were considered for this experiment, and the final decision was made based on the spectral output, lumen output, and economic feasibility.

White light from current LED technology is always the result of either a colored diode coated in a phosphor of contrasting color, or a combination of multiple colored diodes mixing to produce the appearance of a white source. Spectral power distributions (SPD) for LEDs include at least one peak at the wavelength where the colored diode emits its energy. The spectral output of an ETC theatrical fixture with seven unique diodes was tested with the Konica Minolta CL-500A illuminance spectrophotometer as a potential source. The peak wavelengths for red, amber, green, cyan, blue, and indigo were 632 nm, 596 nm, 525 nm, 501 nm, 473 nm, and 443 nm, respectively. The white light combination of these diodes produced a spectrum with noticeable peaks in the indigo and yellow-green regions of the spectrum, as well as a dip in the cyan-blue region. The spectral data for each of the diodes is shown in Figure 13. Large peaks at certain parts of the spectrum were not desirable for establishing continuity throughout the visible spectrum. This fixture was also very large compared to the integrating sphere which would have made illuminating a diffuse surface with this source difficult.

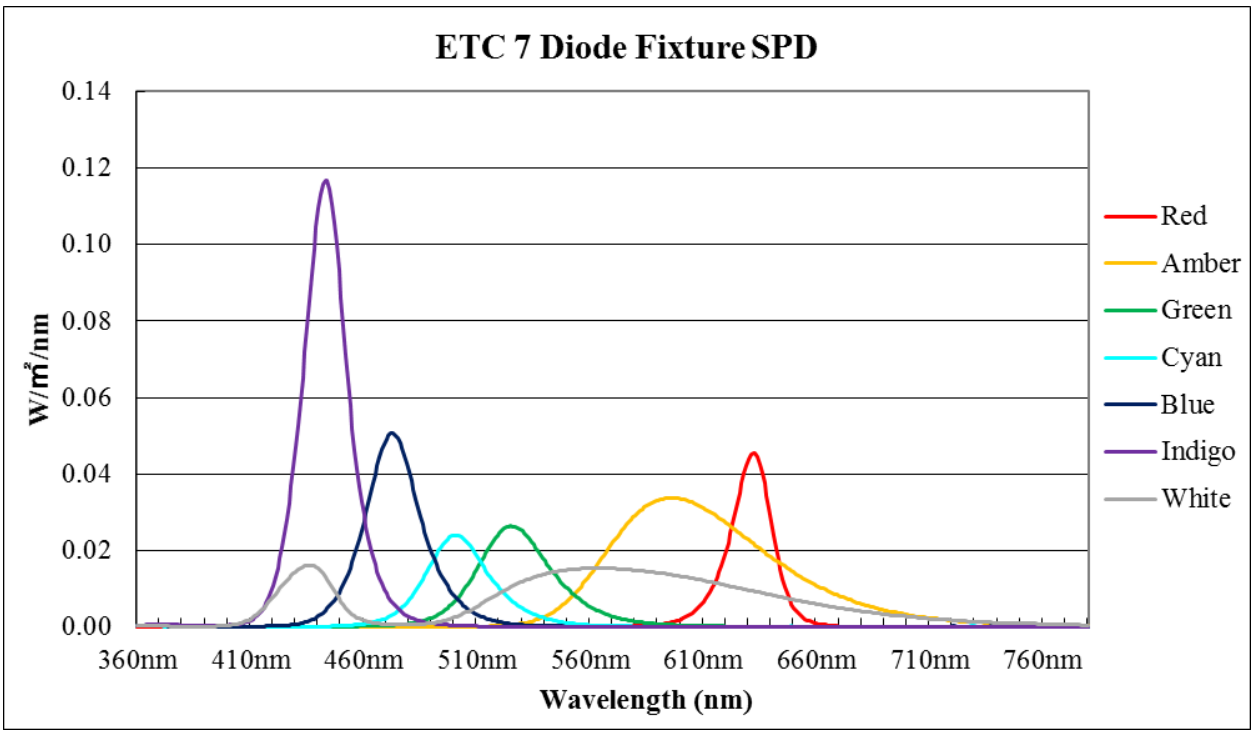

Figure 13: Measured SPD of ETC Source with 7 Diodes

Similar to the seven diode LED fixture, fluorescent lamps contain significant peaks in their spectrum as a result of the phosphors used in the technology. Therefore, a fluorescent spectrum was not ideal for this experiment.

Natural daylight contains all possible visible wavelengths, from the low blues into the deep reds. Fiber optics were considered as a potential source of daylight transmission to be used within the integrating sphere setup. After further consideration, it was determined that the most efficient energy transfer through fiber optics would come from a strong, directional source, which in this case would be the sun. This would require one end of the fiber optic to track the sun to provide a strong light source on the other end. However, the low blue wavelengths that were most desirable from this daylight strategy are attributed to the skylight from the atmosphere scattering light in the sky, rather than the direct sunlight

itself. Scattered light is extremely difficult to transmit through fiber optics, which typically requires a directional source. Additionally, daylight conditions may change rapidly, which would make it difficult to ensure consistent light output between trials. Therefore, a fiber optic daylight source was not ideal for this experiment due to the difficulty to utilize daylight in a controlled environment.

Xenon arc lamps are not commonly used in architectural lighting applications, but they may be found in other specialty applications. A true xenon source produces one of the most even energy distributions across the visible spectrum and has a CCT similar to daylight at 6000K (2). An example SPD of a true Xenon source is shown in Figure 14. Xenon was recommended as a broadband source for spectral measurements by the CIE (25).

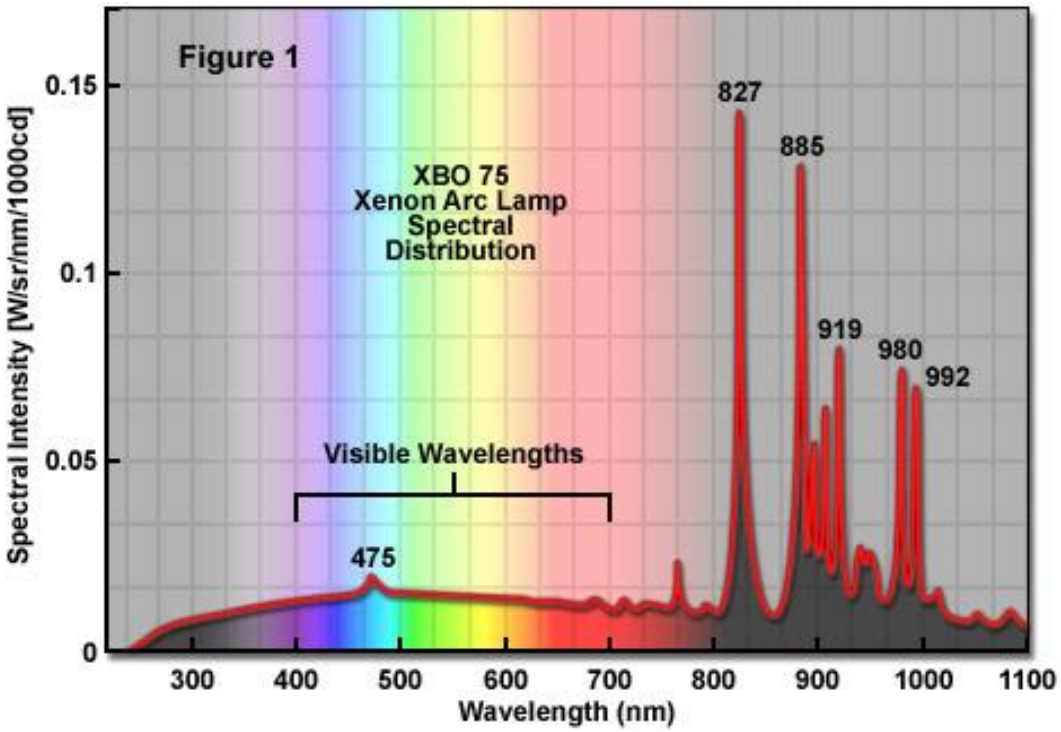

Figure 14: Typical Xenon Lamp Spectrum (38)

High-end automotive headlights are often referred to as xenon sources, so this was pursued as an option for this experiment. A Philips 35 Watt xenon HID lamp was selected as a potential source. This lamp was powered with the appropriate automotive ballast which converted a 12 V DC power input to an 85 V AC power output. The spectral content was then measured with the Konica Minolta CL-500A illuminance spectrophotometer. The lamp, as well as the resulting SPD, are shown in Figure 15 and Figure 16, respectively.

Figure 15: Philips 35 Watt Xenon HID Automotive Headlight

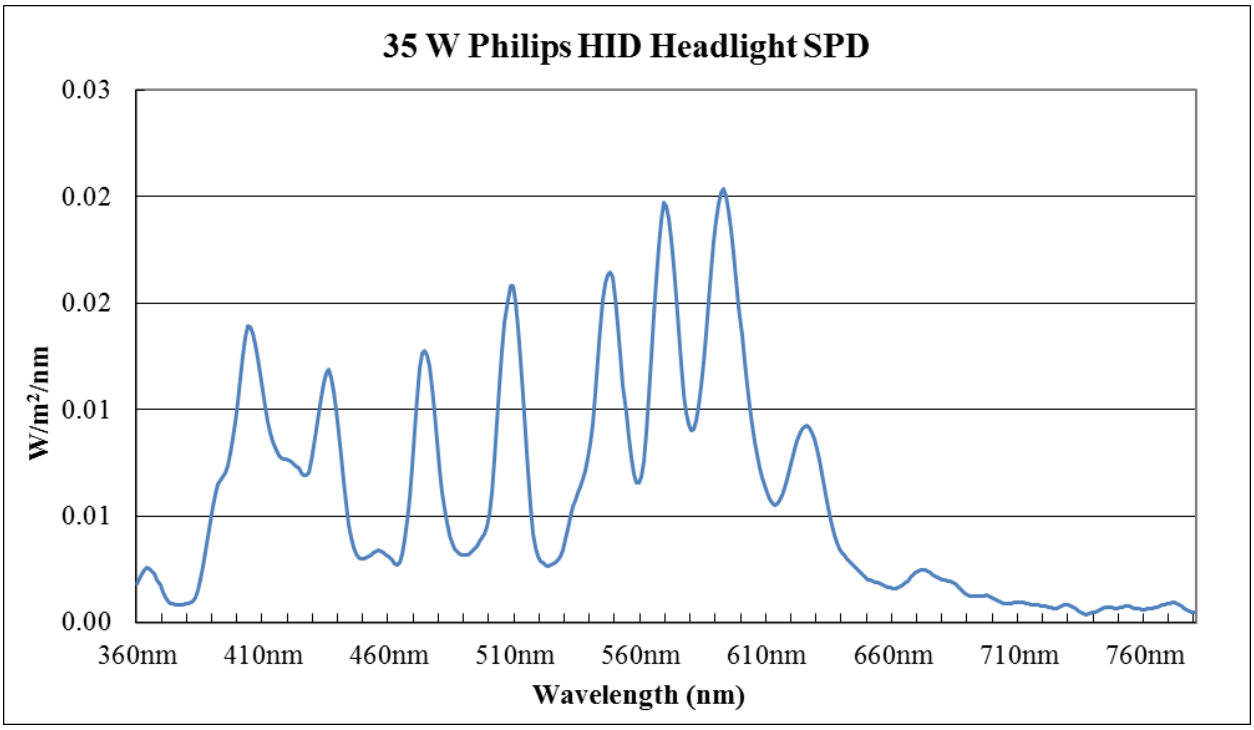

Figure 16: Measured SPD of Philips 35 Watt Xenon HID Automotive Headlight

It is apparent from the measured SPD that this lamp is not a pure xenon arc source because of the many drastic spikes throughout the visible spectrum. Further research explained that while many headlights are referred to as xenon sources, they are actually modified metal halide lamps. High pressure xenon is sometimes used instead of the traditional argon gas to produce some initial light output while the metal halide warms up (39). The immediate light output provided by the xenon or argon component is important in automotive applications for safety reasons, but the gas is only in use for a matter of seconds. Therefore, the stable output of xenon HID headlights is comparable to a metal halide source rather than a true xenon arc source.

Another common application of xenon arc lamps is in projectors. The spectrum of a Canon LV-7265 projector was measured with the illuminance spectrophotometer while a

blank white screen was projected. The resulting SPD is shown in Figure 17. Again, it is apparent that the source in this projector is not a true xenon arc lamp because of the large spikes in the distribution, as well as the lack of energy output in the low blue ranges of the visible spectrum. It turns out that while xenon arc lamps are used in some projectors, they are very expensive due to the rarity of xenon gas, so they are typically only used in very high quality projectors for special applications, such as IMAX movies. An image of a high wattage xenon lamp for IMAX projectors is shown in Figure 18 (40).

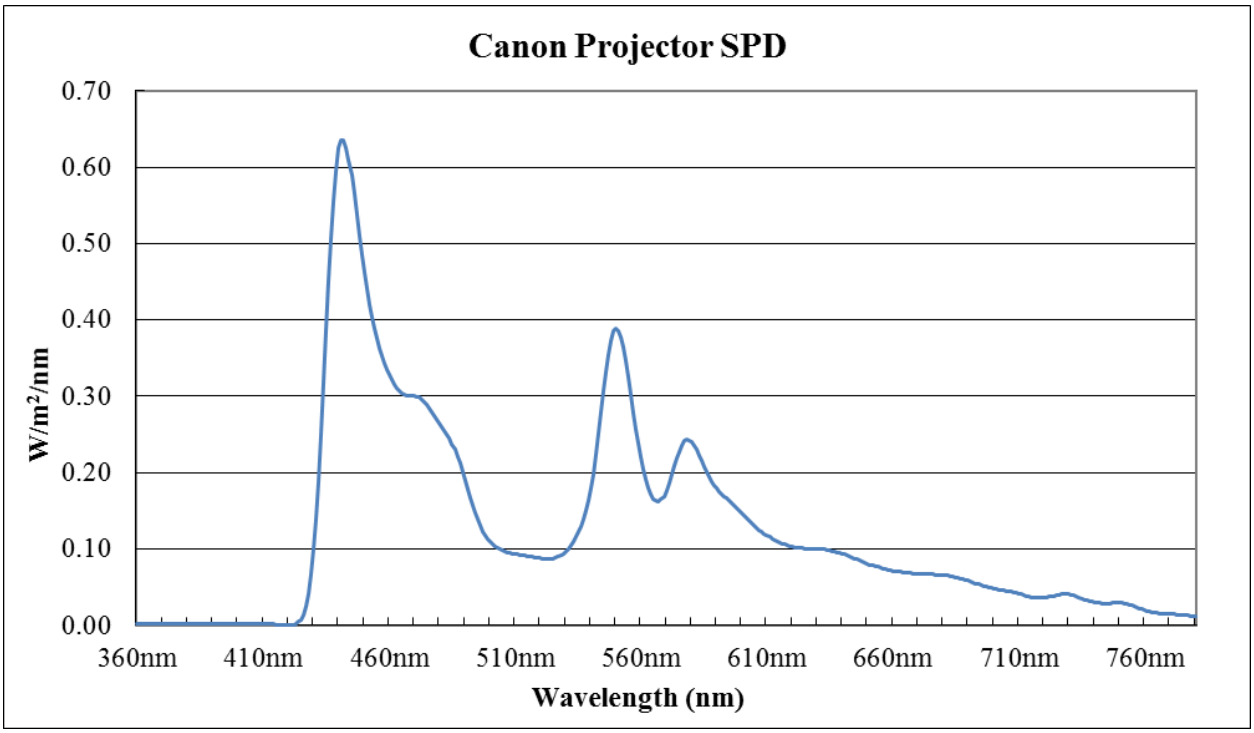

Figure 17: Measured SPD of Canon LV-7265 Projector

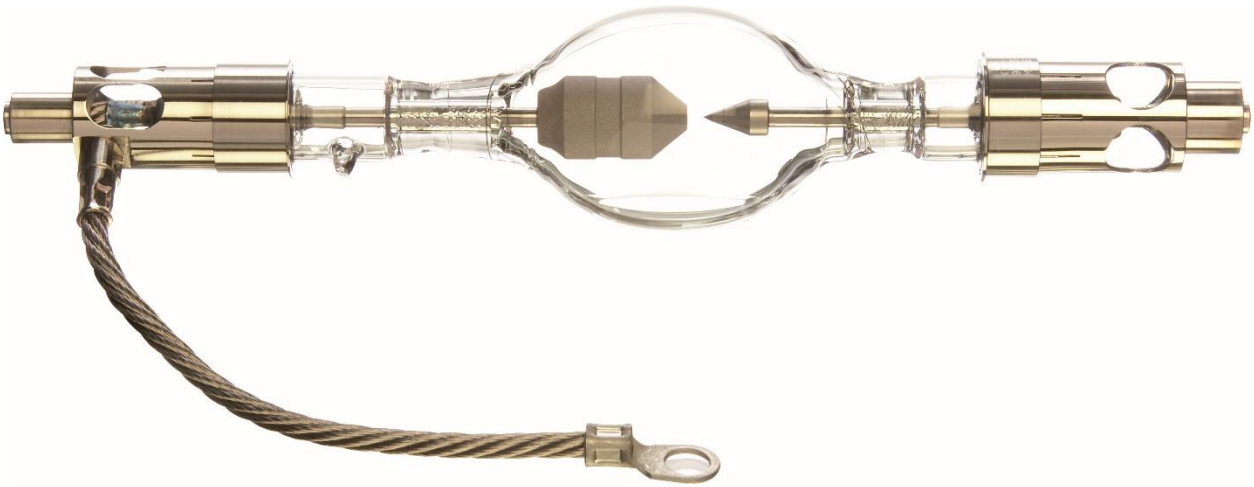

Figure 18: Xenon Arc Lamp for IMAX Movie Projectors

Independent xenon arc lamps intended solely for research were also considered. Upon initial inquiries with a reputable manufacturer, it was clear that only purchasing the lamp and no additional equipment for sockets, power supply, and enclosure was not recommended due to the dangers of handling arc lamps and the potential of them exploding. The entire system of equipment for operating one of these lamps would be recommended for future color research; however, the system was cost prohibitive for the lighting department at this time. As a frame of reference, a "plug and play" xenon light source assembly as shown in Figure 19 was quoted at roughly $7,000 (41).

Figure 19: Xenon Arc Lamp System for Research (41)

Two additional options recommended by the CIE for spectral responsivity measurements were the use of lasers or a monochromator (25). Availability of either the many lasers required to sufficiently cover the visible range, or a single broadband laser, proved to be very limited in selection or documentation, and thus not attainable at this time. Monochromators are an all-inclusive machine which is able to manipulate spectral output, bandwidth, stray light, and wavelength uncertainty for reproducibility of results (25). These machines may be either manual or automatic in operation, and require a broadband source such as xenon to be manipulated by means of a diffraction grating (41). Further explanation of this technology may be found online by the Newport Corporation (41). While a monochromator could easily achieve the light output and control desired for this experiment, it was found to also be cost prohibitive for this project. Specific equipment considered was quoted to roughly cost between $16,000 and $18,000 depending on the light source (41). An example of a Xenon source with monochromator is shown in Figure 20.

Figure 20: Monochromator with Xenon Source (41)

A light source that was initially considered and kept in mind while considering other possible options for this experiment was a traditional tungsten filament source such as incandescent. Incandescent sources emit their energy in a constant, gradual increase from minimal levels in the ultraviolet region to high levels in the infrared. Many modifications have been made to incandescent sources in the past century with various functionality improvements in mind. The tungsten halogen (TH) lamp was first created in 1958 as a way to improve the lifespan of incandescent lamps (2). TH lamps follow a similar spectral distribution pattern to incandescent lamps, but with a decrease in output towards the infrared end of the spectrum. Benefits of a TH lamp compared to a traditional incandescent

include a wider range of available correlated color temperatures (CCT), and approximately 30% higher luminous efficacy (2). There exist many shape and base options which could be utilized in the integrating spheres already created, and most models are affordable and readily available. High quality versions of TH lamps are available from manufacturers that also produce xenon arc lamps and monchromators for research; however, the cost of these sources is hundreds of times greater than the price of most common TH lamps. The additional cost was deemed unnecessary for the level of accuracy desired from this experiment.

A source with high lumen output was important because having a sufficient quantity of light throughout the spectrum was a concern. Low output may cause poor signal to noise ratios, which would affect the accuracy of the measurements. However, the intense heat given off by TH sources was the limiting factor due to the maximum thermal capacity of the small integrating sphere and acrylic lens. A 50 Watt, 12 V DC Philips tungsten halogen lamp with bi-pin base and a spectral output as shown in Figure 21 was chosen for initial testing of the 12 filters. However, this did not end up producing sufficient intensity for certain filters to meet the minimum illuminance of 5.0 lux for the CL-500A with saturated color sources.

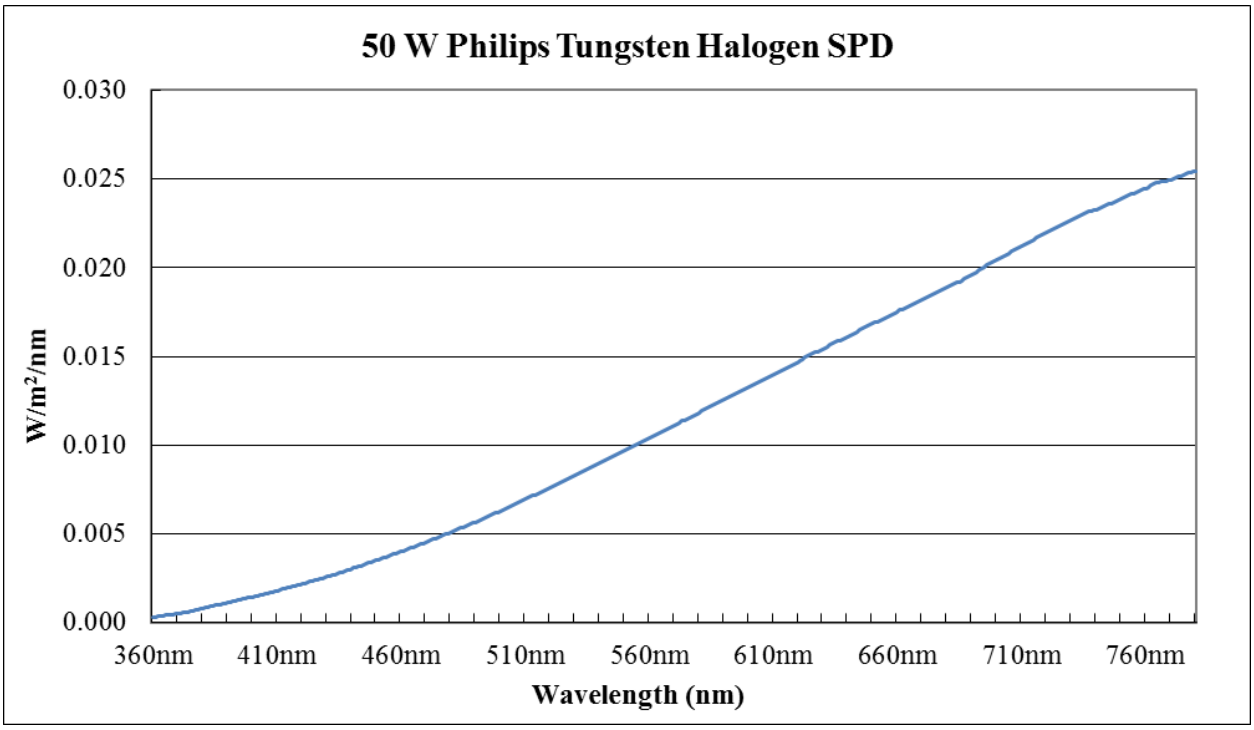

Figure 21: Measured SPD of 50 Watt Tungsten Halogen Lamp

A 75 Watt, 12 V DC TH lamp was also tested with the filters which did not exceed the thermal capacity of the integrating sphere. The SPD of this lamp is shown in Figure 22.

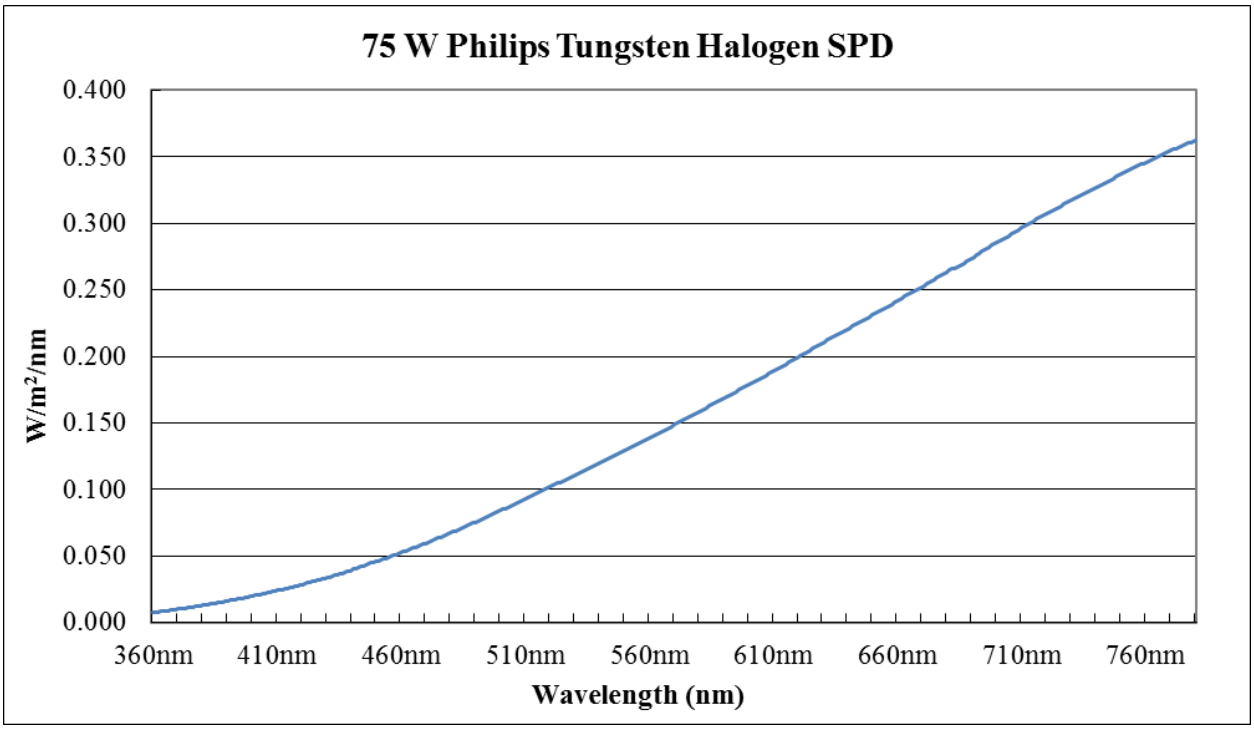

Figure 22: Measured SPD of 75 Watt Tungsten Halogen Lamp

Unfortunately, this source did not produce enough energy for the blue filters to be measured with the CL-500A either. At this point using a higher wattage TH source was a concern because of the heat and the severity of wattage increase that would be required to improve the blue filter readings. The tungsten halogen source was abandoned at this point in favor of another potential light source.

A high intensity, white LED was considered because of its high output in the blue end of the visible spectrum. While the LED did contain peaks within the visible spectrum due to the inherent nature of blue pumped LEDs, the SPD of this source included significant energy at all relevant wavelengths as shown in Figure 23.

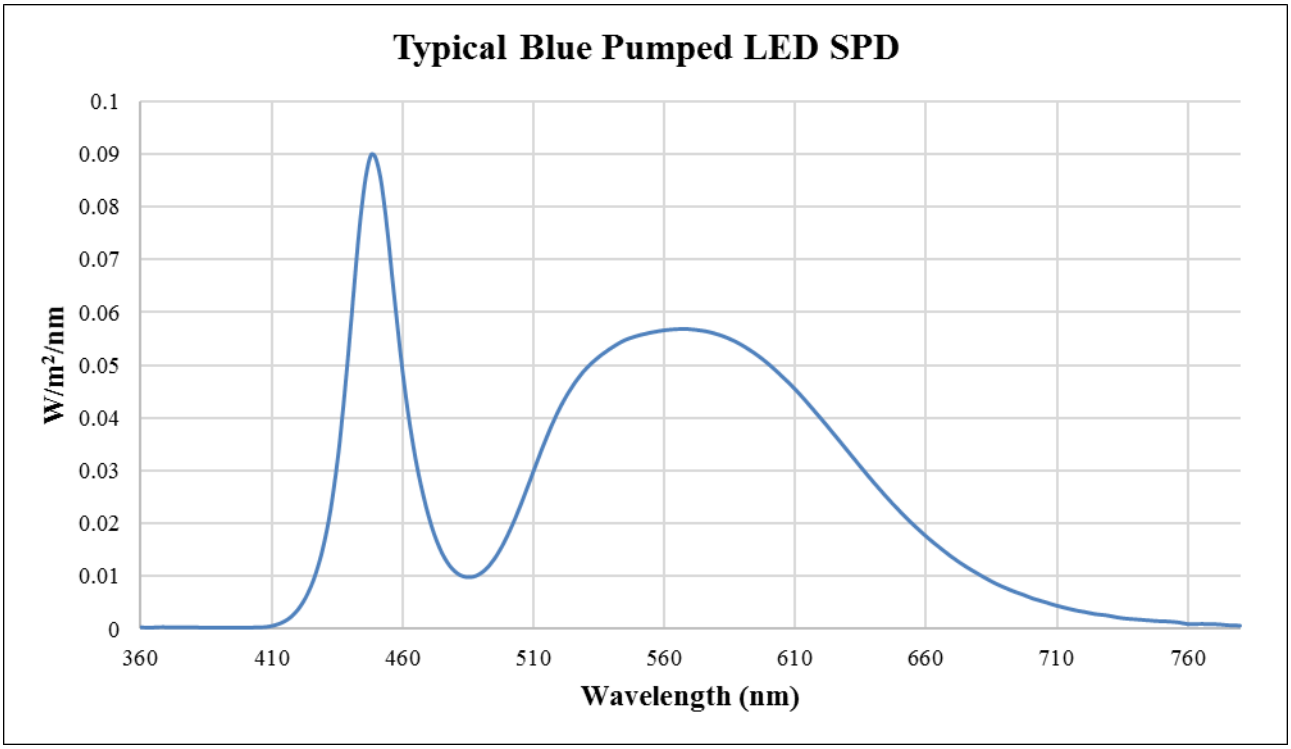

Figure 23: Cool White COB LED Spectrum

The lumen output of this particular chip on board (COB) module was more than 10 times that of the 75 Watt TH lamp, and the heat was controlled via a large heat sink with integral cooling fan. It was determined that the SPD did not need to be smooth as long as sufficient energy was produced at all measured wavelengths within the visible spectrum. Therefore, the chosen source type for this experiment was a Cree XLamp CXA2590 LED array shown in Figure 24. The heat sink with integral cooling fan is shown in Figure 25.

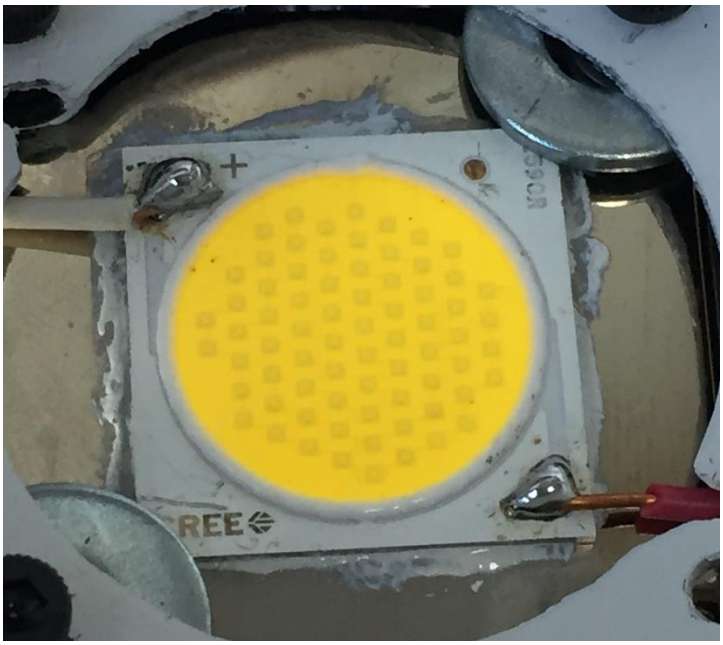

Figure 24: Cree XLamp CXA2590 LED Array

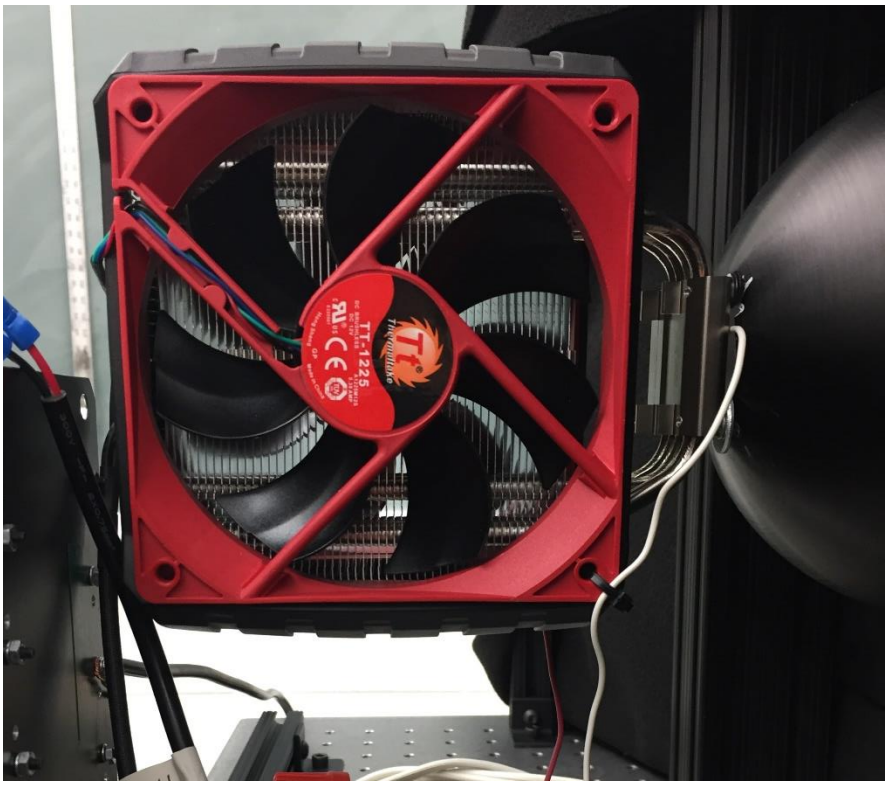

Figure 25: Heat Sink and Fan by Thermaltake

The LED was controlled directly by a Lambda DC power supply that allows the user explicit control of the current and voltage. This array was run at a current of 1.7 A, and a voltage of 72 V. The fan attached to the heat sink operates at 12 V DC, and was powered via a line voltage to low voltage transformer mounted to a metal plate behind the sphere.

3.1.5 Narrow Bandwidth Filters

Filters were used with the LED source to isolate the visible spectrum into narrow bandwidths of radiant energy. Initial spectral data for each filter was provided by the manufacturer, Mega-9, during the selection process, but was later verified through measurements taken with the Konica Minolta CL-500A illuminance spectrophotometer. The distributions provided by Mega-9 were relatively square in shape, which was desirable because the visible spectrum could be broken into small bands while reducing the possibility of missing important data in large gaps between peak wavelengths. It was decided to use a selection of filters with some wavelength overlap so that no parts of the spectrum were overlooked. Small wavelength bands were desired for a thorough evaluation across the visible spectrum. The choice was made to use all 20 to 30 nm full width at half maximum (FWHM) filters, with the exception of one 45 nm FWHM filter for the 555 nm center wavelength filter. The FWHM is defined as 50% of the transmittance on either side of the center wavelength (42). The center wavelength is not necessarily the peak transmission wavelength for every filter. While the filters allow light to pass through at a range of wavelengths, these filters will simply be referred to by their central wavelength for the remainder of this paper. Twelve filters were selected with center wavelengths ranging from 410 nm to 735 nm. Remembering that the FWHM bandwidth extends past these center wavelengths on either side, the extent of the spectrum tested was from 395 nm to

approximately 747 nm. A small region of wavelengths in the far extremes of both ends of the visible spectrum were not measured; however, the typical human sensitivity to these wavelengths as defined by the V(λ) curve is extremely low. The slightly reduced extent of the visible spectrum measured through the selected filter range was deemed acceptable for the purpose of this experiment. Filters came in two different sizes, 12.7 mm and 25.4 mm, depending on availability at the time of purchase. A lens holder for the largest diameter was constructed out of plastic with an insert that could hold the smaller diameter filters as well. This was desired to ensure that the placement of the filters over the acrylic lens would remain consistent between each trial and to block any uncovered acrylic. An image of this holder attached to the sphere over the acrylic lens is shown in Figure 26.

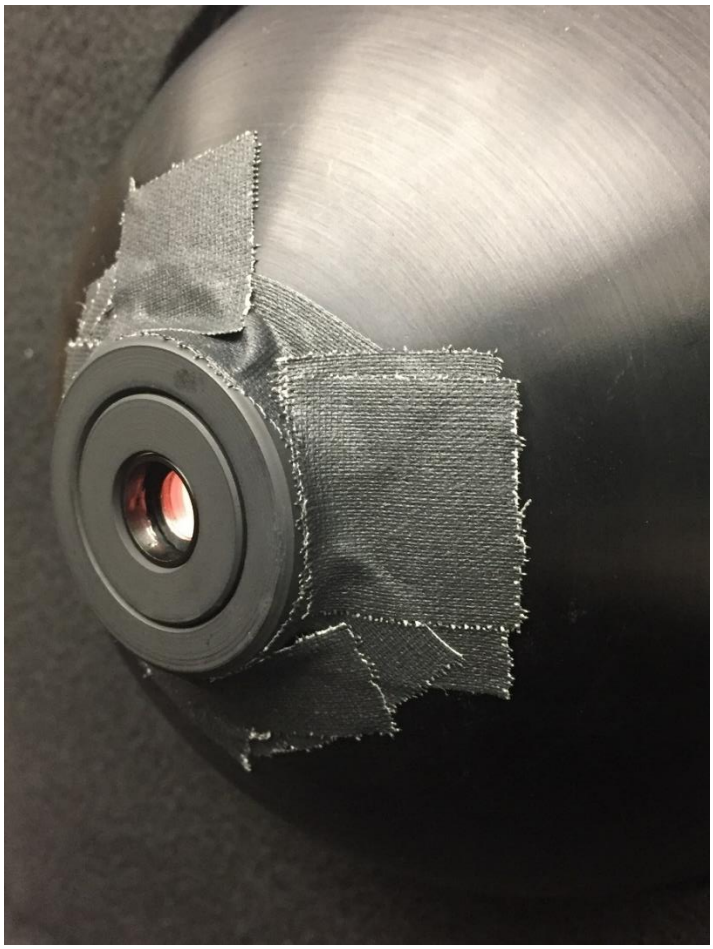

Figure 26: Filter Holder Attached to Integrating Sphere with Small Diameter Filter

Initial images of the filters exposed some imperfections in the black filters holders that allowed small amounts of unfiltered light through. A cover matched to the size of the filter aperture only was cut out of matte black chalkboard paper in both filter diameters and attached over the holder during all trials with gaffer tape. The smaller cover may be seen in Figure 27.

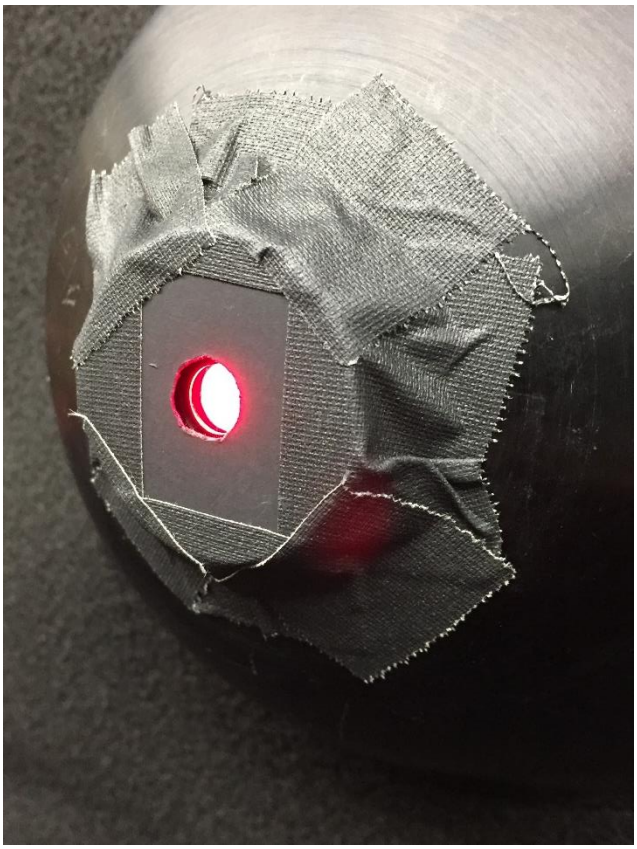

Figure 27: Small Chalkboard Cover to Block View of Filter Imperfections

Specifications of all 12 filters are given in

Table 2. A spectral power distribution which includes all of the filters on one chart covering the visible spectrum with data from Mega-9 is shown in Figure 28.

Table 2: Filter Specifications

Center Wavelength	FWHM (nm)	Diameter (mm)
410 nm	30	12.7
435 nm	30	25.4
465 nm	25	12.7
495 nm	30	25.4
525 nm	30	25.4
555 nm	45	25.4
585 nm	20	25.4
615 nm	30	25.4
645 nm	30	12.7
675 nm	30	12.7
705 nm	30	25.4
735 nm	25	25.4

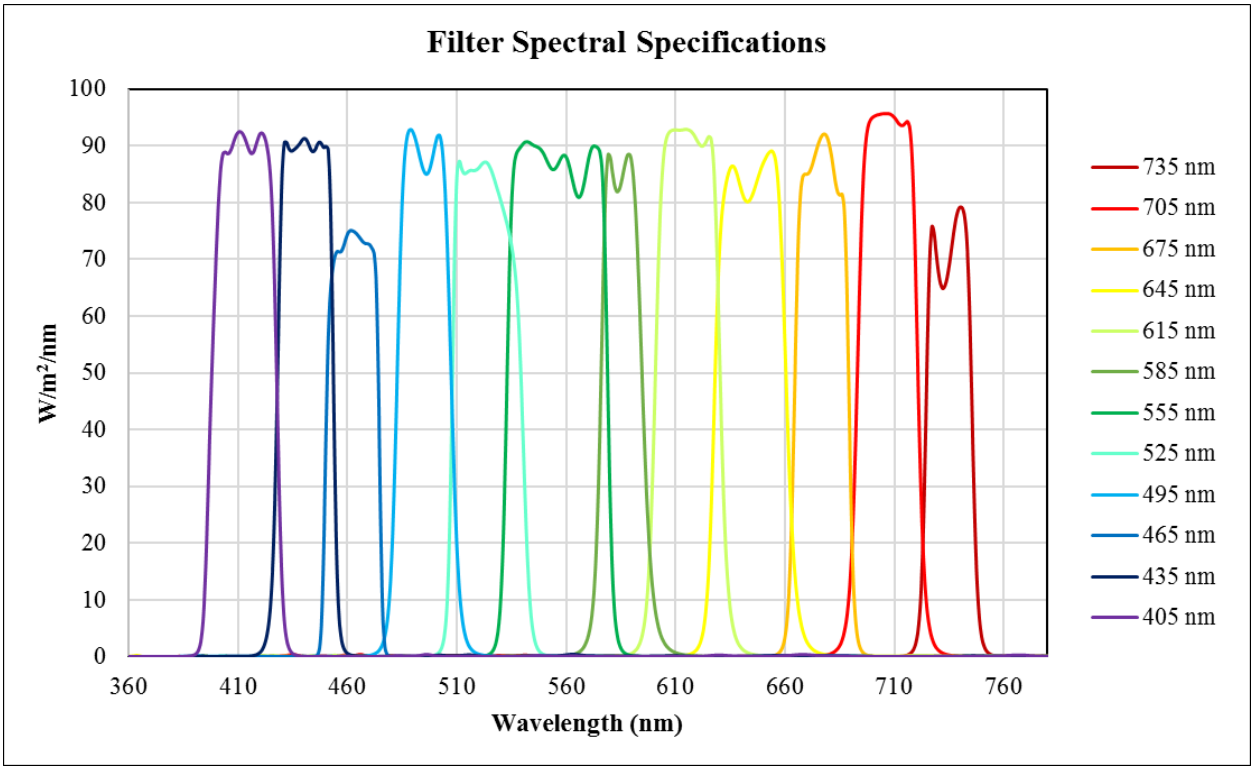

Figure 28: SPDs of All 12 Filters from Mega-9

3.2 Luminance Calculation Methodology

3.2.1 Calculating Luminance from Illuminance at Multiple Distances

Luminance is not dependent on distance, but rather on the intensity over projected area as shown in the following equation.

$$L \equiv \frac{d^2\phi}{dAd\omega\cos\theta}$$

This equation is illustrated in Figure 29 where dA is the luminous source, and the axis origin is the receiver. The solid angle is shown as $d\omega$, the angle of incidence of the light to the receiver is θ.

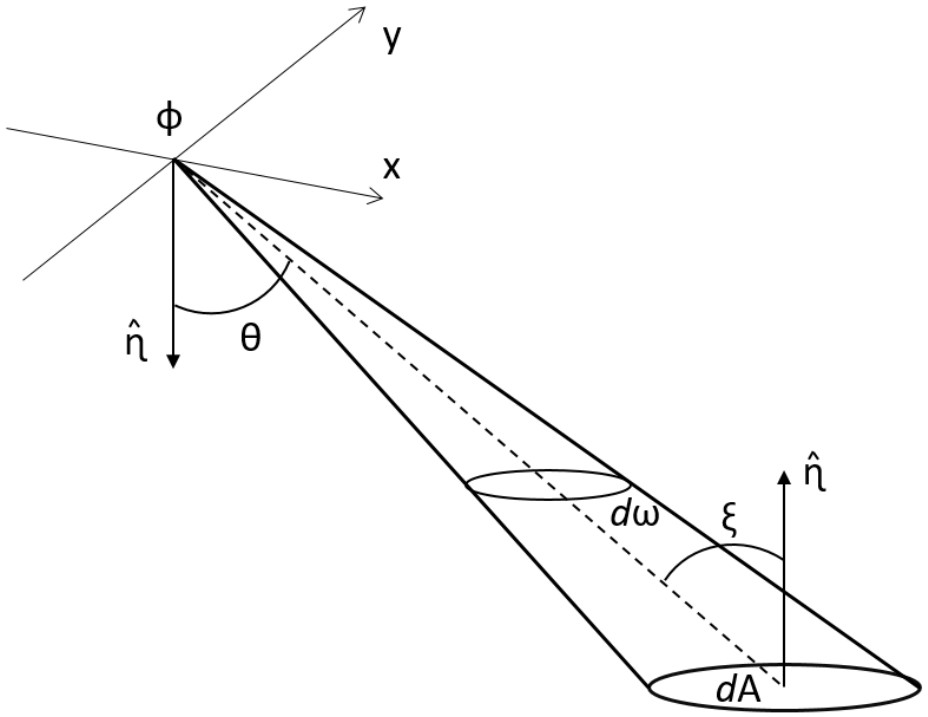

Figure 29: Luminance Definition Diagram

Furthermore, illuminance measurements with a corresponding distance may result in a calculated luminance value. Illuminance is related to luminance with a known solid angle and angle of incidence as shown by the following equation.

$$L = \frac{dE}{d\omega \cos \xi}$$

The illuminance spectrophotometer sensor (receiver) was normal to the light source in all measurements. For this experiment, it was assumed that the luminance across the filter was uniform. This assumption will not alter any results because both the illuminance and luminance measurements were taken as an average from the entire light emitting area, thus the exact luminance at each point is irrelevant. Since the source and receiver surfaces were parallel, ξ was equal to θ in this case. In the luminance equation above, E was a

measured constant, L was a calculated constant, and dω was expanded to its spherical coordinates form as shown below.

$$d\omega = \sin\theta \, d\theta \, d\varphi$$

Taking the denominator of the luminance equation for all incoming incident angles resulted in the following integral,

$$\int_{\varphi=0}^{2\pi} \int_{\theta=0}^{\Theta} \sin\theta \cos\theta \, d\theta \, d\varphi$$

where the upper bound Θ was the half angle of the right angle cone as shown in Figure 30.

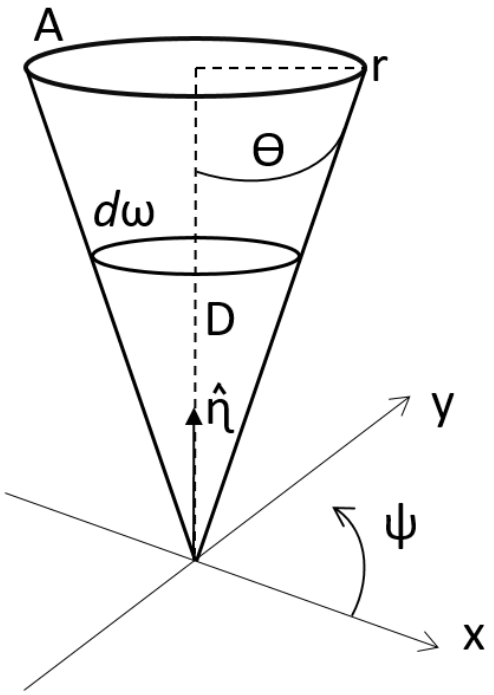

Figure 30: Luminance Definition with a Right Angle Cone

The resulting luminance calculation is shown below,

$$L = \frac{E}{\pi(1 - cos^2\Theta)}$$

which may be simplified with trigonometric identities to the following, final luminance equation.

$$L = \frac{E}{\pi sin^2\Theta}$$

The half-angle of the right angle cone was calculated with distance measurements as follows,

$$\theta = \tan^{-1}\frac{d}{2D}$$

where d was the diameter of the source area, and D was the distance between the source and receiver. The solid angle is often simplified for far-field scenarios to the area of the source, divided by the squared distance between the source and receiver. In this experiment, approximately half of the measurements were taken in the near-field. Which is to say they were taken at a distance of less than five times the largest dimension of the source. Therefore, a large portion of the measurements were taken in the near-field, so the calculations should not use the simplified form of the solid angle. The measurements classified as far-field will still be correct with this calculation because it is based on the true definition of solid angle, rather than simplifying assumptions which do not work for all scenarios in this experiment.

An average illuminance from three trials with the CL-500A was taken at each location, as well as an average distance from the filter lens to the sensor head for each of the seven measurement positions. These values, along with the filter diameter, were used to calculate luminance for each filter at each position, both before and after luminance measurements and images were taken. While the illuminance and distance changed for each trial, the calculated luminance of each filter was expected to stay the same as it is a

characteristic of the source itself, and is therefore independent of distance. These calculated luminance values from each position were averaged to become one final luminance.

3.2.2 Error Propagation Analysis of Calculated Luminance

The uncertainty involved with each measurement is known and may be used to calculate the total uncertainty that is involved with the luminance calculation. The specified error of the CL-500A meter is ±2% for illuminance values. A digital caliper was used for distance and diameter measurements, which is accurate to two decimal places. Therefore, the numerical accuracy of this device would be defined as ±0.005 mm. The maximum variation in multiple distance measurements lead to the conclusion that a larger uncertainty than ±0.005 mm was prevalent in most distance measurements. The uncertainty assumed for the distance between the illuminance spectrophotometer and source was ±0.25 mm. The maximum variation in measurements for the large and small filter diameters were different, which resulted in unique uncertainty values dependent on the filter size. Large filters were determined to have an uncertainty of ±0.25 mm, and ±0.10 mm was used for small filters. The final luminance equation to be evaluated with error propagation is shown below.

$$\bar{L} = \frac{\bar{E}}{\pi\left(\sin^2\left(\tan^{-1}\left(\frac{\bar{d}}{2\bar{D}}\right)\right)\right)}$$

The analysis of this error propagation was made very difficult by the presence of trigonometric functions, thus it was rewritten with the following identity.

$$sin^2\left(\tan^{-1}(x)\right) = \frac{x^2}{x^2+1}$$

The rewritten luminance calculation thus became the following equation.

$$L = \frac{E\left(\left(\frac{d}{2D}\right)^2 + 1\right)}{\pi\left(\frac{d}{2D}\right)^2}$$

The equation above was evaluated based on error analysis principles for quotients, products, and multiplying by exact numbers, such as Pi (43). The uncertainty was calculated as follows,

$$\delta L = \frac{\sqrt{\left(\frac{\left(\frac{\delta\bar{E}}{|\bar{E}|}\right)}{\sqrt{N_E}}\right)^2 + \left(\frac{2\left(\frac{\delta\bar{d}}{|\bar{d}|}\right)}{\sqrt{N_d}}\right)^2 + \left(\frac{2\left(\frac{\delta\bar{D}}{|\bar{D}|}\right)}{\sqrt{N_D}}\right)^2}}{\sqrt{N_L}}$$

where $\delta\bar{E}$ is the average illuminance uncertainty, $\delta\bar{d}$ is the average filter diameter measurement uncertainty, and $\delta\bar{D}$ is the uncertainty of the average distance between the sensor and the source. N represents the number of data values that were averaged for each measurement. This resulted in a maximum uncertainty of ±0.8% for all results of the illuminance to luminance calculation. The following results for luminance differences in the rest of this report should be considered with this ±0.8% uncertainty in mind.

3.3 Initial Testing of Source and Filter Characteristics

The integrating sphere with acrylic lens was mounted to an optical bench with the LED attached to the port on the opposite side of the acrylic. Black fabric was used to cover the optical bench to reduce any light reflections between the source and the meters as shown in Figure 31.

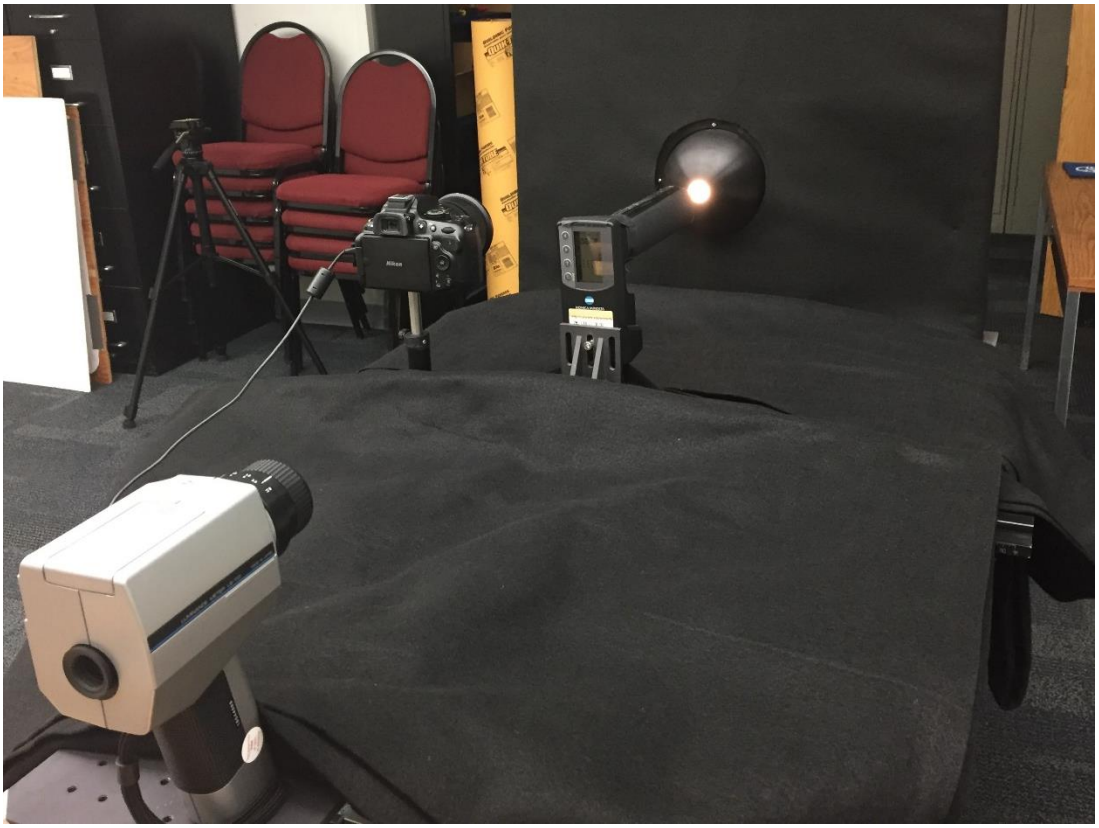

Figure 31: Integrating Sphere and Meter Setup on Optical Bench

All additional light sources in the room were turned off to ensure that no other sources of light would influence the measurements. It was assumed that the integrating sphere would trap any heat given off by the source which would change the output of the LED. To test this hypothesis, the luminance meter was setup directly normal to the acrylic lens and measurements were taken every 30 seconds after an initial warmup time of 15 minutes. The fan on the heat sink was running the entire time the source was in use. It was determined that luminance measurements had stabilized after 20 minutes, which was the minimum amount of time the sphere warmed up each time it was turned on for this experiment.

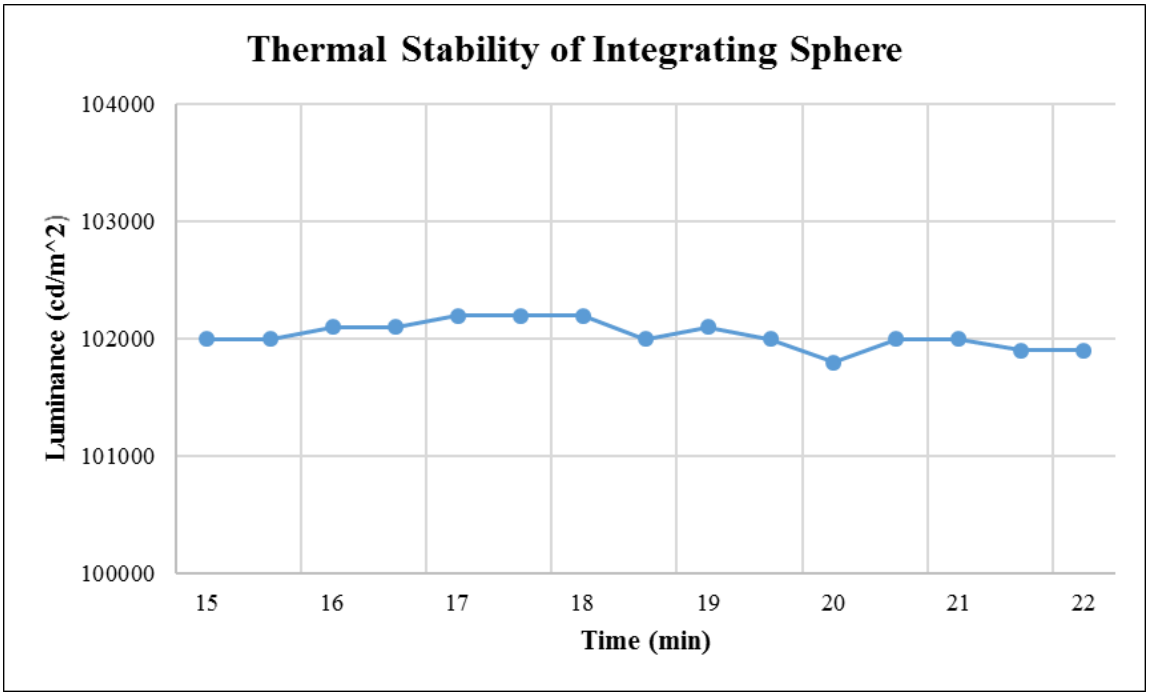

Figure 32: Thermal Stability of LED in Integrating Sphere

Another important characteristic of this setup to consider was the distribution of light from the acrylic lens of the sphere coupled with the filters. Tests were performed to investigate the uniformity and Lambertian nature of the acrylic, as well as both a large and small diameter filter. First, spatial uniformity was observed by taking luminance measurements at various locations of each surface. A diagram of the measurement locations for the acrylic and large filter, as well as a different pattern for the smaller filter are shown in Figure 33 and Figure 34 respectively.

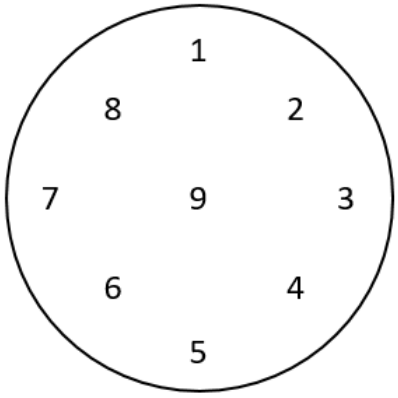

Figure 33: Uniformity Measurements of Acrylic and Large Filter

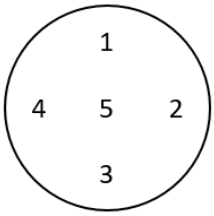

Figure 34: Uniformity Measurements of Small Filter

All luminance values for the acrylic were within a difference of 7.46%. The difference in luminance values of the large and small filters were 5.56% and 7.45%, respectively. These differences in value are small enough to classify the light output as uniform across the entire source.

The distribution was also tested to determine if the sphere source was Lambertian. If these characteristics of the source were true, luminance would remain the same when measured from different angles. This would provide some forgiveness in luminance measurements if the meter was not directly normal to the source. This was tested by first setting up the luminance meter normal to the acrylic lens, then marking out five degree intervals in each direction up to 30 degrees. These marks followed a straight line out from the initial measurement because luminance does not depend on distance, so the meter was

simply rotated to face the source. Luminance measurements from the acrylic condition are shown graphically in Figure 35. These results show that placing the meter within 30 degrees from normal to the acrylic lens source would result in a negligible difference in luminance.

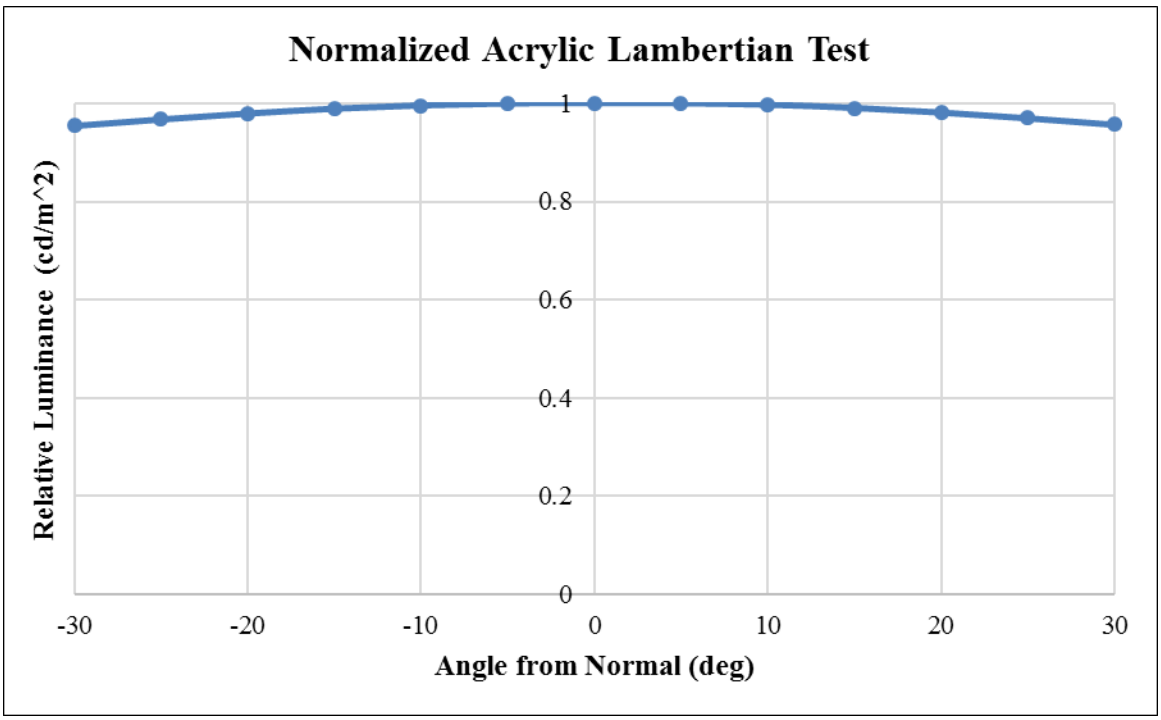

Figure 35: Luminance Versus Angle from Normal for Acrylic Lens

The same test was repeated with one large and one small radius filter over the acrylic to determine if the distribution characteristics would hold true after filtration of the source. When the filters were viewed from straight on versus off-axis, the color appearance changed. Following the change in visual appearance, the luminance values measured at each degree interval also changed drastically, as shown in the graphs of luminance values at each angle in Figure 36 and Figure 37.

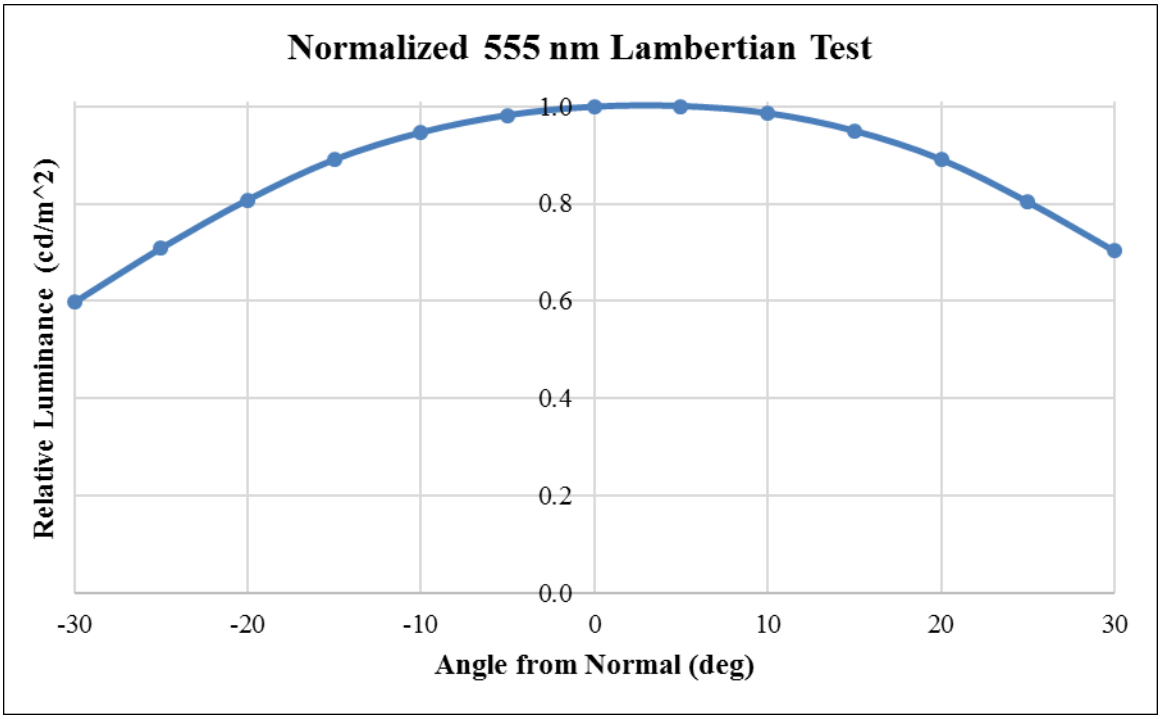

Figure 36: Luminance Versus Angle from Normal for Large Filter

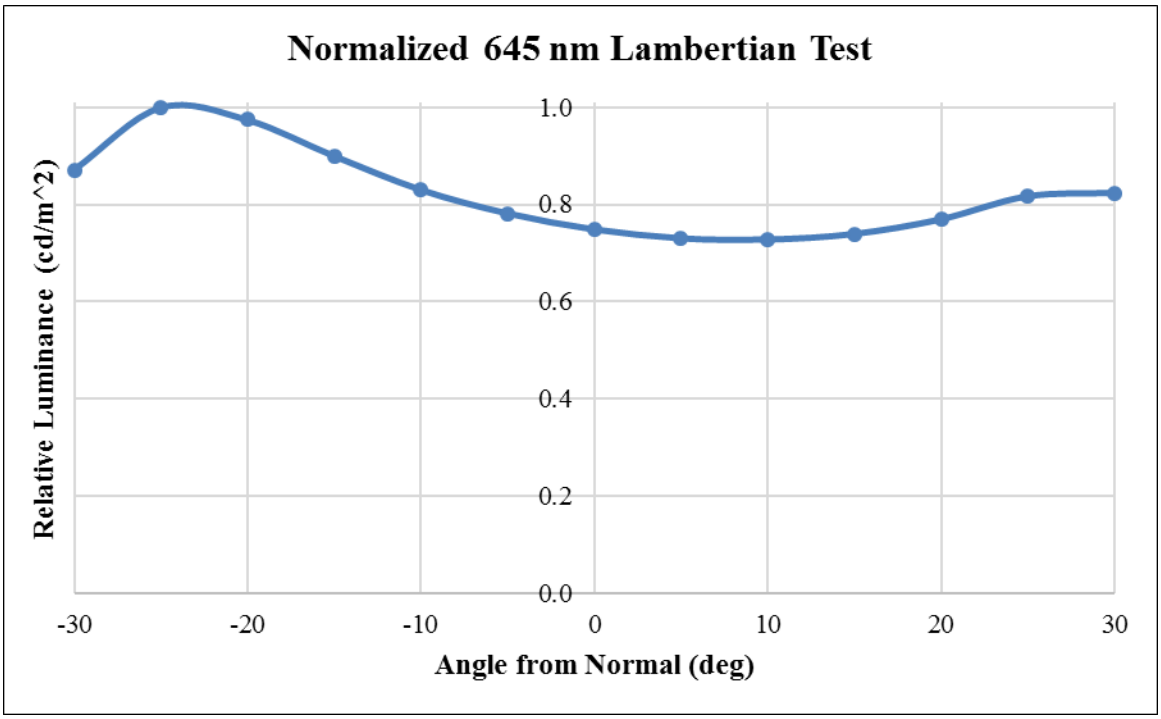

Figure 37: Luminance Versus Angle from Normal for Small Filter

The distribution testing was performed with the initial 50 Watt TH source and was not repeated with the LED for two reasons. First, if the acrylic surface was still uniform and homogeneous, as was confirmed with both the TH and LED sources, and the same acrylic was used for both sources, then the distribution should be the same. Secondly, the results did not demonstrate Lambertian characteristics for the filters. Therefore, this assumption of the source was not used to design the final experimental setup. Based on these results, it was determined that all measurements for this experiment should be taken from the same viewing angle which was normal to the source. This observation was crucial in designing the experimental setup with the narrow bandwidth filters.

3.4 Luminance Meter Measurement Experimental Setup

As previously noted, it was determined that all measurements needed to be taken from the same viewing angle of the source in order to produce consistent luminance results. However, luminance is not dependent on distance, as described in section 3.2.1. With a normal viewing angle and known distance between the source and illuminance spectrophotometer, the luminance may be calculated from an illuminance measurement and corresponding distance, as shown in the following equation

$$L = \frac{\bar{E}}{\pi\left(sin^2\left(arctan\left(\frac{r}{D}\right)\right)\right)}$$

where r is the radius of the light source, D is the distance between the source and receiver, and $\bar{E}$ is the average illuminance. These measurements are also illustrated in Figure 38.

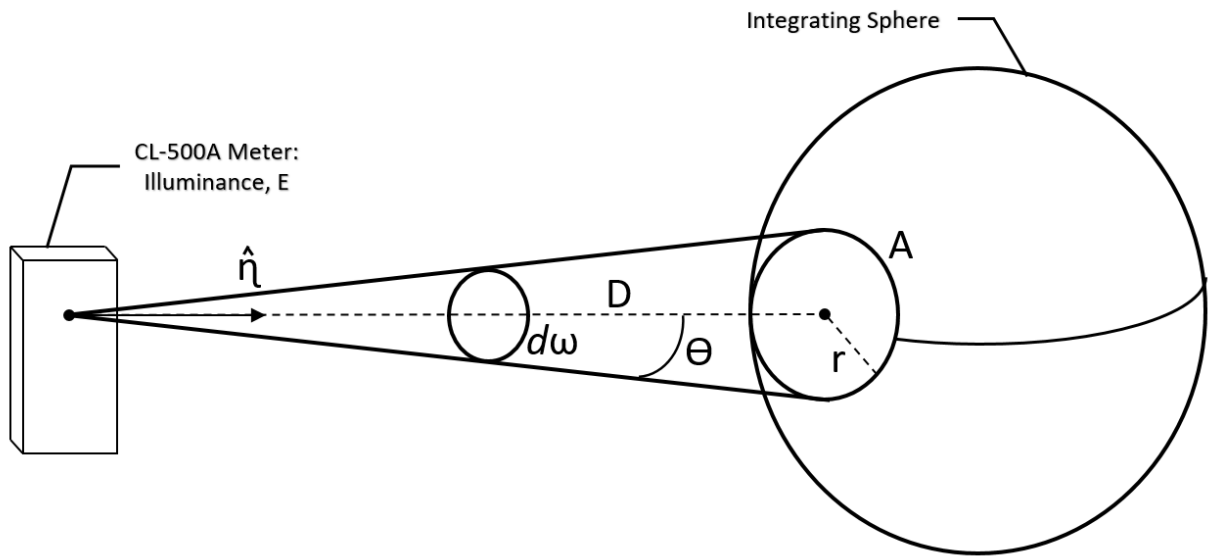

Figure 38: Luminance Calculation Diagram

The luminance meter was mounted on a tripod directly normal to the source. Without additional lenses, this meter has a minimum measuring distance of 1.014 m due to the properties of the focusing lens (22). The minimum distance was taken into account, and the luminance meter was located far enough away from the source so that the 1/3° viewing area encompassed almost all of the filter area. This view area is represented by a small black circle which is visible through the viewfinder. Since there were two filter diameters, there were two distance positions of the luminance meter. The intention behind including the majority of the filter area, rather than taking measurements of the filter center with the meter closer to the source, was to replicate the view of the source that the illuminance spectrophotometer would see. The focus of the luminance meter was reset at each distance position. While luminance does not depend on distance, it was observed during initial measurements that the luminance value measured by the LS-110 did in fact change when the focus changed. Therefore, careful attention was paid to the focus of the luminance

meter and the focal distance was checked against a distance from the source measurement whenever the position changed.

Two separate luminance measurement conditions were collected with the luminance meter for each trial, one without a CCF applied, and one with the corresponding CCF from Table 1 programed into the meter. Luminance measurements of the source were taken six times for each condition. First, the acrylic lens of the sphere was evaluated without any filters as the base case. Next, the filters were attached one at a time to the acrylic lens with the holder and cover as previously mentioned. The optical bench was covered in black felt and a black felt shroud was constructed around the sphere to block any light that may escape out of the back port of the integrating sphere as shown in Figure 40.

The CL-500A was required to be very close to the source for some filters in order to receive at least 5.0 lux for the saturated color data. However, the distance measurement was also important for calculations, and at short distances, any possible measurement error could have a dramatic effect on the luminance calculations later. Thus, it was decided that three illuminance measurements and two distance measurements for seven unique distances, both before and after LS-110 and camera measurements were taken, would help to reduce these potential sources of measurement error. The locations of the CL-500A were marked on the optical bench to maintain consistency between trials. Filters which provided relatively low illuminance values, versus those resulting in high illuminance, did not use all seven of the same distances. Certain low output filters needed to remain close to the source for all seven positions in order to maintain illuminance values over 5.0 lux. Higher output filters were able to both include more variation in distances, as well as utilize the baffle when far enough away from the source that it could fit between the meter and integrating

sphere. The baffle was not deemed necessary for measurements where the meter was very close to the source, as the sensor did not have a substantial view of the surrounding room. The illuminance spectrophotometer was mounted to a magnet that was able to be switched on and off to hold the position of the meter steady during measurements. The sensor head was normal to the light source for all measurements, and the meter was tethered to a computer to initiate data collection and record results. This setup is shown in Figure 39 and Figure 40.

Figure 39: Experimental Setup for Luminance Measurements

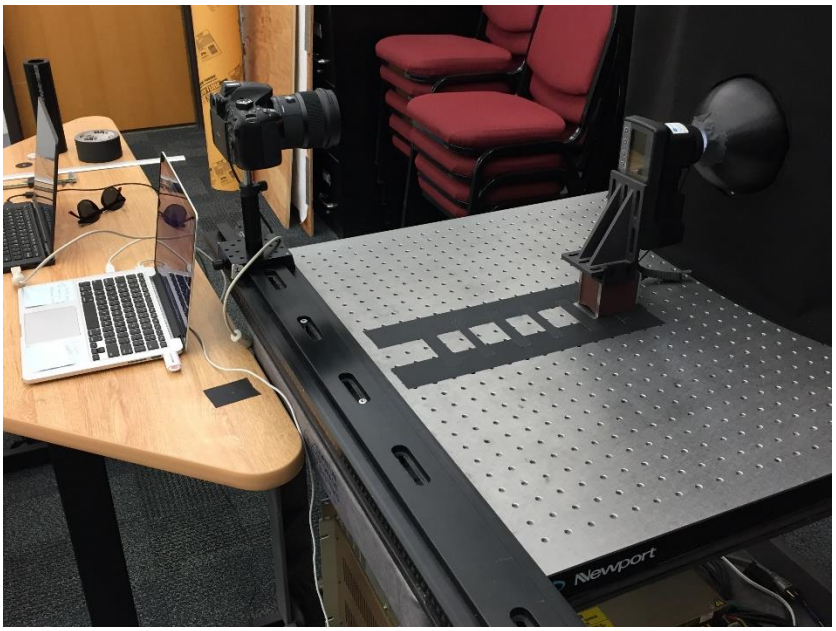

Figure 40: Experimental Setup for Illuminance and Spectral Measurements

3.5 Results and Analysis

3.5.1 Photometric Filter Response

Radiometric data at each wavelength was collected by the illuminance spectrophotometer for every filter and the acrylic condition. While the filters all produced a narrow spike in energy at their specified central wavelength, a few also included low amounts of energy at other parts in the visible spectrum. This was especially true for the 410 nm, 705 nm, and 735 nm filters. Further analysis was required to understand how significant of an effect this additional energy would have on the various measurements taken.

First, it is important to understand that the CL-500A multiplies the V(λ) photopic luminous efficiency function by the data points at each wavelength in order to transform

the radiometric information into photometric information. Reference the following equation of luminous flux for this transformation.

$$\phi \equiv 683 \int_0^{\infty} \phi_{e\lambda}(\lambda) v(\lambda)\, d\lambda$$

Then, all of the values within the visible spectrum are summed together in order to produce a single illuminance value. These illuminance values were crucial for the calculated luminance comparison to the luminance meter, which also accounts for the V(λ) function with all of its measured values.

Irradiance was plotted for a typical SPD of each source and filter combination, which means that the photopic efficiency of this energy was not yet considered. Graphs were produced of both solely the radiometric and photometric information from each filter, as well as both metrics on one chart. Since data was taken from various distances, which changes the irradiance and illuminance, an average of the data from the middle position was used for this part of the analysis. An example with the 705 nm filter is shown in Figure 41 - Figure 43 but the same information for filters can be found in the Appendix.

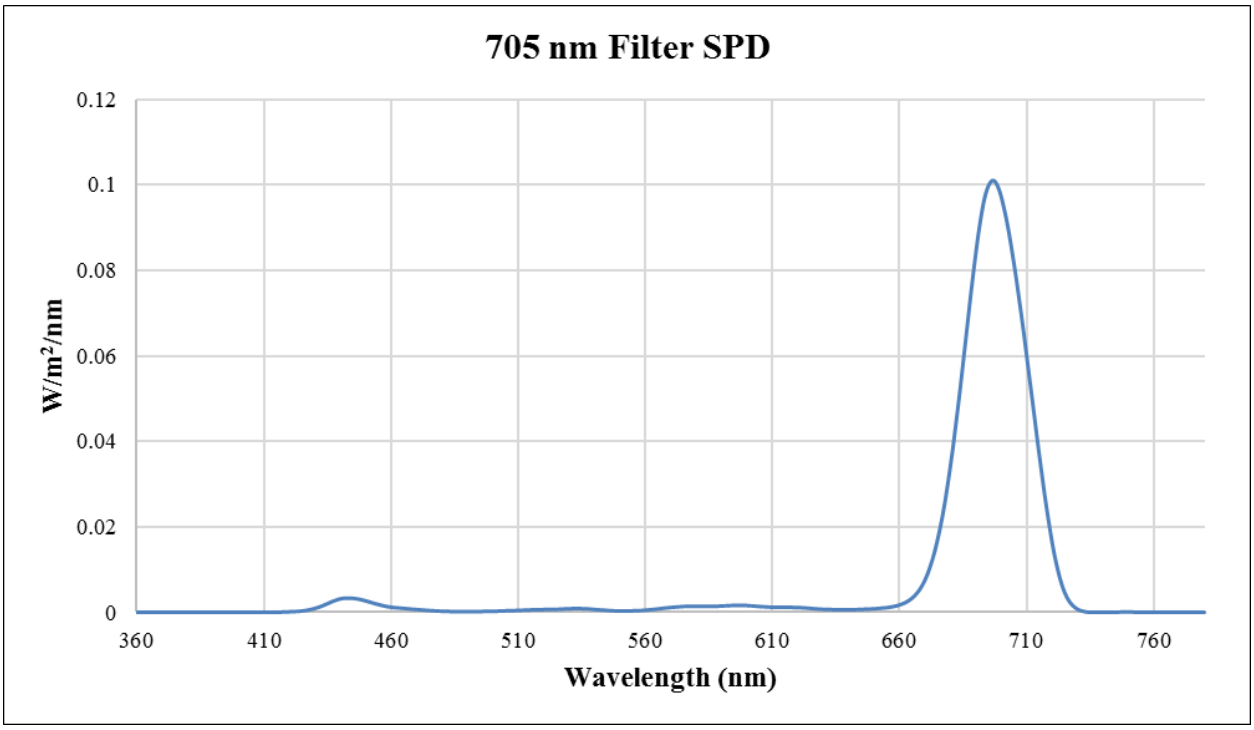

Figure 41: Irradiance of 705 nm Filter Throughout the Visible Spectrum

The radiometric SPD of the 705 nm filter shown in Figure 41 appears to have a large, narrow spike around 705 nm as would be expected, but a few small bumps are visible around 440 nm, as well as between 560 nm and 610 nm. These may seem insignificant in comparison to the larger spike; however, their location in the spectrum and their relationship to the V(λ) function are extremely important. When this information was converted to a photopic response, which has its peak sensitivity at 555 nm and decreases towards either end, the same initial measurements become those seen in Figure 42 below.

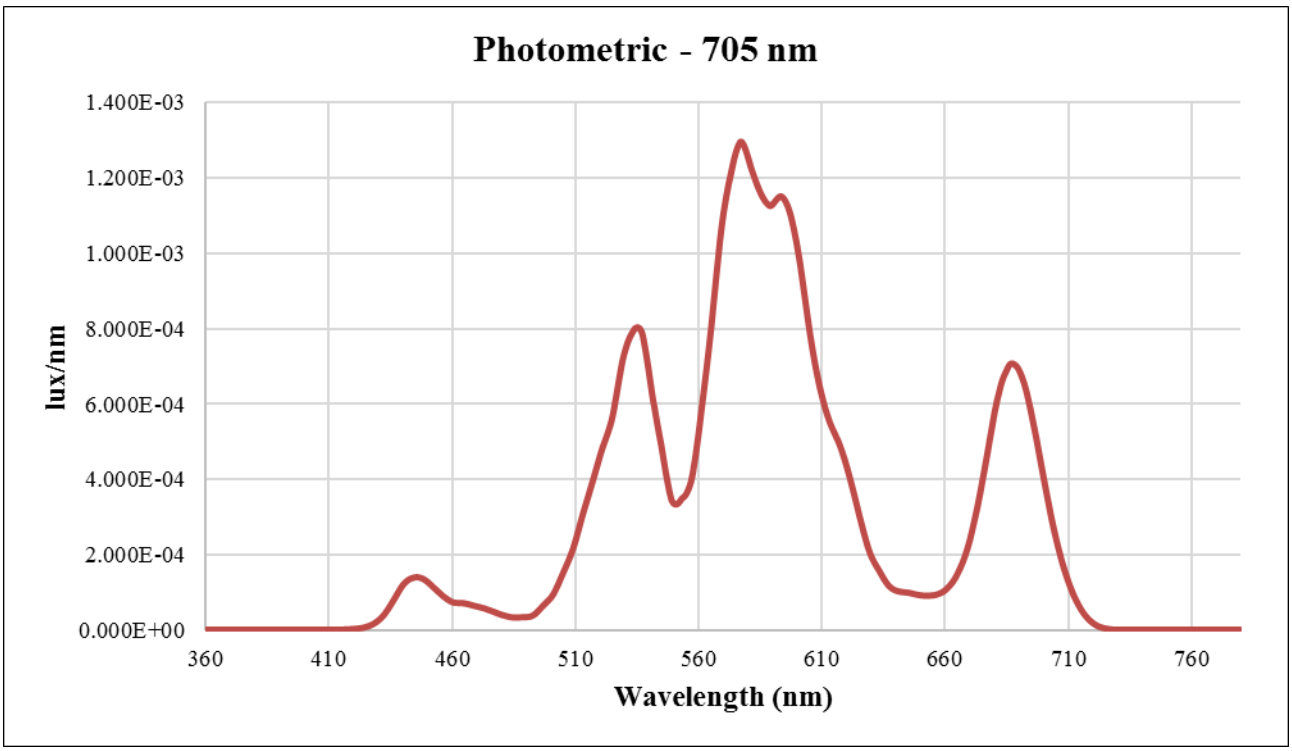

Figure 42: Illuminance Produced by LED Through 705 nm Filter at Each Wavelength

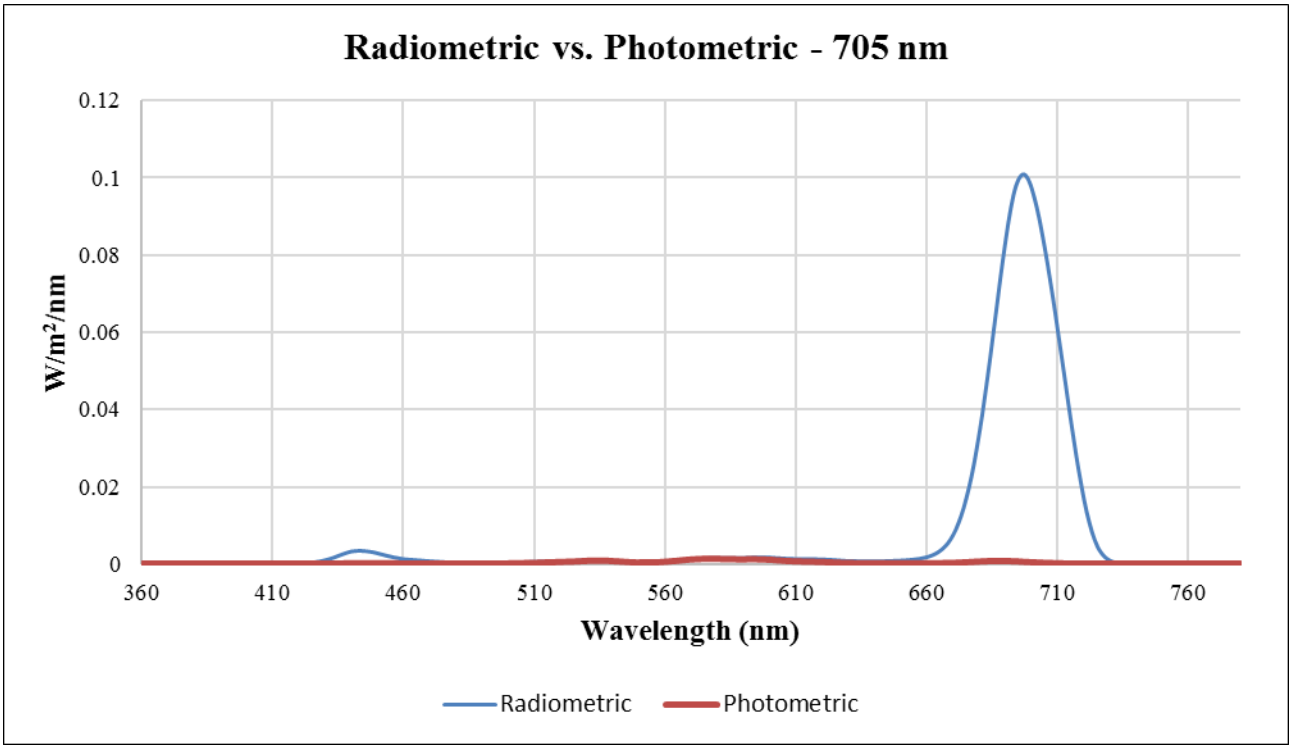

Figure 43: Radiometric and Photometric Data for 705 nm Filter

Clearly the small bumps, that seemed insignificant in the SPD, became very significant when the photopic response was taken into account. The large spike around 705 nm is still visible, but it is outweighed by the energy at the center wavelengths and other parts of the visible spectrum. As shown in Figure 43, the plot of both metrics on one chart illustrates how little of an impact the measured radiometric data has when V(λ) is applied. This realization was problematic for data from this filter because while the wavelengths of interest could be isolated in the data from the illuminance spectrophotometer, the same process would not be possible for the measurements from the luminance meter.

Upon analysis of all of the filters, it was determined that the 410 nm and 735 nm filters resulted in similar issues throughout the visible spectrum, as is shown in Figure 44 and Figure 45, respectively. As shown in Figure 45, the 735 nm filter also produced noticeable radiation in the center of the spectrum on the SPD, which appeared in testing with the LED source. However, this was not as apparent when initially tested with the tungsten halogen source, because less energy was being emitted at the central wavelengths.

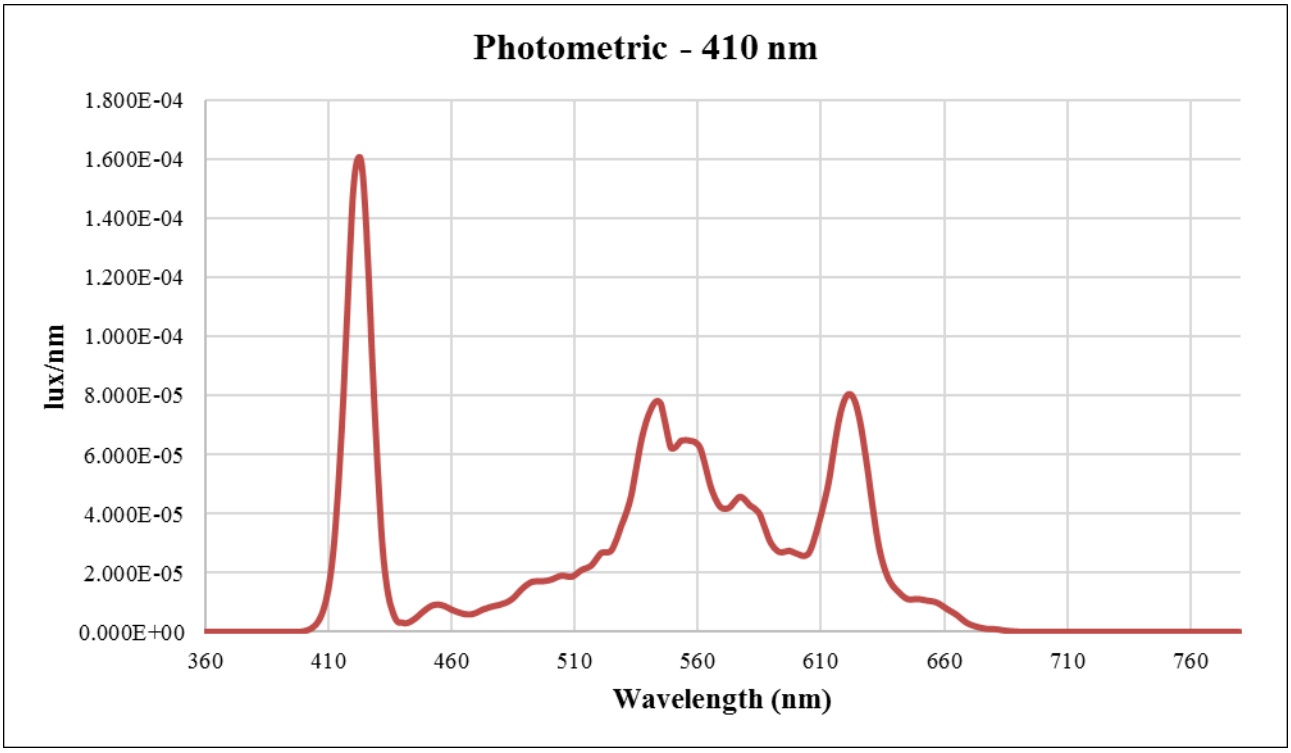

Figure 44: Illuminance Produced by LED Source with 410 nm Filter at Each Wavelength

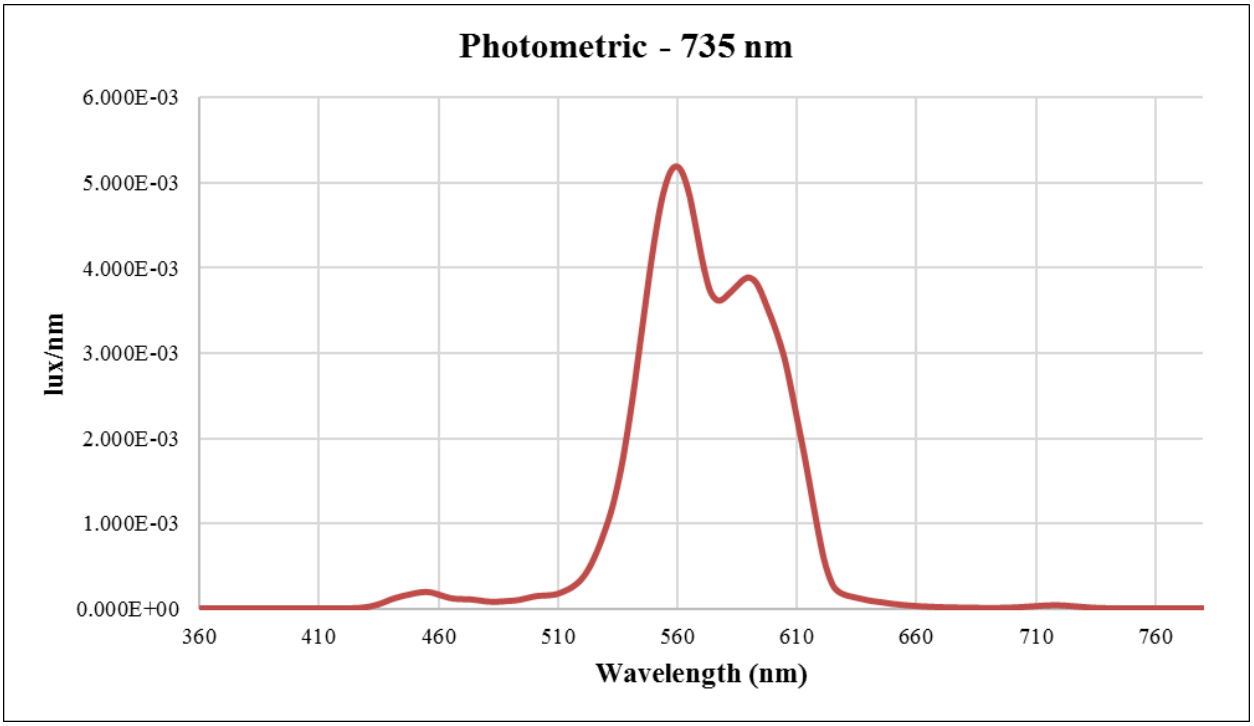

Figure 45: Illuminance Produced by LED Source with 735 nm Filter at Each Wavelength

The remaining nine filters produced more reliable photopic information that was not heavily influenced by minor transmission of light at other parts of the spectrum. However, as shown below in Figure 46, the 435 nm filter did result in one small bump around 555 nm. The light in this central part of the spectrum ended up to be approximately 30% of the light produced in the 435 nm spike. This filter was still considered in testing, but this potential source of error was kept in mind for the additional analysis.

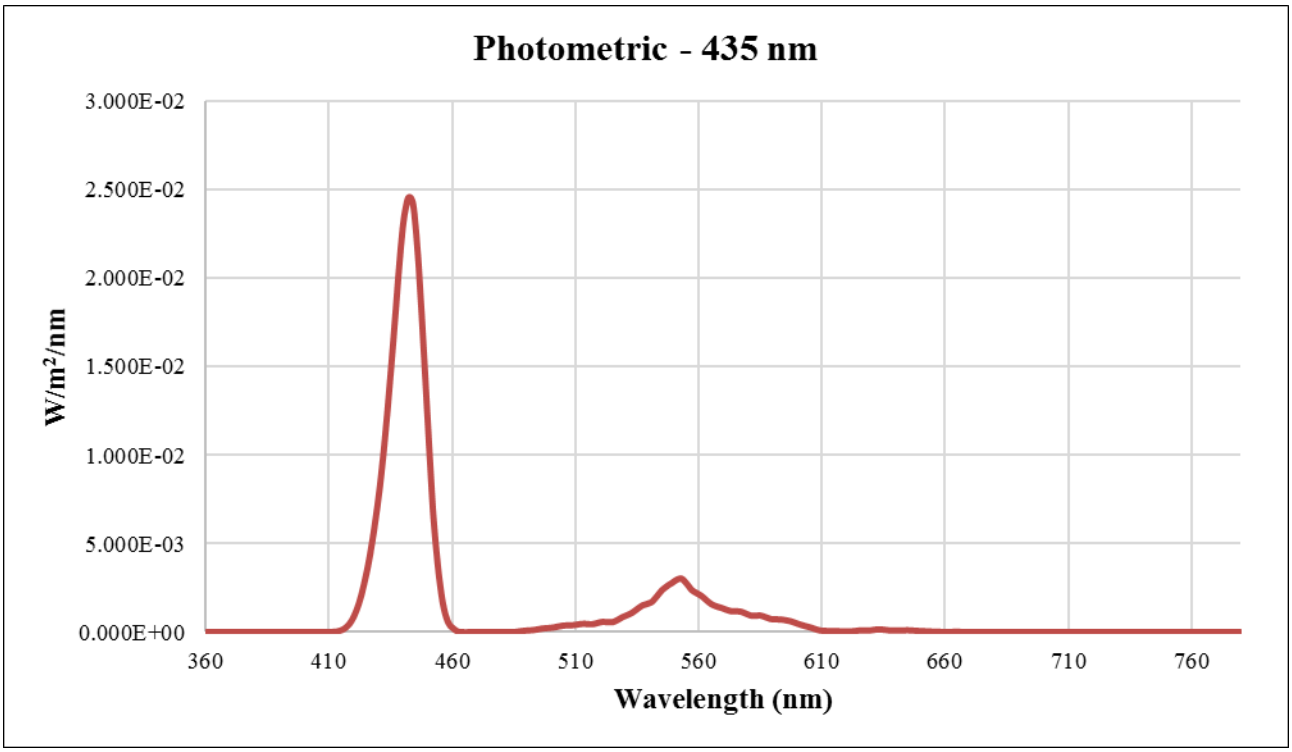

Figure 46: Illuminance Produced by LED with 435 nm Filter at Each Wavelength

The issue with the accuracy of some of the narrow bandwidth filters for this experiment, is likely due to the fact that photometric testing is only one of the many uses that this manufacturer supplies filters for including astronomy observation and biochemical analysis (42). If the photopic efficiency function did not need to be applied to the radiometric output of the filters, there would not have been an issue. However, in order to match the systems already in place by the other instruments in question, this step was

necessary. For future research with narrow bandwidth filters, the application of the action spectrum of interest is a crucial step to understanding the effectiveness of the filters.

3.5.2 Comparing Calculated Luminance to Measured Luminance

The calculated luminance from each position was statistically analyzed with quartile ranges and standard deviations. If any of the calculated luminance values for each condition fell outside of the first or third interquartile range, they were considered to be an outlier and were excluded in further calculations. Similarly, if any of the values were greater than two standard deviations away from the mean, they were also considered to be an outlier and excluded from the average luminance calculation. Only the 465 nm and 675 nm filters contained one outlier, which were excluded, while the acrylic condition contained two outliers, which were also excluded. An average of the valid trials for each filter and acrylic condition was calculated to compare with the LS-110 luminance meter results.

An example of the statistical analysis results for half of the 465 nm filter luminance calculations is shown in Table 3. The mean luminance value of this filter was 1389.8 cd/m^2, with a standard deviation of 7.7 cd/m^2. The first interquartile range was found to be 1385.7 cd/m^2, and the third was 1398.0 cd/m^2. Trial 6 was an outlier in this case because the luminance was greater than two standard deviations from the mean, and was outside of the first and third interquartile range. Thus, this trial was excluded from the average luminance calculation for this filter.

Table 3: 465 nm Filter Statistical Analysis Results

Trial	L (cd/m²)	Within 1σ?	Within 2σ?	Within 1st & 3rd Quartiles?
1	1395.4	Yes	Yes	Yes
2	1389.4	Yes	Yes	Yes
3	1400.6	No	Yes	Yes
4	1390.4	Yes	Yes	Yes
5	1382.1	No	Yes	Yes
6	1414.9	No	No	No
7	1380.7	No	Yes	Yes

The calculated luminance was compared to the average luminance measured by the LS-110 meter. A chart of the differences in values for each condition is shown in Figure 47.

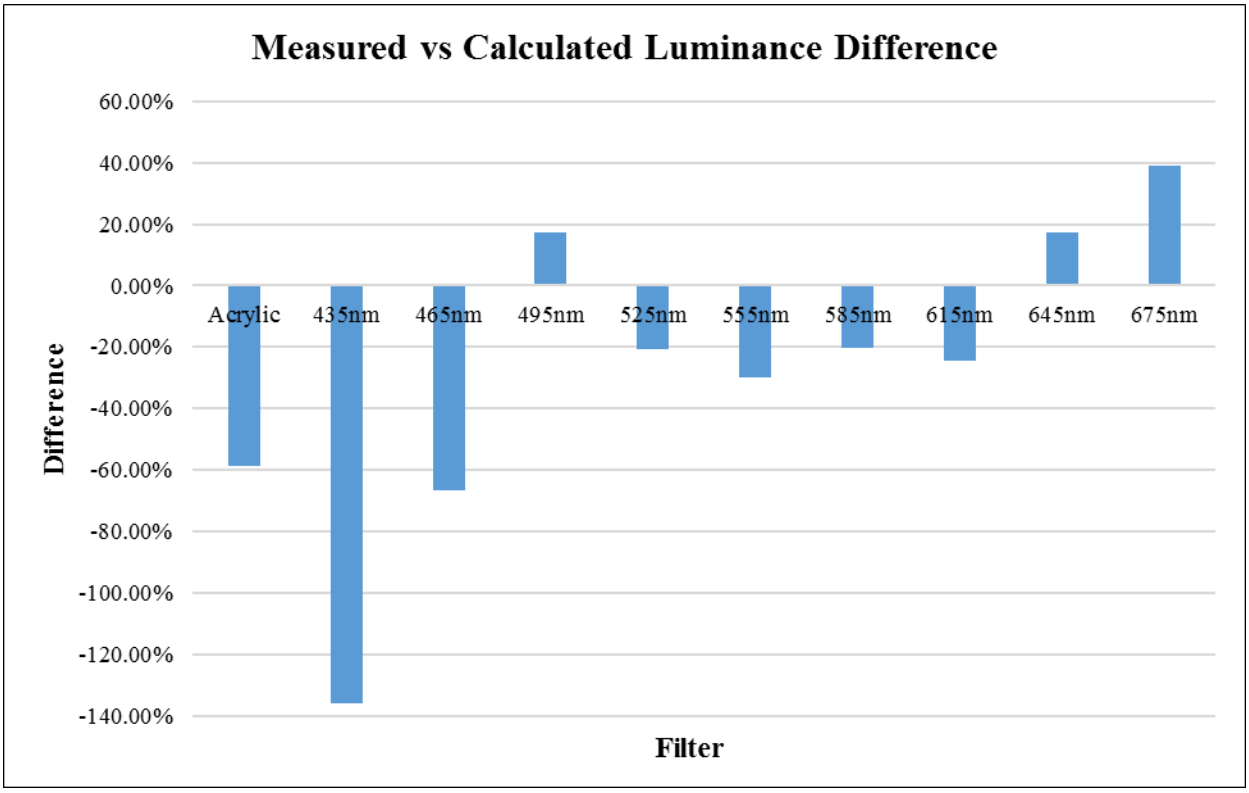

Figure 47: Difference Between Measured Luminance with LS-110 and Calculated Luminance

Negative percentages in the figure above signify that the calculated luminance was greater than the measured luminance. Conversely, positive results indicate that the measured luminance was greater than the calculated luminance for the 495 nm, 645 nm, and 675 nm filters. An absolute version of the same results is shown in Figure 48.

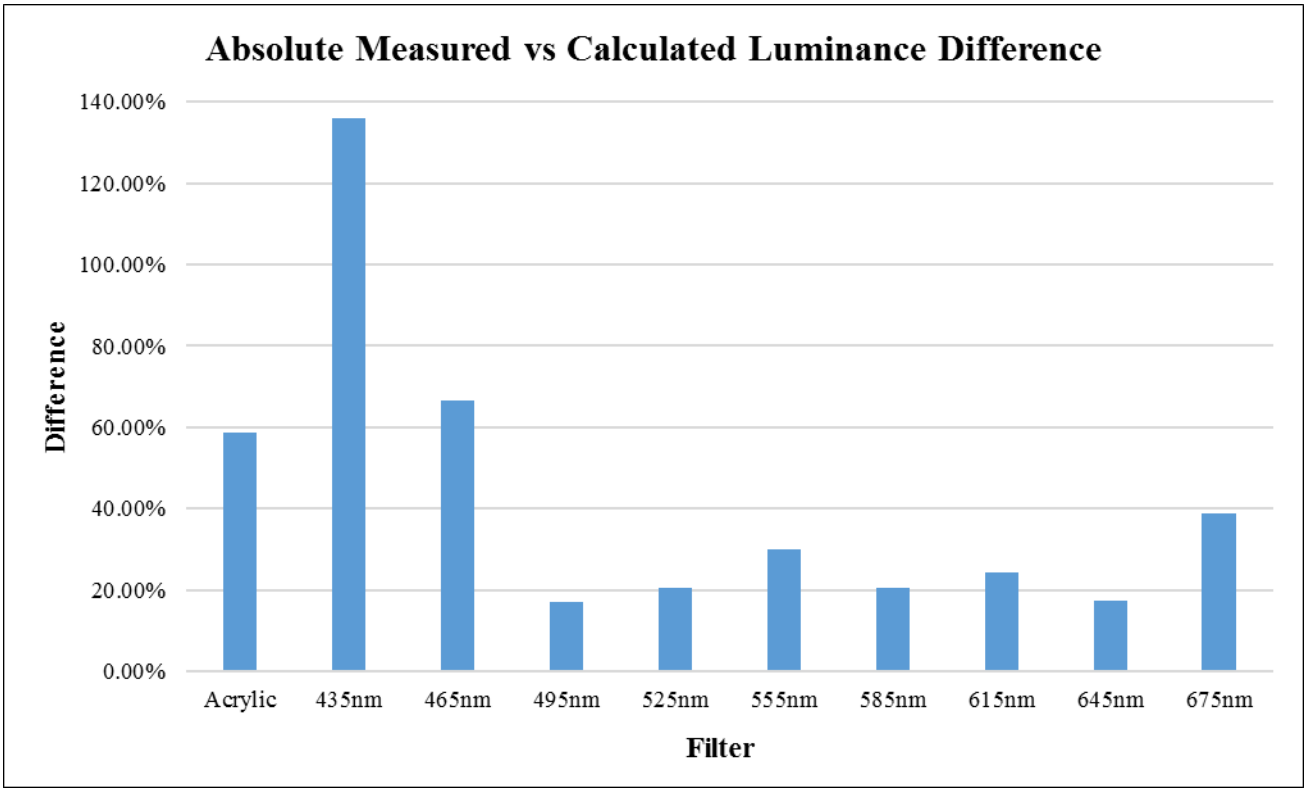

Figure 48: Absolute Difference Between Measured Luminance with LS-110 and Calculated Luminance

The accuracy of the luminance meter appears to be best in the green region of the spectrum, towards the peak of V(λ). The accuracy decreases towards the red and blue ends of the spectrum, where V(λ) converges to zero. A similar trend was predicted as the result of this experiment because it shows that the sensitivity of the meter is similar to the sensitivity of the human eye. This would be an ideal pattern for measurements pertaining to the human visual system. The expected minimum error would have occurred at 555 nm where the peak photopic sensitivity occurs. One possible explanation for the increased difference at 555 nm, compared to the neighboring 525 nm and 585 nm filters, is the relatively wide bandwidth of this central filter. The 555 nm filter was the only filter with a 45 nm FWHM, while the neighboring filters have 20 and 30 nm FWHM specifications, respectively. It is possible that the luminance difference for the 555 nm filter also included

some potential error from additional wavelengths accounted for in the neighboring filter as well.

Another potential explanation of these results comes from considering the spectral sensitivity response function provided by Konica Minolta in the specifications for the LS-110 meter.

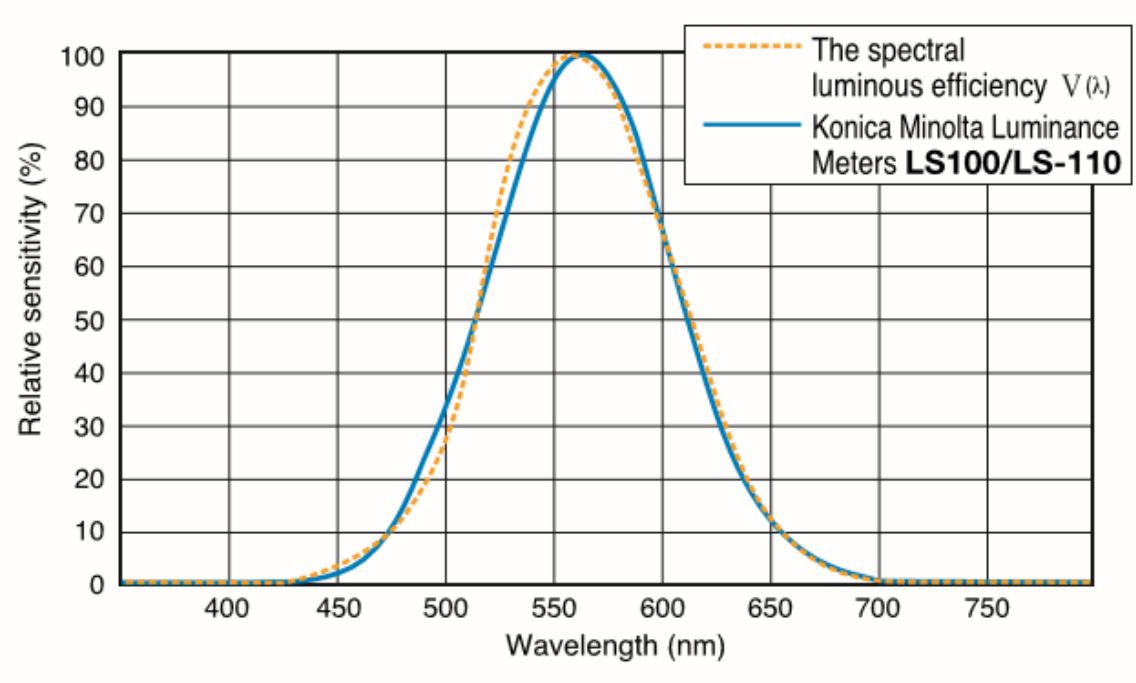

Figure 49: LS-110 Sensitivity Compared to V(λ) (23)

The blue curve in Figure 49 demonstrates the sensitivity of the LS-110 compared to V(λ), the dotted orange curve. This chart may be used to better understand the measured versus calculated luminance differences with both positive and negative percentages from back in Figure 47. The 495 nm filter resulted in a higher measured luminance than was calculated. This section of the LS-110 specification shows an overestimated response compared to V(λ) in this region while it dips below V(λ) in the adjacent areas where the calculated percentages were negative. The 645 nm and 675 nm filters also resulted in

positive differences like the 485 nm filter. Right around 645 nm the two curves appear to overlap, and just to the right of this point the LS-110 response appears to cross V(λ) again towards the red end of the spectrum.

The acrylic condition with broadband white light and no filter also resulted in a large difference. Explanations for this error will be thoroughly discussed in the following chapter. There are specified CCFs for unique white light sources, and it was anticipated that an LED color-correction would improve the accuracy of these results. Different color correction factors were applied to all of the luminance results for both the filtered and white light conditions. Accuracy of blue filters on the far end of the spectrum improved slightly, as well as the 555 nm filter in the green region. However, CCFs did not significantly improve the accuracy of the results in most cases. Therefore, CCFs were not used in the final results of this experiment. A complete investigation of the various possible effects of luminance values in this experiment is included in the Appendix.

3.6 Discussion

The uncertainty of this luminance calculation method was determined to be ±0.8%. With that uncertainty in mind, the results of the luminance meter measurement compared to the luminance calculation resulted in noteworthy differences throughout the visible spectrum. The luminance difference was smallest near the center of the spectrum, and increased towards either end. This pattern inversely correlates to the V(λ) curve of photopic sensitivity, which makes sense because the meter is meant to include visual effects in a similar manner to the human eye. Differences were largest on the blue end of the spectrum, which has typically resulted in the highest error in previous luminance measurement

research. Differences were lowest in the green region, and slightly higher, but still less than the blues, towards the red end of the spectrum.

Application of a CCF helped improve the accuracy of some saturated color sources. However, if the region of the spectrum specified for a particular CCF does not accurately correspond to the wavelengths that it is meant for, errors may increase. For example, if a blue CCF is applied to the blue-green section of the spectrum, this can increase error rather than correct for it. Similarly, white light sources other than incandescent have inherent errors in luminance measurements. Application of a CCF does little to improve these differences in the case of this LED source.

More research is still needed before exact error corrections throughout the spectrum are identified and error reduction strategies could be applied. In order to further reduce uncertainty and gain a better understanding of the entire spectrum on a more detailed level, a monochromator with a xenon source would be recommended for future research of this kind. The equipment would not likely provide sufficient signal for the CL-500A illuminance spectrophotometer. Instead, a more sensitive meter such as the Ocean Optics QE65000 spectral radiometer, or a similar instrument, would be recommended. It is estimated that the price of equipment for this modified setup would cost over $40,000.

Chapter 4: Spectral Responsivity Errors of Lighting Meters

The results of the calculated versus measured luminance comparison led to further questions about the accuracy of the luminance meter. It was expected that saturated sources would cause various measurement errors, but the large difference in the LED condition was not anticipated. This is believed to be due to the fact that the source was LED rather than incandescent, which was the basis of calibration for the LS-110 luminance meter. Consequently, additional research on the spectral responsivity of the two meters used in this experiment was conducted.

4.1 Experiment Specific Meter Information

4.1.1 CL-500A Illuminance Spectrophotometer

The CL-500A illuminance spectrophotometer has a 128-pixel resolution. While this is much better than standard illuminance meters with one-pixel type, this is still not ideal for measuring single wavelengths. Considering a range of roughly 380 nm across the visible spectrum, this would mean the average pixel is responsive to approximately 3 nm bandwidths. The instrument outputs data in 1 nm increments, which must be the result of either interpolation or an opponent process in the internal software. Meters with less than 1 nm bandwidths do exist, but these are likely of higher precision than necessary for most applications.

4.1.2 LS-110 Luminance Meter

It was later confirmed by the LS-110 luminance meter manufacturer, Konica Minolta, that the LS-110 is not the ideal instrument for measuring LED sources. The sensor for this meter uses only one type of pixel, which covers the visible spectrum from 360

nm to 740 nm. This is in contrast to meter sensors with many unique sensitivities like the CL-500A. The LS-110 sensor is covered by a single V(λ) correction filter which adjusts the responsivity of the sensor to match the responsivity of the human eye at each wavelength which was shown in Figure 49. The calibration source for this meter, like most industry meters, is the CIE Standard Illuminant A incandescent lamp.

4.2 Investigation of the Acrylic Condition Luminance Calculation

Additional illuminance and luminance measurements of the acrylic condition were taken with both the 50 W and 75 W tungsten halogen sources mentioned earlier in the Broadband Light Source Selection section. Multiple trials of the same COB LED module were conducted as well. The LED test initially presented as the Acrylic condition in Chapter 3 will be referred to as LED_1. An additional trial of this LED module that was taken for comparison with the TH sources will be referred to as LED_2. Four additional COB LED trials were also conducted with another, equivalent integrating sphere and LED module. These results will be presented as LED_{3A} through LED_{3D}. Each of the LED trials were based on equivalent sources with the same SPD. The measured and calculated luminance values from these trials were compared in Table 4.

Table 4: Acrylic Condition Results with Various Source Types

Illuminant	Avg L, LS-110 (cd/m^2)	Avg L, Calculation (cd/m^2)	Avg Difference
50 W TH	5769	6942	-20.3%
75 W TH	8027	9339	-16.3%
LED_1	90950	144426	-58.8%
LED_2	120583	155808	-29.2%
LED_{3A}	101950	124593	-22.2%
LED_{3B}	81173	118703	-46.2%
LED_{3C}	82902	132372	-59.7%
LED_{3D}	98495	133268	-35.3%

The results above show noticeably lower luminance differences for the TH sources than the LED trials. The average TH difference was 18.3%, while the average LED difference was 41.9%. Another noteworthy result is that the six LED trials produced a wide spread of differences, from 22.2% to 59.7%. The results have consistently shown that there is certainly an increased difference in luminance values when using an LED source rather than an incandescent source. Based on the difference in spectrum of the calibration source and tested LED, this large difference in luminance values was not surprising. However, an average 18% difference with the TH trials raised some concern because this should theoretically have an almost identical spectrum to the meter calibration source, CIE Standard Illuminant A. In order to better understand this difference, further testing and analysis of the TH source used in this experiment was conducted.

The 50 W and 75 W TH trials presented in this section were tested at 12 V and allowed to reach thermal equilibrium inside of the integrating sphere. The average correlated color temperature (CCT) of the 75 W lamp, as measured through the acrylic lens of the integrating sphere, was 2815 K across all trials. The spectrum of the lamp was also tested at 12 V when illuminated outside of the integrating sphere and resulted in a CCT of 2994 K. In order to achieve a closer CCT to that of CIE Standard Illuminant A at 2856 K, the TH source was dimmed to 10.5 V. The CCT of the bare lamp run at 10.5 V and measured outside of the integrating sphere then became 2868 K. The lamp was then immediately placed inside of the integrating sphere and produced a CCT of 2852 K. It was predicted that the characteristics of the integrating sphere were changing the spectrum of the TH sources, but the change did not initially appear to be drastic. The two measured spectra for the 75 W TH source, both inside and outside of the integrating sphere, are shown in Figure 50.

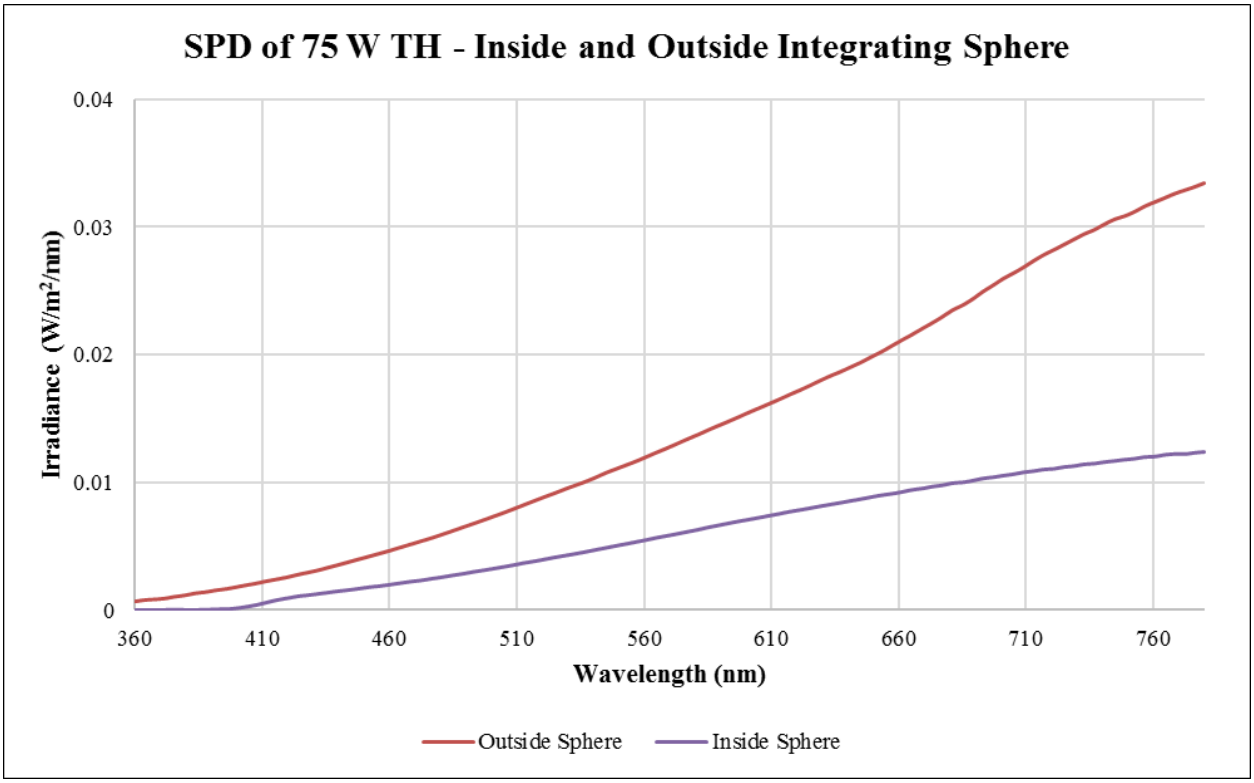

Figure 50: SPD of 75 W TH Taken Inside and Outside of Integrating Sphere

While the measurement of the lamp inside of the integrating sphere was significantly dimmer, the shape of the curves appeared to be fairly similar. However, when the two spectra were normalized at their peak, 780 nm, there was a noticeable difference between the two conditions. The normalized spectra are shown in Figure 51.

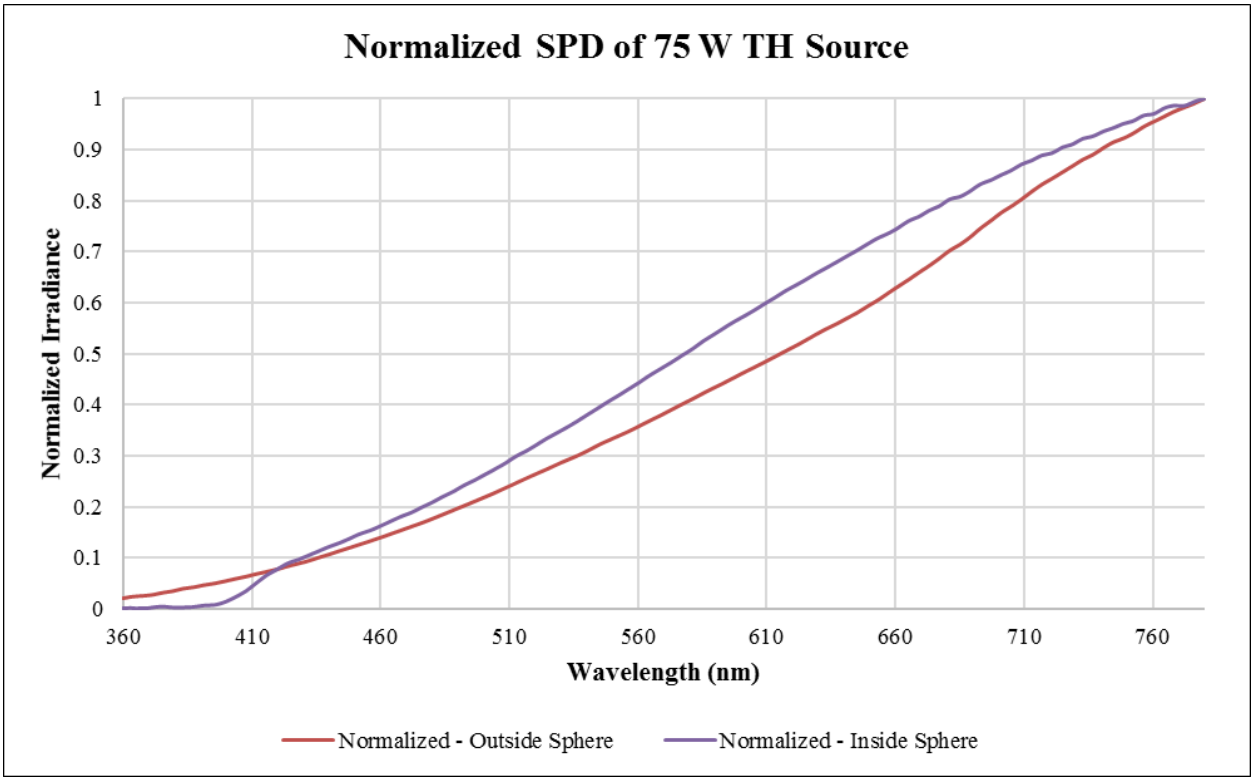

Figure 51: Normalized SPD of 75 W TH Taken Inside and Outside of Integrating Sphere

A large gap between the two spectra occurs throughout almost the entire visible spectrum. This unanticipated, altered spectrum due to the integrating sphere is likely due to a combination of the spectral reflectance of the diffuse white paint used on the interior, and the transmittance properties of the acrylic lens used to cover the aperture. The acrylic lens was made from a material commonly used for acrylic diffusers in luminaires throughout the lighting industry. The integrating sphere with acrylic lens was necessary for the setup used in this experiment. The alteration to the spectra of the TH sources when placed inside of the integrating sphere explains why there may be an 18% average difference in luminance values found for the 50 W and 75 W TH sources.

These results prove that there is an inherent error in this luminance meter for scenes that involve light sources other than CIE Standard Illuminant A. Additional review

of the literature confirmed that error margins of luminance values vary depending on the SPD of the light source (34). The CCF capabilities of the luminance meter attempt to correct for this error by providing multiple white light source correction factors. As was mentioned in a previous section of this report, and is included in the Appendix, the various white source CCFs did not drastically improve the measurement. In fact, all of the white color-corrected luminance values resulted in a difference of over 50% for the LED_1 case of this experiment. The exact extent of luminance measurement error dependent on source spectrum may require more thorough documentation.

4.3 Application of Findings to Luminance Experimental Data

Research on spectral responsivity errors and the specifications of the CL-500A and LS-110 justify the conclusions found through this experiment. The application of the V(λ) filter over the sensor in the LS-110 luminance meter affects the accuracy of luminance values, depending on the spectral characteristics of the source. The measurement of the CL-500A is believed to be reliable, based on the additional testing of a standardized light source and the known sensor capabilities. Any potential distance or diameter measurement uncertainty due to human factor or experimental errors was reduced by testing seven different distance locations for multiple trials. Thus, the calculated luminance values, with the exception of the addressed measurement uncertainty, resulted in a more accurate luminance value than the LS-110 for this experiment. The blue region of the spectrum resulted in larger differences than the red overall because the correction filter manages to fit the V(λ) curve much more accurately at red wavelengths than blue wavelengths. This is made evident by the incandescent spectrum of the calibration source, which outputs very little energy on the blue end in comparison to the red end of the spectrum. Going forward, a

spectrally sensitive meter should be used for all measurements in applications which involve fluorescent, LED, daylight, or any source other than incandescent.

Chapter 5: HDRI Spectral Responsivity

This experiment was initiated in order to better understand spectral responsivity errors in HDR derived luminance values. The unexpected discovery of the inaccuracy in broadband LED source luminance measurements with the LS-110 changed the course of this experiment. These findings have since invalidated the calibration method used for this HDRI experiment. However, some noteworthy lessons about HDRI luminance measurement systems were discovered along the way. A background on the HDRI collection that occurred during the luminance calculation experiment described in Chapter 3 will be presented in this chapter. Then, findings which pertain to future HDRI applications, and suggested next steps for HDRI, will be proposed.

5.1 Equipment

5.1.1 Camera, Lens, Aperture Decision

A firm conclusion of the recent vignetting research at the University of Colorado Boulder was the recommendation to use vignetting correction filters for all future HDRI analysis. Therefore, the lens and aperture combination selected for this experiment was based on the minimum overall error after vignetting correction filters were applied. The pattern of vignetting effects was taken into account also to select a combination with minimal errors in the center of the image. The Sigma Prime lens with f/5.6 aperture was chosen as the optimal system out of those tested (3). In order to lessen the potential for any significant error due to vignetting in this experiment, the filtered light source of interest was always arranged near the center of the frame where vignetting effects are known to be minimal (3). A summary of all relevant camera settings for this experiment is included in Table 5.

Table 5: Nikon D5200 Test Settings

Bracket Step Size	4
Aperture	f/5.6
ISO	100
Image Type	JPEG Fine + RAW

5.1.2 HDRI Software

There are many tethering software options available for the Nikon D5200 camera to streamline the process of photographing multiple exposures. *Sofortbild* (44), a Mac compatible program, was chosen as the best option for this experiment based on previous research (3). The chosen HDRI compilation software was also decided based on the software used for the recent vignetting correction study conducted on this equipment (3). This decision was made in hopes that a calibrated HDRI luminance analysis system can be created for the specific equipment at the University of Colorado Boulder. RAW file types were compiled with *raw2hdr* (45), which was executed through the command terminal on a Mac operating system. After HDRI compilation, a vignetting correction filter was applied to the image through a MATLAB script adapted from previous research (3). The corrected image was then viewed and analyzed through a Windows based software called *hdrscope* (46). This software was ideal because it allows the image to be calibrated to an average value within a chosen circular area, similar to how the luminance and illuminance meter values were collected in the experiment.

5.1.3 Calibration Source Decision

A calibration point was required in each image to convert relative luminance values to absolute luminance values. It was decided that this would be a light source as well, rather than a reflecting surface, to keep the subject of interest and calibration point at similar luminances and thus reduce error in the calibration (32). Two additional integrating spheres with LEDs and acrylic lenses were used, which closely matched the setup of the narrow bandwidth filter source. As mentioned in the Literature Search, it is best for the calibration point to have a similar luminance to the subject of interest. Since the filters produced a wide range of luminance values from roughly 400 cd/m^2 to 44,000 cd/m^2, based on LS-110 measurements, the two calibration source luminance options were roughly 7,000 cd/m^2 and 28,000 cd/m^2, as measured on the acrylic. Neutral density filters were used to create additional luminance conditions by covering the acrylic aperture. These resulted in additional calibration options of roughly 300 cd/m^2 and 1,400 cd/m^2.

As mentioned in previous chapters, the LED acrylic condition resulted in large luminance differences. Since the calibration of the HDRI was based on LED sources before this discovery as well, the calibration luminance values have significant errors of their own. This issue is what ultimately affected all luminance values found through the calibrated HDRI in this experiment. In retrospect, the possibility of an incandescent calibration source may have been reliable because the LS-110 measurements should be accurate for this source type. However, the luminance values produced from incandescent sources in the diffuse sphere setup were significantly lower than some of the most luminous filter conditions. The difference in relative luminance between the calibration and subject of interest would create its own issues with the calibration accuracy.

5.2 Vignetting Correction Filter Creation

To create a vignetting correction filter for the Nikon D5200 with Sigma Prime lens at f/5.6 aperture, the camera was setup to view the inside of a 4-foot diameter integrating sphere at LTI Optics. Uniformity of the sphere interior was confirmed with many radial measurements made by the LS-110 luminance meter. Bracketed LDR images of this uniform, diffuse surface were combined to create a single HDRI. The HDRI was then called into MATLAB via a script written at the University of Colorado Boulder to analyze the decrease of luminance values towards the periphery of the image along multiple radial lines of pixels. The luminance value at each evaluated pixel was then compared through the script to produce a vignetting function that quantifies the rate at which luminance falls off towards the edges of the image. The inverse of this function may be applied to any HDRI from the same lens and aperture combination via a MATLAB script to reverse the effect of vignetting on the image.

$$2.06x^6 - 4.86x^5 + 3.58x^4 - 0.66x^3 - 0.32x^2 + 0.65x + 1.00$$

The function above was generated for the Sigma Prime lens with f/5.6 aperture. This was used to correct for vignetting in all HDR images before analysis for the images assessed in this report.

5.3 HDRI Experimental Setup

The Nikon D5200 camera with Sigma Prime lens was mounted to a sliding rail attachment on the optical bench near to the illuminance spectrophotometer. The two calibration light sources were placed near the edge of the image frame. The additional

spheres were positioned a few inches behind the main sphere to avoid significant contribution of stray light to any measurements taken for the main sphere.

A bracket of low dynamic range images was taken of the acrylic lens as well as each of the nine filters. This occurred in the middle of each test condition, after one trial of the luminance and illuminance measurements had been collected. The second trial of meter data for each condition was collected after the images were captured. A summary of the maximum and minimum exposure settings for each filter is shown in Table 6.

Table 6: Exposure Settings for Each Filter Condition

Condition	**Min Shutter**	**Max Shutter**
Acrylic	30	1/1000
435nm, 465nm, 495nm, 525nm, 555nm, 585nm, 615nm, 645nm	30	1/500
675 nm	30	1/1250

5.4 Importance of LDR Bracket Selection for HDRI Luminance Analysis

The range of luminance values was very large for some photos, because there was a black background with a bright light source. A wide range of exposure times were captured for all images to be sure that no important information was overlooked. The large amount of high resolution images took up a lot of memory, and the process became quite time consuming, but ultimately was very informative. Figure 52 shows an example of the LDR taken for the 615 nm filter to illustrate the effect of exposure times.

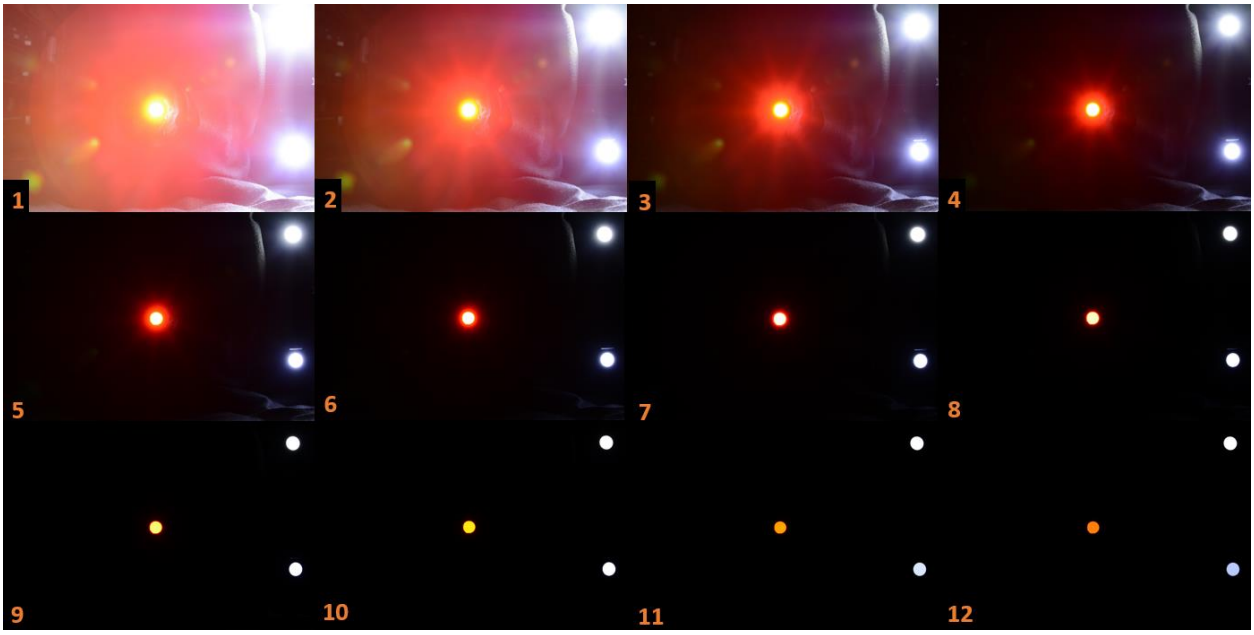

Figure 52: 615 nm LDRI Bracket

HDRI were created using three unique criteria to determine how important the bracket selection process was to the image accuracy. First, HDRI were created by combining all bracketed images that were taken for each trial. Next, the LDRI were reviewed in Photosphere, a Mac compatible program, to view histogram information of each bracket. Histograms are available for luminance, RGB, or red, green, and blue pixels separately. The histograms provide information on the frequency of each value in the image. The range of pixel values for a given image is shown on the horizontal axis, and the frequency of that value is represented by the vertical axis. The majority of the surrounding area in these images was extremely dark, and the area of interest, being the filter or acrylic, was very small in comparison to the field of view. Therefore, the histograms for almost all of the exposure times did not contain much information. Approximately three out of every 12 bracketed images on average contained what appeared to be useful histogram information for typical HDRI. Some LDRI did not show any visible information on the histograms except for a short spike at zero which accounted for the black background. Each

type of histogram available in Photosphere was evaluated, and those images with any significant information were selected and combined into a HDRI. This HDRI combination type typically included a fairly large range of brackets, but excluded the quickest exposures. An example of each set of histograms for the 615 nm filter is shown in the following series of figures.

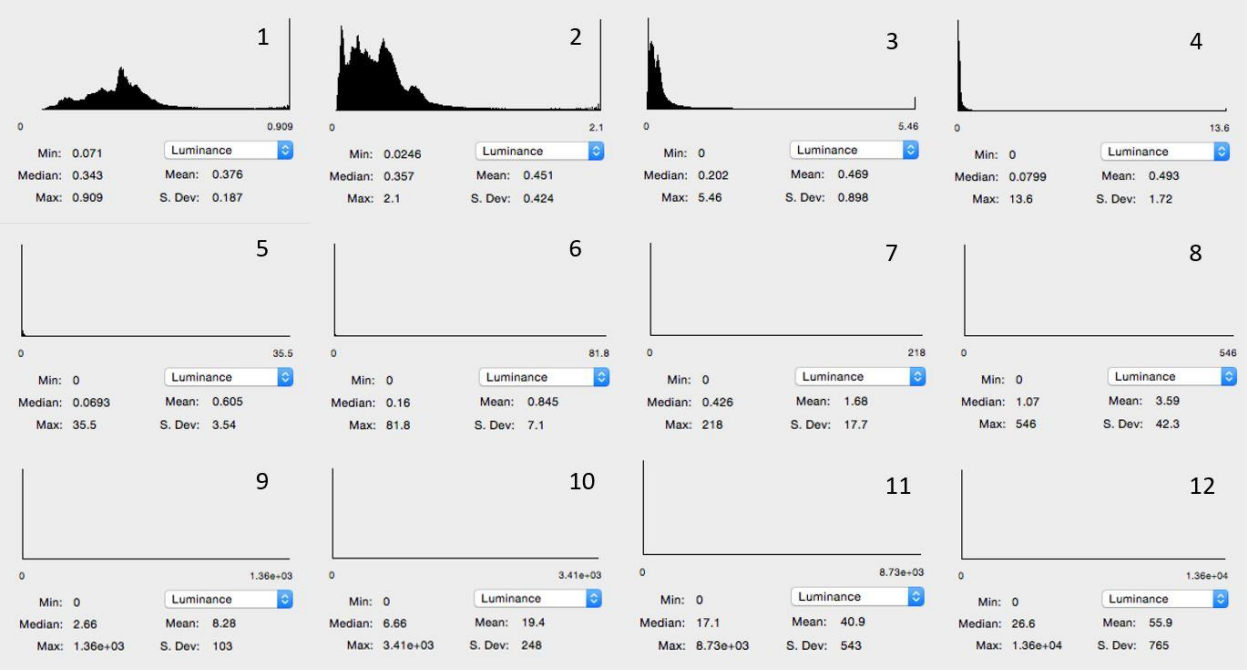

Figure 53: 615 nm Luminance Histograms

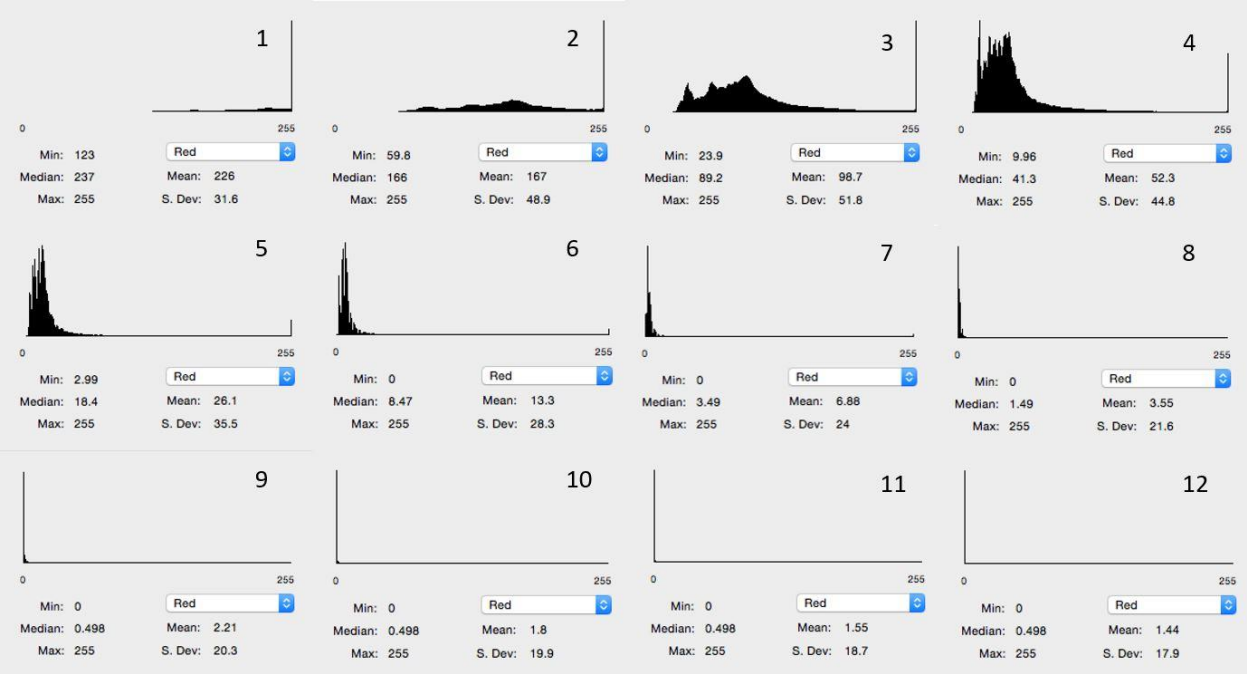

Figure 54: 615 nm Red Histograms

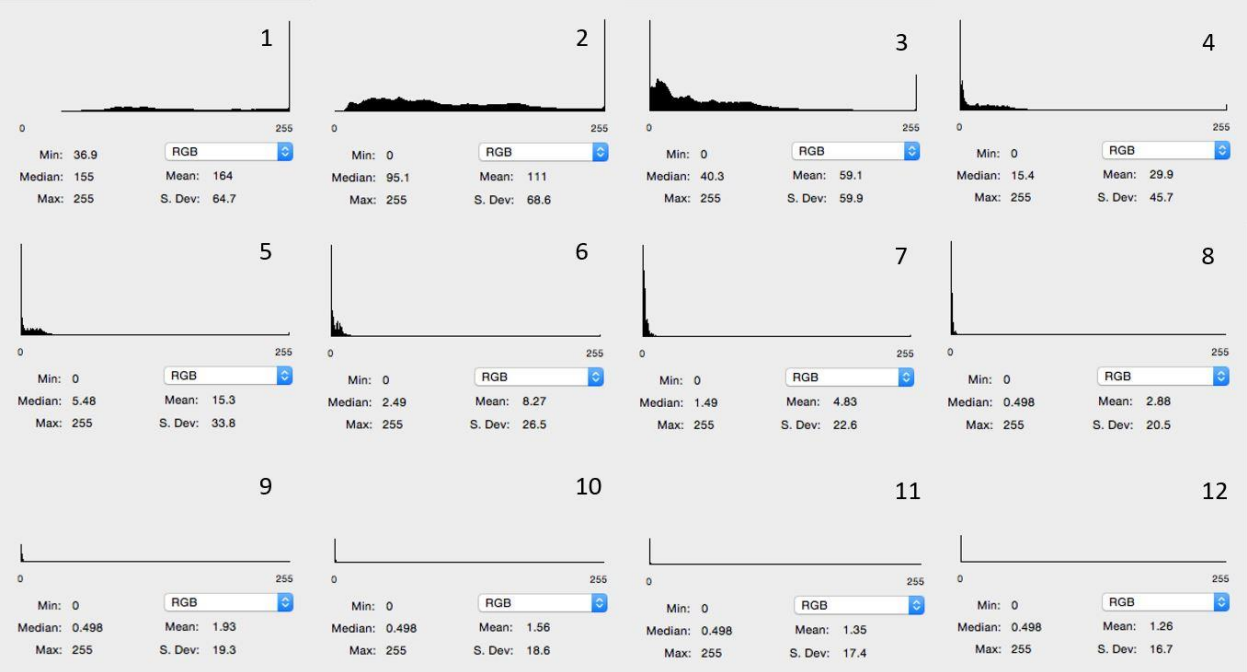

Figure 55: 615 nm RGB Histograms

A final set of bracketed images were selected for HDRI generation, which was based on relative luminance values on a pixel-by-pixel basis. Photosphere initially attempts to

assign luminance values to the LDR bracketed images. These are uncalibrated values, which means they simply provide a relative comparison of luminance. Pixels which are completely saturated will all report the same value. This is often the case with long exposure times, because the camera sensor reaches its limit in certain areas, while trying to gather enough useful information in other areas of the scene. The shorter the exposure, the more variation becomes detectable between relative pixel luminance values. The value of this relative luminance also increases with shorter exposures, and becomes more realistic. For example, the 30 second exposure typically resulted in a luminance of approximately 4 cd/m^2 for all filters, and both calibration sources. These three different light sources clearly have unique luminance values when viewed in person, which was also confirmed by LS-110 luminance measurements. When the exposure times became shorter, the software began to recognize variation in the relative luminance values of the light sources. This final method of bracket selection chose to combine LDRs once the three source luminance values were no longer equal, and included all of the following brackets as well. These typically consisted of a shorter range of brackets towards the end of the numbered set.

Again, the three methods described were to combine all bracketed images, combine a selection based on histogram information, or combine a selection based on relative luminance values. The three HDRI for each filter condition were then corrected for vignetting, and calibrated in hdrscope to the source with the closest luminance to the measured filter luminance. Then, the area of the filter was selected to attain an average luminance value.

The differences in HDRI luminance compared to the standard luminance measurements taken with the LS-110 meter varied greatly in some cases, depending on the

combination selection method. For example, the 615 nm case resulted in a difference of -18.0% from the LS-110 measurements for the combination including all brackets. The relative luminance based combination for this filter resulted in a relatively similar difference of -15.5% by using only brackets eight to 13. However, the histogram based combination for this filter showed a difference of -67% by combing brackets three to ten. It is assumed that the reason for such high errors in this last combination is due to cutting out the shortest exposures, which provide the most accurate luminance information for the calibration source. Clearly the brackets selected for HDRI generation are important and need to be carefully considered for accurate luminance results because errors may be dangerously large, or small, if misrepresentative brackets are selected. Therefore, it is best to err on the side of caution and include all of the available luminance data from each exposure and be consistent between trials. The decision was made to use all bracketed images for the remainder of the HDRI analysis so that no crucial information was unintentionally omitted.

5.5 Results and Analysis

All final HDRI for each condition are included in the Appendix. A graph of the difference between the HDRI derived luminance value compared to both the measured and calculated luminance values from Chapter 3 is shown in Figure 56. The LS-110 luminance meter comparison is shown in light blue, and the calculated luminance from CL-500A measurements is in red. The data shown in Figure 56 is difficult to fully appreciate for the majority of the filters when the scale is so drastically increased by the large difference

percentages of the blue filters. Figure 57 presents the same information as Figure 56 but with an adjusted scale to make the other data decipherable.

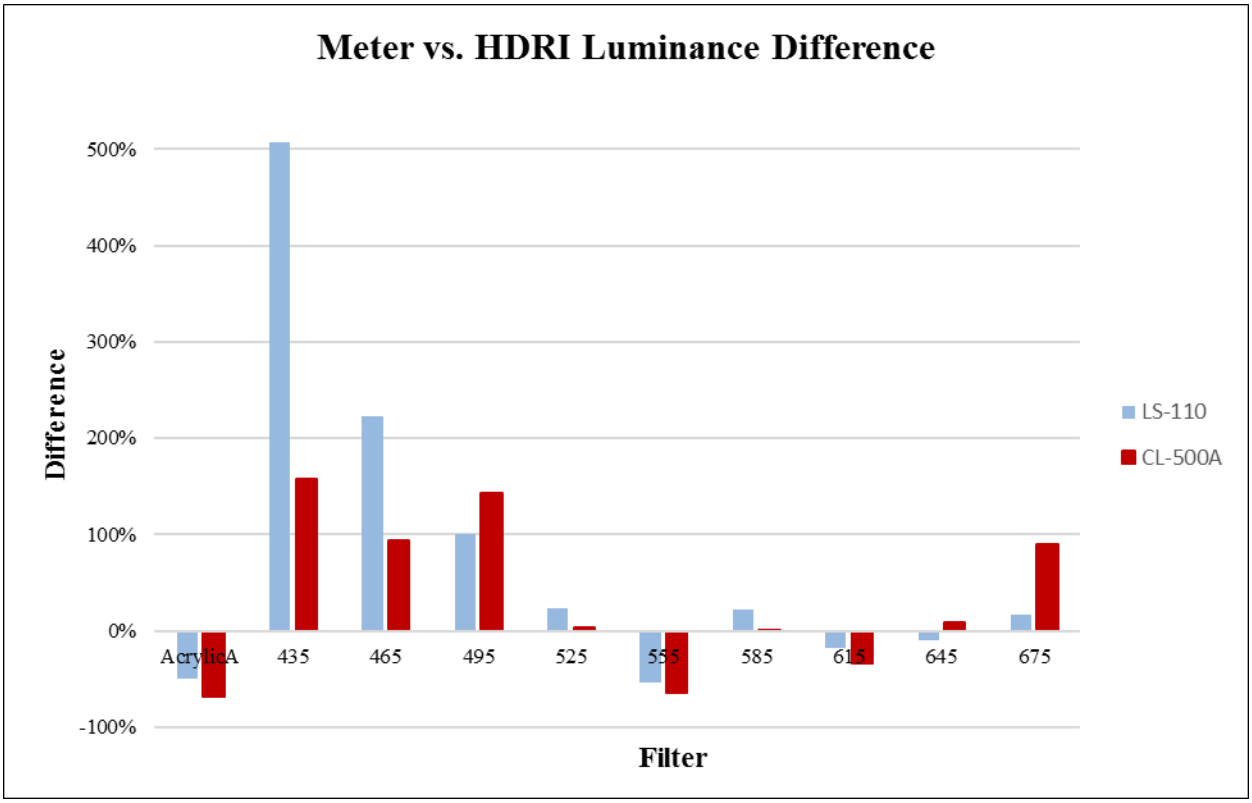

Figure 56: Measured and Calculated Luminance Versus HDRI Derived Luminance

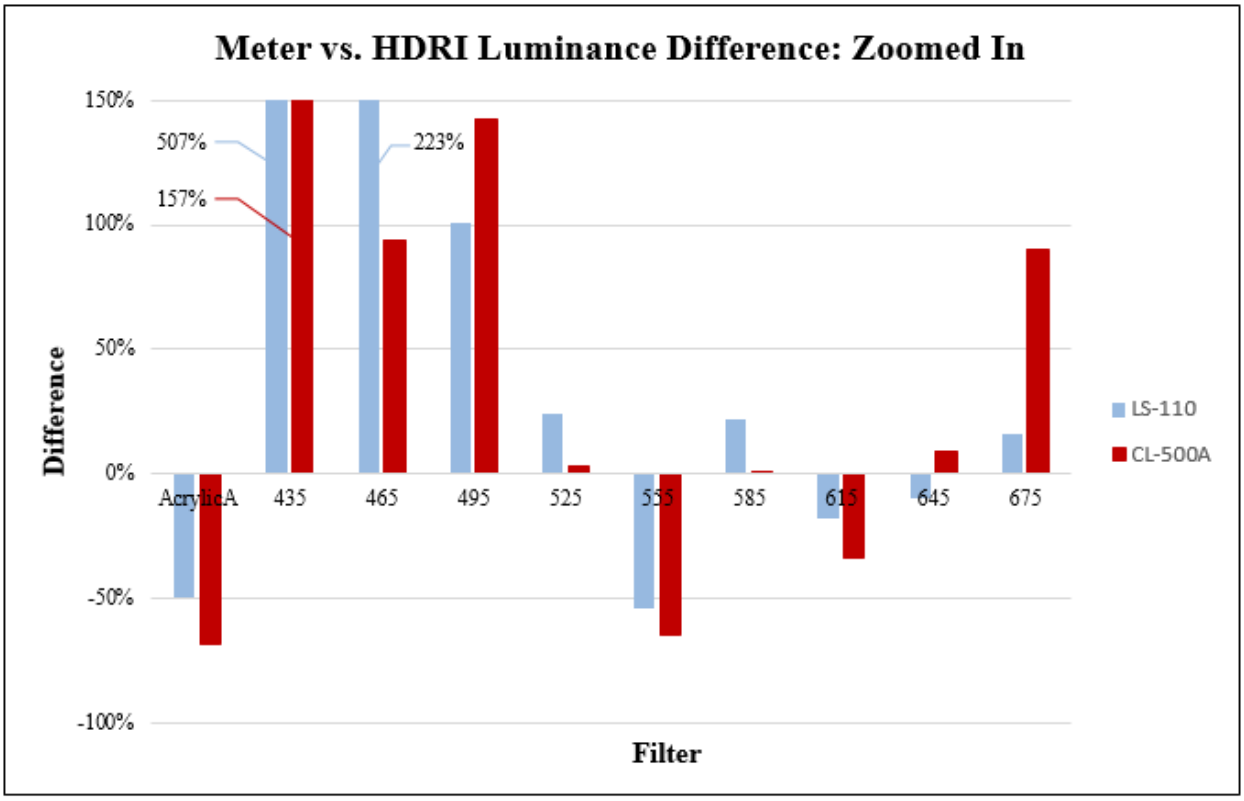

Figure 57: Close-up of Measured and Calculated Luminance Versus HDRI Derived Luminance

Positive percentages in this comparison mean that the HDRI generated luminance was greater than the measurement from the meter. The acrylic condition did not result in as large of errors as would be expected, based on the results from the previous chapter. This is likely because the source the image was calibrated to was also a white LED which may have negated most of the error in the luminance measurement. The blue filters on the left side of the spectrum showed extreme differences between the HDRI value and the meters. This aligns with past research which has always found blue to have the highest luminance error, as is true in this experiment as well. The difference between the LS-110 measured luminance and the HDRI is over 500% in the worst case of the 435 nm filter.

While the exact percentages presented here may not be accurate due to the calibration source measurement, the overall trends throughout the spectrum are still relevant. It is understandable that the HDRI luminance difference may not inversely correlate to V(λ) the way that the luminance differences appeared to, because this is dependent on the sensitivity response of each sensor pixel. Unlike the meters which include a V(λ) response filter automatically applied to the data, the camera sensor is comprised of RGB pixels which are sensitive to certain wavelengths. There was no definitive trend to whether the LS-110 measured luminance or calculated luminance was more accurate when compared to the HDRI value.

5.6 Discussion

An unintentional, yet significant discovery of this HDRI experiment was the importance of which LDR images are selected from the bracket for luminance accuracy. It is best to err on the side of caution with bracket selection and make sure the full range of luminance values is included in the HDRI. Additionally, RAW file formats should be used for luminance analysis when saturated colors are a concern. Compression along the RGB channels of the camera sensor occurs when saving JPEG files, which adds additional complexity to understanding the spectral component issues.

The spectral error of the luminance meter was not noticed in past experiments because the meter was assumed to be accurate for white light sources. An HDRI generated luminance was generally calibrated by and compared to LS-110 luminance values which, in hindsight, consistently contained large errors for LED sources. Going forward, HDRI should not be calibrated to standard luminance values from a meter without spectral

capabilities. Furthermore, absolute measurements from two different scenes or images will not be comparable by means of a traditional luminance meter if they contain different light sources. Only relative luminance values within one scene may be compared without spectrally-based measurements.

Since there was inaccuracy in the luminance measurements of the two LED sources used to calibrate the HDRI, this affected all of the HDRI by an unknown amount. Therefore, the differences found through this experiment still require further experiments with a modified calibration system. The results of this experimental setup showed extreme differences between measured luminance and HDRI derived luminance for blue sources. The LS-110 measurement differed from the HDRI derived luminance of the three filters on the blue end of the spectrum by an average of 277%. These same measurements only differed by an insignificant amount for the green and red regions of the visible spectrum.

The responsivity of the camera image sensor was further investigated to try and make sense of any patterns in the HDRI luminance results. It turns out that there is a wide variation of image sensors used in the DSLR industry, and even within particular camera manufacturers. Nikon, along with other manufacturers, does not provide much information on their image sensors other than the pixel array size, and whether it is CMOS or CCD. The specific properties of these sensors are proprietary information. However, many camera, semi-conductor, and micro-processor enthusiasts seek to understand these specifications for a more thorough understanding of their industry. There exist many websites which provide reverse-engineered information of cameras by taking apart and analyzing products already on the market. While these sources may not be as reliable as the manufacturer themselves, they provide substantial insight on camera image sensors.

Nikon digital cameras typically contain image sensors designed by Sony or Nikon themselves (47). A couple of their DSLR models break from the mold and use Toshiba image sensors instead. The Nikon D5200 used in this experiment is one of those rare cases (48). A Toshiba 5105 24.1 Mp CMOS sensor with HEZ1 markings was found in this particular model (48). It is known that Toshiba sensors use copper metallization for their pixels, while Nikon, Sony, and Canon, among others, use aluminum (49). A report including the color filtration and RGB pixel specifications is available for purchase, listed at $18,500 (48). This report likely contains the information necessary to understand the sensor accuracy of this camera throughout the visible spectrum. However, the fact that each camera has its own sensor with unique color sensitivity makes the task of spectral pixel correction a much larger task than anticipated. A correction model for color luminance accuracy, would be dependent on each camera make and model. While a solution may be possible for a particular HDRI luminance system, this would not apply to a widespread application to all camera setups.

Chapter 6: Conclusion

Incandescent sources have been the basis of calibration for many meters and systems for a long time. With the ever increasing abundance of LED technology, the spectral content of calibration sources has become more important. This experiment proved that luminance measurements with an industry standard meter result in significant errors of saturated color sources throughout the visible spectrum. These inconsistencies at certain wavelengths compound into errors for broadband white light sources, other than a standard incandescent lamp, as well. The spectral responsivity of the meter sensor, and V(λ) correction filter, affects the accuracy of measurements for both saturated color sources, and many white light sources.

The largest differences between measured and calculated luminance were found for the narrow bandwidth filters towards the blue end of the visible spectrum, with over a 130% difference at the 435 nm filter. Most blue LEDs reach their peak output around 450 nm, which has a luminance measurement error greater than 60% for broadband meters. The calculated versus measured differences decrease toward the center of the visible spectrum, referred to in this report as the green filters. These saturated sources still resulted in measurement differences, but the severity is reduced, at 24% on average. Continuing towards the opposite side of the visible spectrum, the errors continue to increase towards the red wavelengths. These differences were not nearly as drastic as the blue errors with an average of only 11%, but the farthest red 675 nm filter resulted in a difference of 39%. These results agree with previous illuminance and luminance research described in Chapter 2 which has consistently found the largest errors for blue objects.

The saturated sources were anticipated to result in significant luminance measurement errors, however the concerns that were raised about the LED white light source were not expected at the start of this experiment. LEDs have very different spectral characteristics from a standard incandescent source. The SPD of white light from a LED source may be the result of RGB diodes, a blue or indigo diode with yellow phosphor, or a combination including even more diodes, such as amber. Since white light LEDs may have such a wide variety of spectral outputs, the spectral content, rather than a simple correlated color temperature metric, is crucial for understanding the accuracy of luminance measurements in that scene. An average difference of roughly 42% was found for the broadband LED source in this experiment when compared to tungsten halogen lamps. While only LED and TH white light sources were tested in this experiment, the argument can be made that this is an issue for daylight, fluorescent, metal halide, and other source types as well. Any source with a very different spectrum than incandescent, which includes most modern sources, will likely encounter increased measurement error. Some correction factors are provided by manufacturers for various fluorescent and metal halide sources, but the spectra of these source types is more predictable than that of a white LED. Therefore, LED measurement error will be difficult to accurately account for without an understanding of the spectral characteristics of that particular LED module.

The HDRI analysis in this experiment was calibrated using the LS-110 luminance meter and an LED source, before it was discovered that this measurement may have at least 42% error. Since the calibration process included substantial error, the HDRI derived luminance values were not reliable. Therefore, the HDRI luminance values found in this experiment still require further investigation, but some were still significantly greater than the initial calibration error. HDRI derived luminance differences in the blue region were

typically near 150% when compared to the calculated luminance. It is expected that white LEDs would result in HDRI luminance errors also because a significant portion of the LEDs spectrum was output in the blue wavelengths.

Camera color correction may be possible for a particular HDRI luminance measurement system, but is unlikely for widespread application because of the unique sensor types in each camera model. The sensitivity of these sensors could turn out to be similar enough, but this conclusion would require more research on the sensor specifications used in popular camera models. An accurate representation of absolute luminance values from a calibrated HDRI requires a substantial amount of error analysis and quantification for each measurement system. The lens, aperture, image sensor, and luminance calibration instrument each produce unique errors that must be corrected. These sources of error all need to be understood separately, and cohesively, in order to justify any absolute values derived from HDRI. The spectral characteristics of a light source have proven to be crucial in determining the accuracy of lighting measurements, in both HDRI derived luminance values and standard lighting measurements.

References

1. DiLaura, David L, et al. *The Lighting Handbook: Reference and Application.* Tenth. s.l. : Illuminating Engineering Society of North America, 2011.

2. Murdoch, Joseph B. *Illuminating Engineering: From Edison's Lamp to the LED.* Second. s.l. : Visions Communications, 2003.

3. Stanley, Mio J. *On the development and error analysis of a high dynamic range imaging system for luminance measurements.* s.l. : University of Colorado Boulder, 2016.

4. Herrman, John. Ultimate Light Bulb Test: Incandescent vs. Compact Fluorescent vs. LED. *Popular Mechanics.* [Online] September 20, 2011. [Cited: December 23, 2016.] http://www.popularmechanics.com/technology/gadgets/reviews/g164/incandescent-vs-compact-fluorescent-vs-led-ultimate-light-bulb-test/?.

5. Luminous Efficacy. [Online] http://ceae.colorado.edu/~beamer/Images/Luminous%20Efficacy.JPG.

6. DiLaura, David. Colorimetry. [ed.] University of Colorado Boulder. s.l. : Rocky Mountain Lighting Academy.

7. Reinhard, Erik, et al. *High Dynamic Range Imaging: Aquisition, Display, and Image-based Lighting.* Second. Burlington : Elsevier Inc., 2010.

8. *Color appearance in high-dynamic range imaging.* Akyuz, Ahmet O and Reinhard, Erik. 3, 2006, Journal of Electronic Imaging, Vol. 15.

9. Kang, Henry R. Issues of Digital Color Imaging. [ed.] The Society of Photo-Optical Instrumentation Engineers. *Computational Color Technology.* Bellingham : Spie Press, 2006, pp. 407-444.

10. *High dynamic range imaging and its application in building research.* Jacobs, Axel. 1, 2007, Advances in Building Energy Research, Vol. 1, pp. 177-202.

11. *Errors in the Standard Photometric System when Measuring the Brightness of General Illumination Light Sources.* Alman, D. H. October 1977, Journal of the Illuminating Engineering Society, pp. 55-62.

12. *Lamp colour properties and apparent brightness: a review.* Fotios, Steve A. 3, Sheffield : s.n., March 10, 2001, Lighting Research and Technology, Vol. 33, pp. 163-181.

13. Illuminance Meter T-10A/T-10MA Instruction Manual. *Konica minolta.* [Online] 2016. http://www.konicaminolta.com/instruments/download/instruction_manual/light/pdf/t-10a_instruction_eng.pdf.

14. *The usage of digital cameras as luminance meters.* Wüller, Dietmar and Gabele, Helke. [ed.] Russel A. Martin, Jeffrey M. DiCarlo and Nitin Sampat. 2007. SPIE-IS&T Electronic Imaging. Vol. 6502.

15. *Measurement and specification of lighting: A look at the future.* Goodman, T M. 2009, Lighting Research and Technology, Vol. 41, pp. 229-243.

16. Understanding Standard Illuminants in Color Measurement. *Konica Minolta.* [Online] [Cited: December 11, 2016.] http://sensing.konicaminolta.us/2013/11/understanding-standard-illuminants-in-color-measurement/.

17. *Daylight measurement error.* Hayman, Simon. 2, Sydney : s.n., 2003, Lighting Research and Technology, Vol. 35, pp. 101-110.

18. LED Lighting - Error Consideration for Illuminance Measurement . *Gossen.* [Online] http://www.gossen-photo.de/pdf/LED_Beleuchtung_Messfehlerbetrachtung_GB.pdf.

19. What is the difference between radiometers, spectrometers, and spectroradiometers? *Konica Minolta.* [Online] [Cited: December 11, 2016.] http://sensing.konicaminolta.us/2013/11/what-is-the-difference-between-radiometers-spectrometers-and-spectroradiometers/.

20. van der Steen, Marcel. Measuring Illuminance Correctly. *Olino Renewable Energy.* [Online] http://www.olino.org/us/articles/2009/12/07/measuring-illuminance-correctly.

21. Perre, Ivan. PLS 2014: Is measuring LED illuminance with a lux meter accurate? [Online] October 8, 2014. http://www.slideshare.net/theilp/pls-2014-is-measuring-led-illuminance-with-a-lux-meter-accurate.

22. Luminance Meter LS-100 LS-110 Instruction Manual. [Online] http://www.konicaminolta.com/instruments/download/instruction_manual/light/pdf/ls-100-110_instruction_eng.pdf.

23. Luminance Meters: LS-100/LS-110. [PDF]. s.l. : Konica Minolta.

24. Illuminance Spectrophotometer CL-500A Instruction Manual. [Online] http://www.konicaminolta.com/instruments/download/instruction_manual/light/pdf/cl-500a_instruction_eng.pdf.

25. International Commission on Illumination, TC 2-48. CIE 202:2011. *Technical Report: Spectral Responsivity Measurement of Detectors, Radiometers and Photometers.* Vienna, Austria : CIE, 2011.

26. *The comparison of CCD and CMOS image sensors.* Zhang, Lihua, et al. 2009. Proceedings of 2008 International Conference on Optical Instruments and Technology: Advanced Sensor Technologies and Applications.

27. *Recovering high dynamic range radiance maps from photographs.* Debevec, Paul E and Malik, Jitendra. 1997. Proceedings of the 24th Annual Conference on Computer Graphics and Interactive Techniques, SIGGRAPH. pp. 369-378.

28. *Inter-camera color calibration by correlation model function.* Porikli, Fatih. s.l. : Image Processing, 2003. 2003 IEEE International Conference. Vol. 3, pp. 133-136.

29. D5200 Reference Manual. [Online] http://cdn-10.nikon-cdn.com/pdf/manuals/dslr/D5200RM_NT(11)01.pdf.

30. *Development of new daylight glare analysis methodology using absolute glare factor and relative glare factor.* Suk, Jae Yong, Schiler, Marc and Kensek, Karen. 2013, Energy and Buildings, Vol. 64, pp. 133-122.

31. *Determining lens vignetting with HDR techniques.* Jacobs, Axel and Wilson, Mike. Bulgaria : s.n., 2007. Proceedings of XII National Conference on Lighting.

32. *Accuracy of luminance maps obtained from high dynamic range images.* Moeck, Martin. 2, 2007, Leukos, Vol. 4, pp. 99-122.

33. *Validation of high dynamic range imaging to luminance measurement.* Anaokar, Smita and Moeck, Martin. 2, 2005, Leukos - The Journal of the Illuminating Engineering Society of North America, Vol. 2, pp. 133-144.

34. *Evaluation of high dynamic range photography as luminance data aquisition system.* Inanici, Mehlika N. 2, 2006, Lighting Research and Technology, Vol. 32, pp. 123-136.

35. *Variation of calibration factor over time for high dynamic range photography in a single daylit interior scene.* Chung, Tse-Ming and Ng, Roger T.h. 2, 2010, Journal of Light & Visual Environment, Vol. 34, pp. 87-93.

36. *An Assessment of High Dynamic Range Luminance Measurements with LED Lighting.* Tyukhova, Yulia and Waters, Clarence. December 3, 2013, LEUKOS: The journal of the Illuminating Engineering Society of North America.

37. Ohno, Yoshihiro. *NIST Measurement Services: Photometric Calibrations.* Optical Technical Division. Gaithersburg : National Institute of Standards and Technology, 1997. p. 85, NIST Special Publication 250-37.

38. Fundamentals of Xenon Arc Lamps. *Zeiss: Make it visible.* [Online] [Cited: December 21, 2016.] http://zeiss-campus.magnet.fsu.edu/articles/lightsources/xenonarc.html.

39. Klipstein, Don. Automotive Xenon Metal Halide HID Lamps. [Online] 2013. http://donklipstein.com/d2.html.

40. Cinema Xenon Lamps. *Philips Lighting.* [Online] http://www.usa.lighting.philips.com/products/special-lighting/cinema.html.

41. Newport. [Online] Newport Corporation, 2016. https://www.newport.com/.

42. Catalogue 2015. *Mega-9.* [Online] 2015. http://www.mega-9.com/en/Catalogue2015En.pdf.

43. Taylor, John R. *An Introduction to Error Analysis: The study of uncertainties in Physical Measurements.* Second. Sausalito : University Science Books, 1997.

44. *Sofortbild.* [Online] http://www.sofortbildapp.com/.

45. Jacobs, Axel. WebHDR. [Online] 2014. http://www.jaloxa.eu/webhdr/.

46. hdrscope. [Online] http://courses.washington.edu/hdrscope/.

47. List of all Nikon DSLR cameras and their sensor manufacturer/designer. *Nikon Rumors.* [Online] December 16, 2015. [Cited: December 5, 2016.] http://nikonrumors.com/2015/12/16/list-of-all-nikon-dslr-cameras-and-their-sensor-manufacturerdesigner.aspx/.

48. Product Detail. *chipworks.* [Online] [Cited: December 5, 2016.] https://chipworks1.force.com/DefaultStore/ccrz__ProductDetails?viewState=DetailView&cartID=&sku=IPR-1212-801&&store=DefaultStore.

49. Inside the Nikon D5200 DSLR - Toshiba found! *chipworks.* [Online] January 8, 2013. [Cited: December 5, 2016.] http://www.chipworks.com/about-chipworks/overview/blog/inside-nikon-d5200-dslr-toshiba-found.

50. *Technical guide: Integrating sphere theory and applications.* [Web] s.l. : Labsphere: A Halma Company, September 2, 2016.

51. International Commission on Illumination, TC 2.2. CIE 53-1982. *Technical Report: Methods of Characterizing the Performance of Radiometers and Photometers.* Vienna, Austria : International Commission on Illumination, 1996.

52. Denso D2S D2R HID Xenon OEM Ballast w/Ignitor for Lexus Toyota Mazda D2 DDLT002. *Genssi.com.* [Online] http://www.genssi.com/index.php/denso-d2s-d2r-hid-xenon-oem-ballast-w-ignitor-for-lexus-toyota-mazda-d2-ddlt002.html.

53. Xenon Standard Xenon. *Philips.* [Online] 2016. http://www.usa.philips.com/c-p/85122C1/xenon-standard-xenon/overview.

54. International Commission on Illumination. *Colorimetry - Part 4: CIE 1976 L*a*b* Colour Spaces.* s.l. : CIE, 2008. Standard. CIE S 014-4/E:2007 (ISO 11664-4:2008).

Glossary

Lighting Specific Terminology

Photometric – A measurement of radiation quantities, accounting for the human visual response (1).

Photopic Vision – Characterization of human vision for light levels over 10 cd/m^2, primarily controlled by cones in the retina for color and detail oriented tasks (1).

Radiometric – A measurement of optical radiation quantities (1).

Scotopic Vision – Characterization of human vision for light levels below 0.001 cd/m^2, primarily controlled by rods in the retina (1).

List of Abbreviations

CCD – Charge-Coupled Device

CCT – Correlated Color Temperature

CFL – Comact Fluorescent

CIE – International Commission on Illumination (Comission international de l'éclairage)

CMOS – Complementary Metal Oxide Semiconductor

COB – Chip on Board

CRI – Color Rendering Index

DSLR – Digital Single-Lens Reflex

HDRI – High Dynamic Range Image

IES – Illuminating Engineering Society

LDRI – Low Dynamic Range Image

LED – Light Emitting Diode

RGB – Red, Green, Blue

SPD – Spectral Power Distribution

TH – Tungsten Halogen

Appendix A: SPD of Filters with LED Source

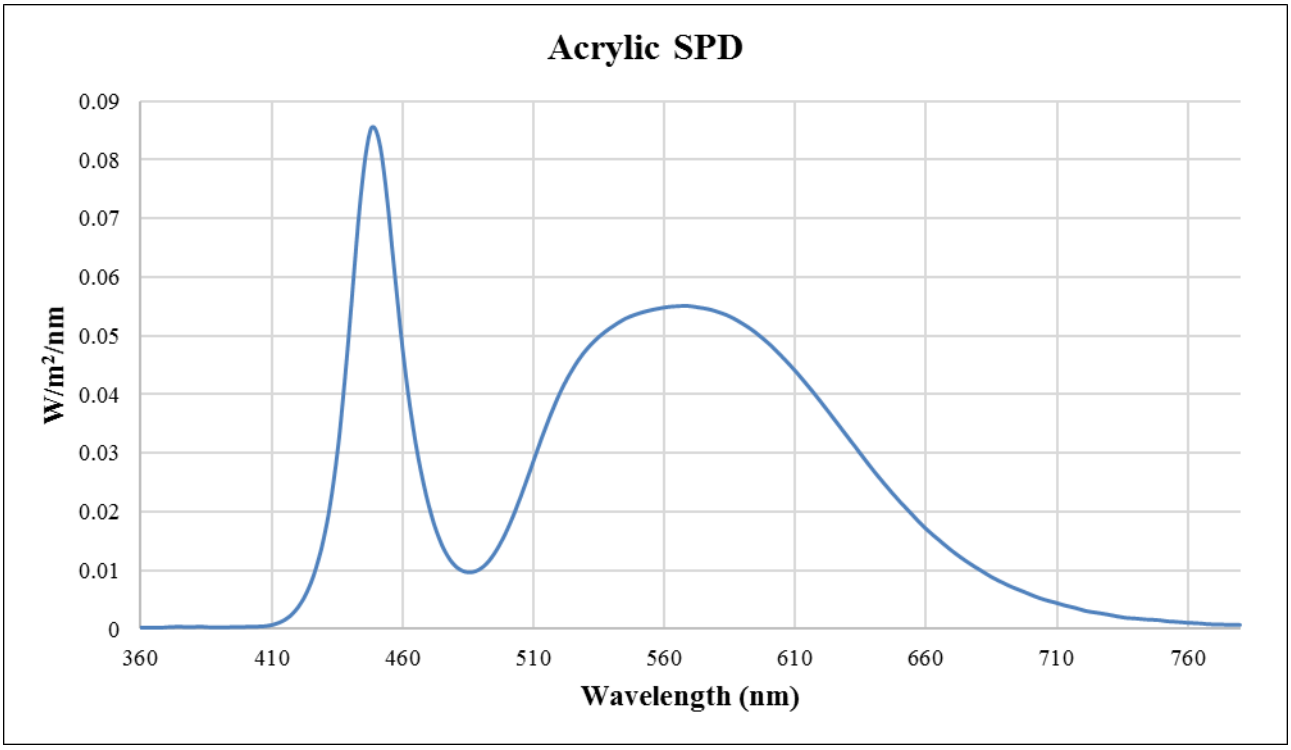

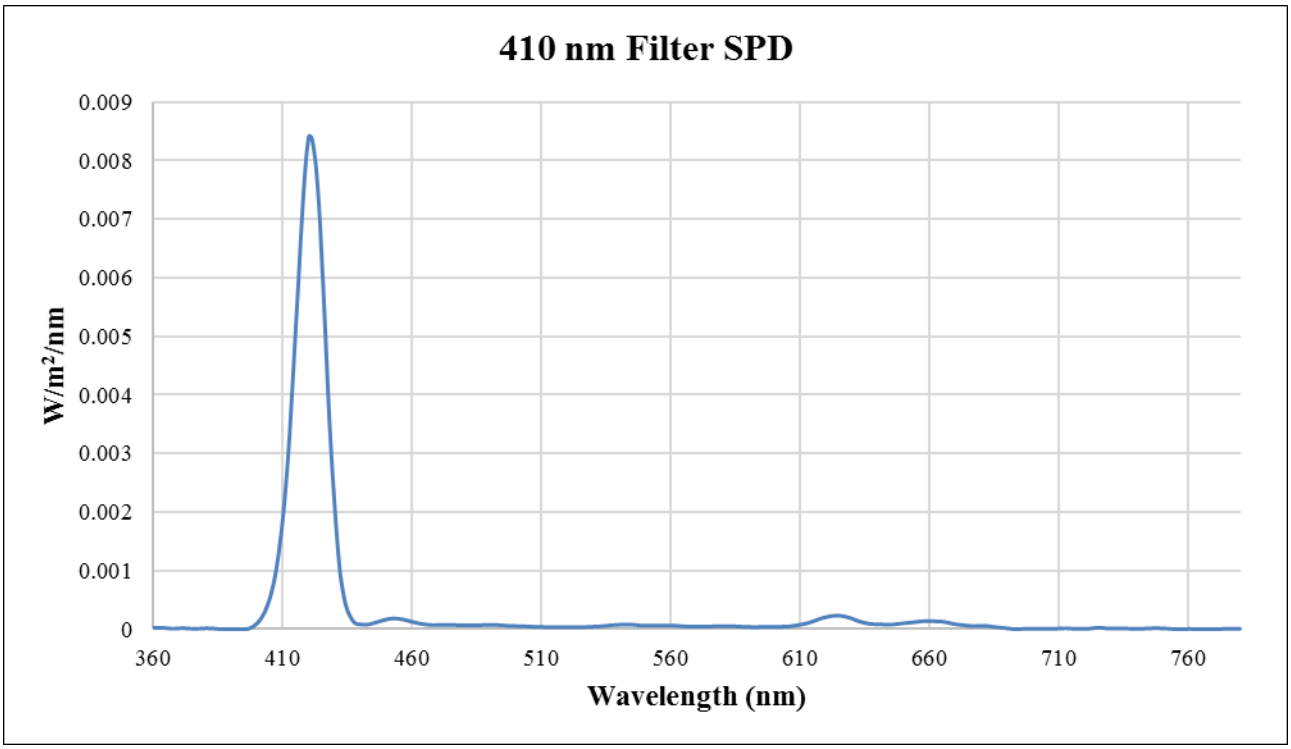

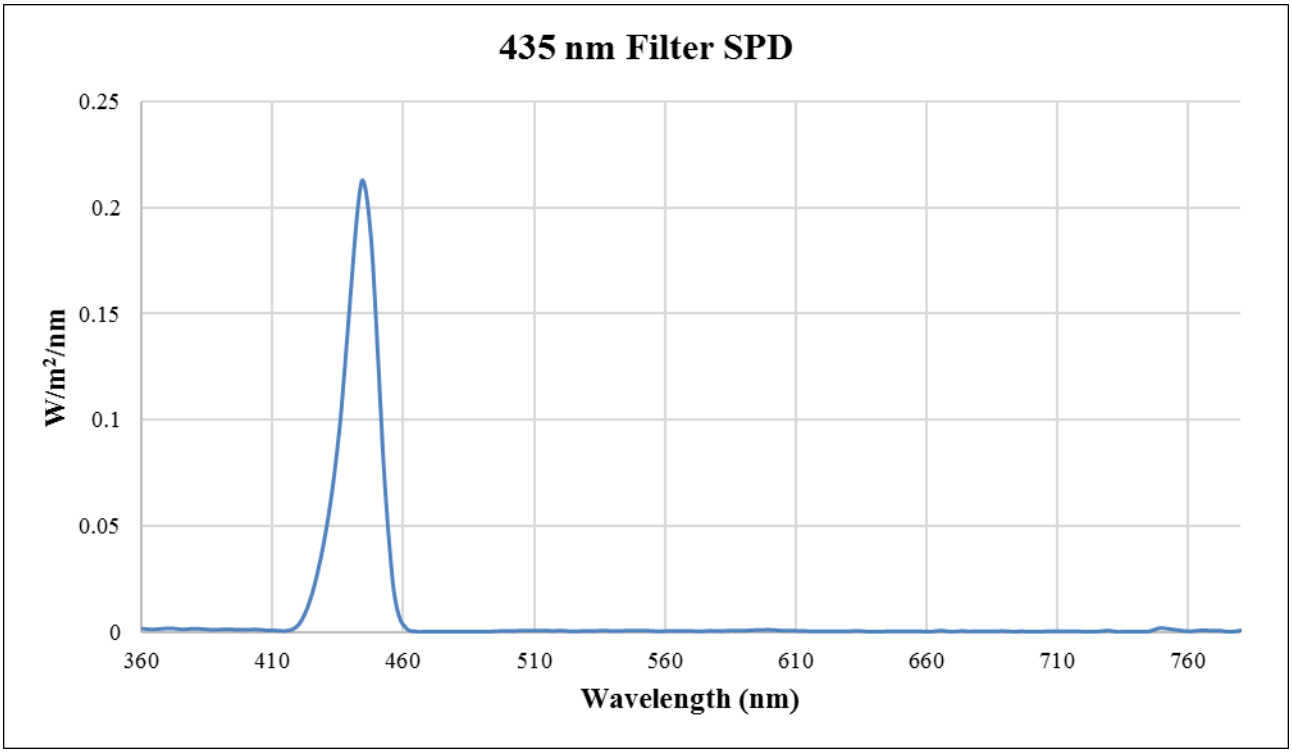
435 nm Filter SPD
0.25
0.2
0.15
0.1
0.05
0
W/m²/nm
360
410
460
510
560
610
660
710
760
Wavelength (nm)

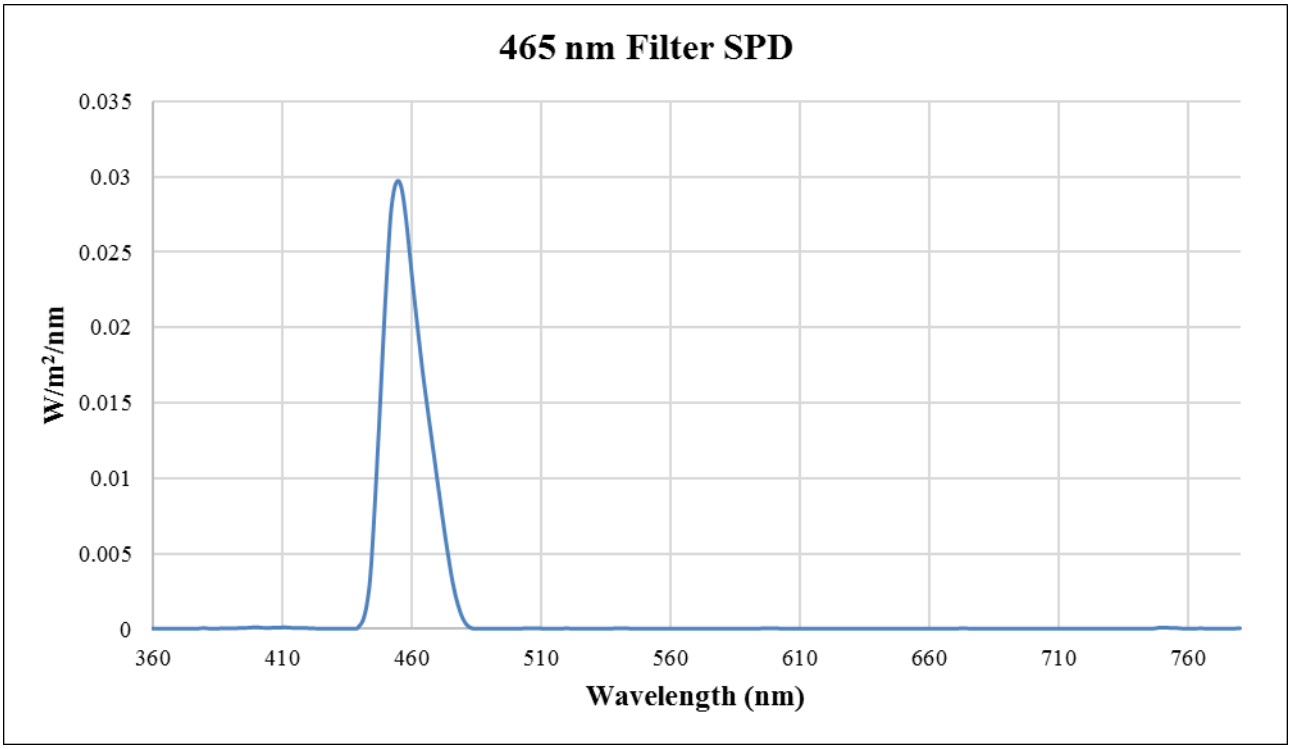
465 nm Filter SPD
0.035
0.03
0.025
0.02
0.015
0.01
0.005
0
W/m²/nm
360
410
460
510
560
610
660
710
760
Wavelength (nm)

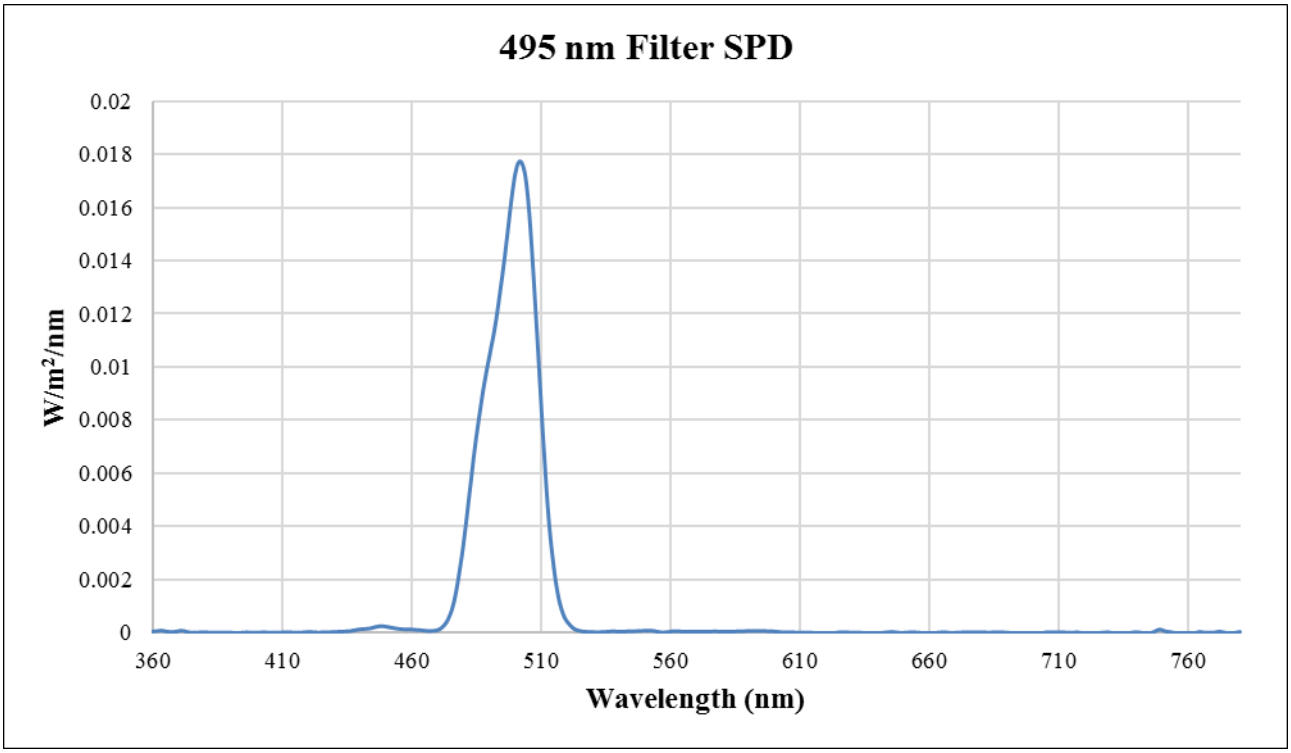
495 nm Filter SPD
0.02
0.018
0.016
0.014
0.012
0.01
0.008
0.006
0.004
0.002
0
W/m²/nm
360
410
460
510
560
610
660
710
760
Wavelength (nm)

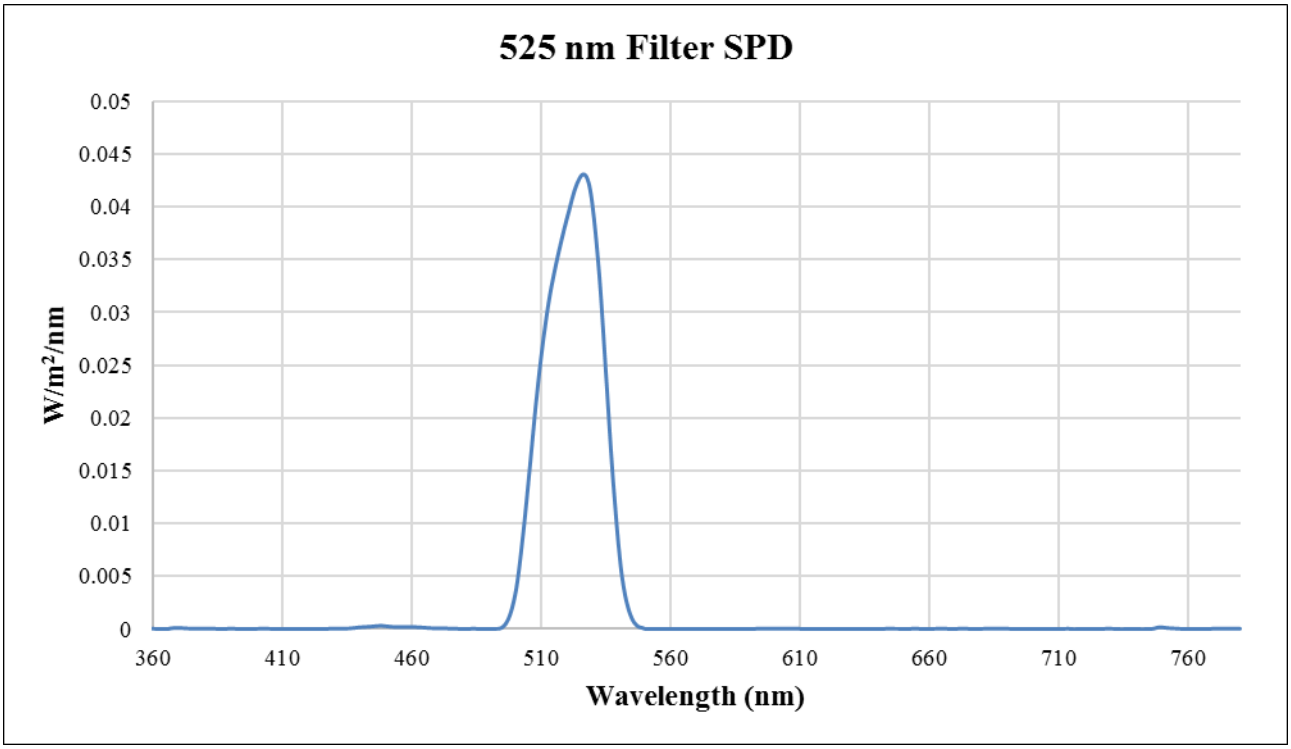
525 nm Filter SPD
0.05
0.045
0.04
0.035
0.03
0.025
0.02
0.015
0.01
0.005
0
W/m²/nm
360
410
460
510
560
610
660
710
760
Wavelength (nm)

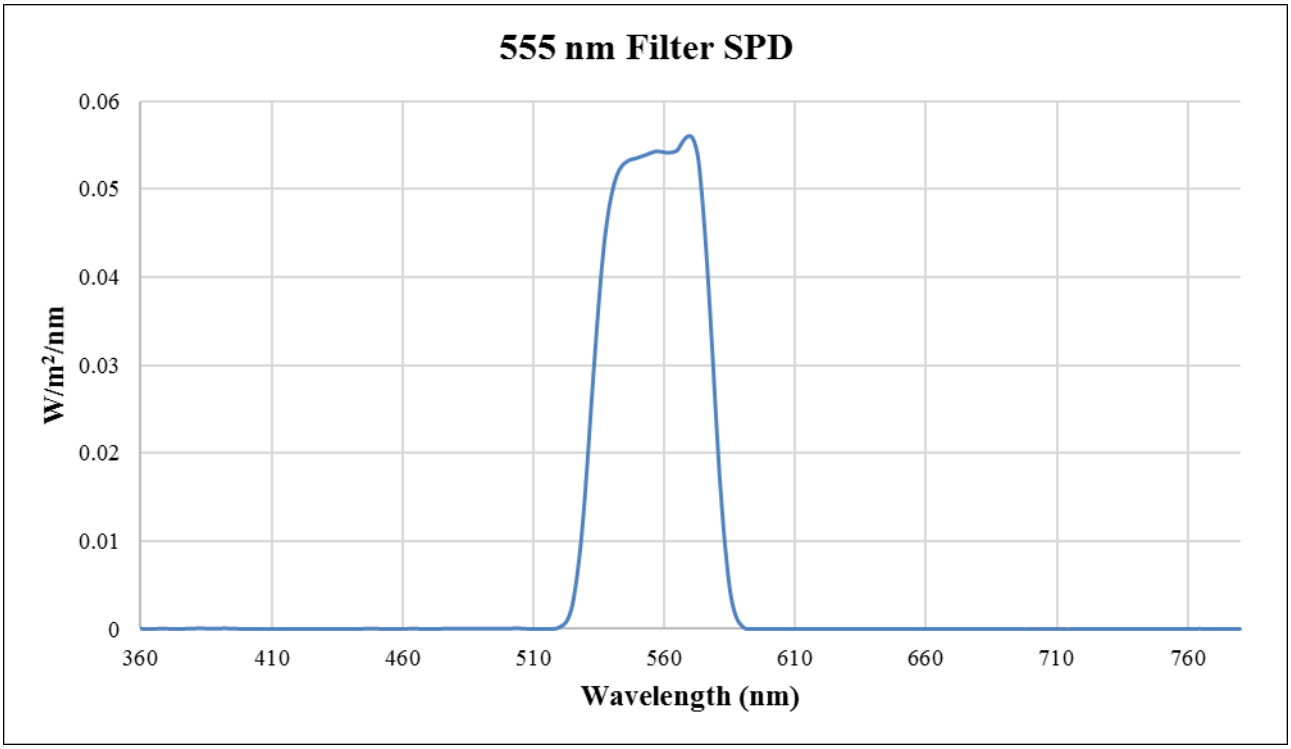
555 nm Filter SPD
0.06
0.05
0.04
0.03
0.02
0.01
0
W/m²/nm
360
410
460
510
560
610
660
710
760
Wavelength (nm)

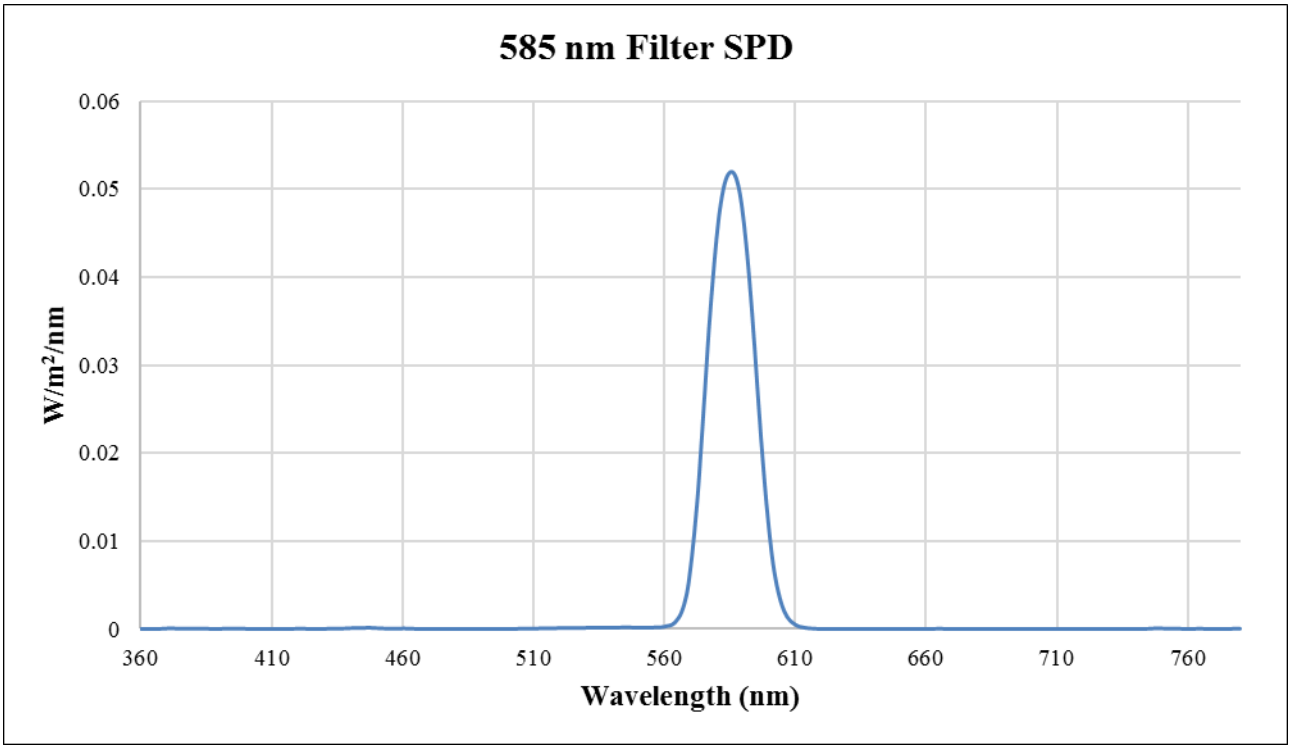
585 nm Filter SPD
0.06
0.05
0.04
0.03
0.02
0.01
0
W/m²/nm
360
410
460
510
560
610
660
710
760
Wavelength (nm)

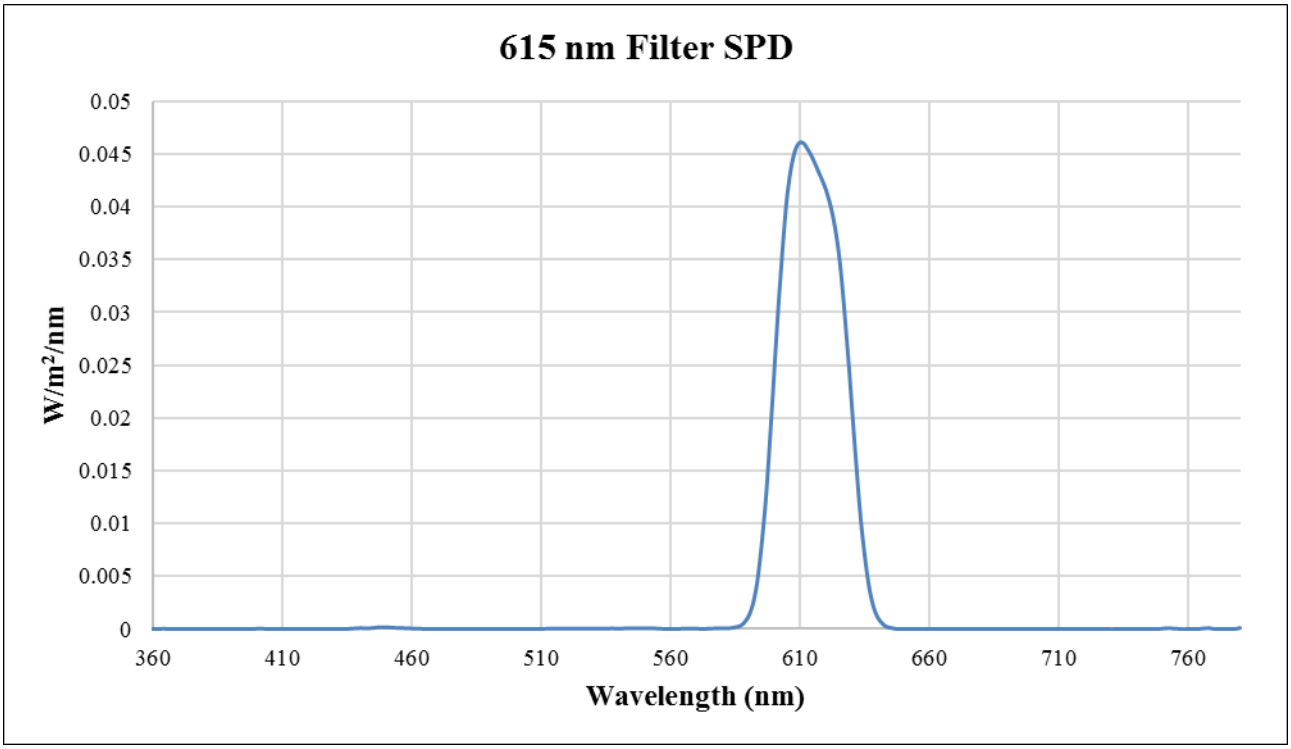
615 nm Filter SPD
0.05
0.045
0.04
0.035
0.03
0.025
0.02
0.015
0.01
0.005
0
W/m²/nm
360
410
460
510
560
610
660
710
760
Wavelength (nm)

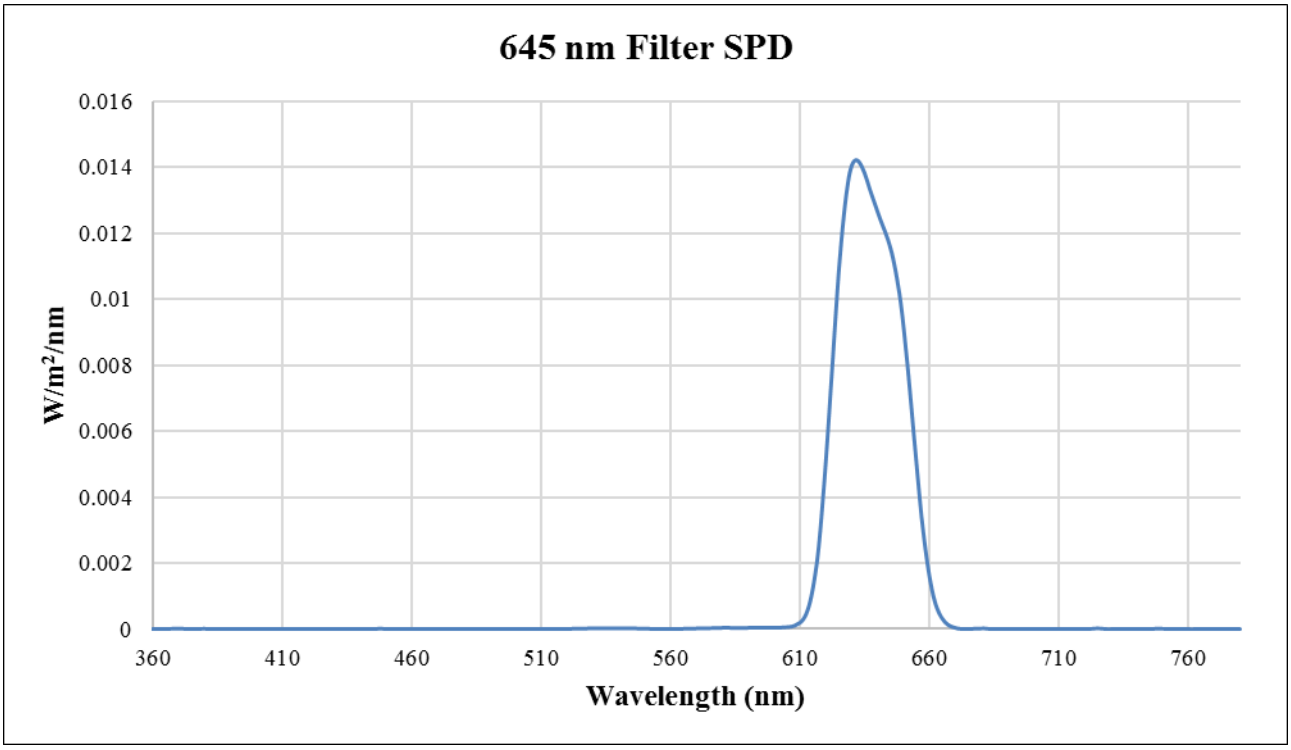
645 nm Filter SPD
0.016
0.014
0.012
0.01
0.008
0.006
0.004
0.002
0
W/m²/nm
360
410
460
510
560
610
660
710
760
Wavelength (nm)

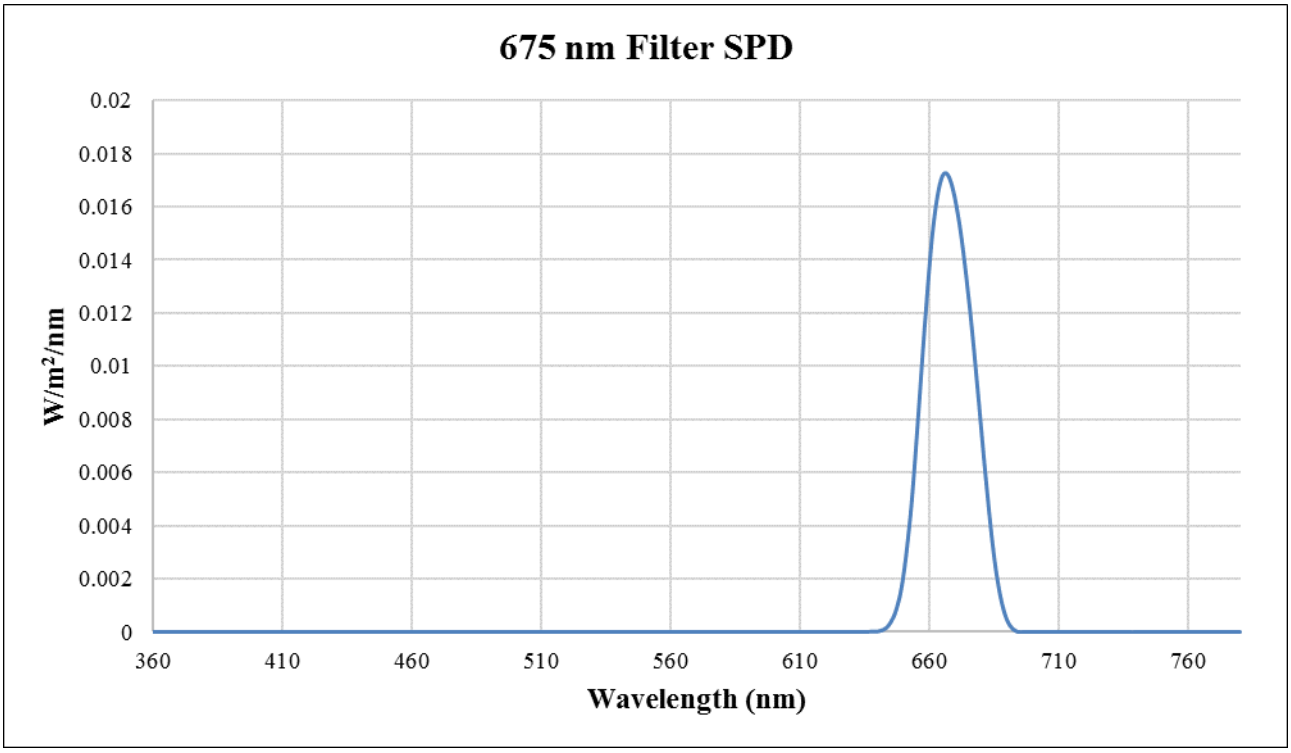
675 nm Filter SPD
0.02
0.018
0.016
0.014
0.012
0.01
0.008
0.006
0.004
0.002
0
W/m²/nm
360
410
460
510
560
610
660
710
760
Wavelength (nm)

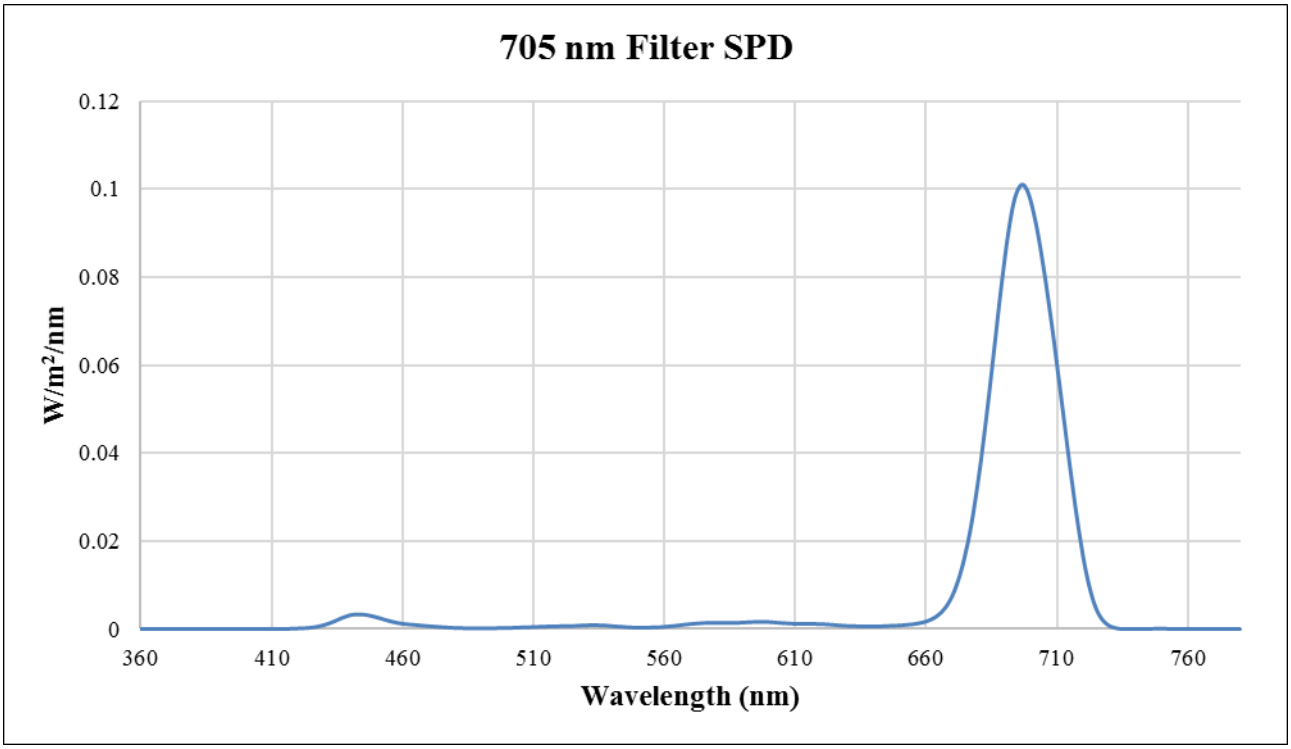
705 nm Filter SPD
0.12
0.1
0.08
0.06
0.04
0.02
0
W/m²/nm
360
410
460
510
560
610
660
710
760
Wavelength (nm)

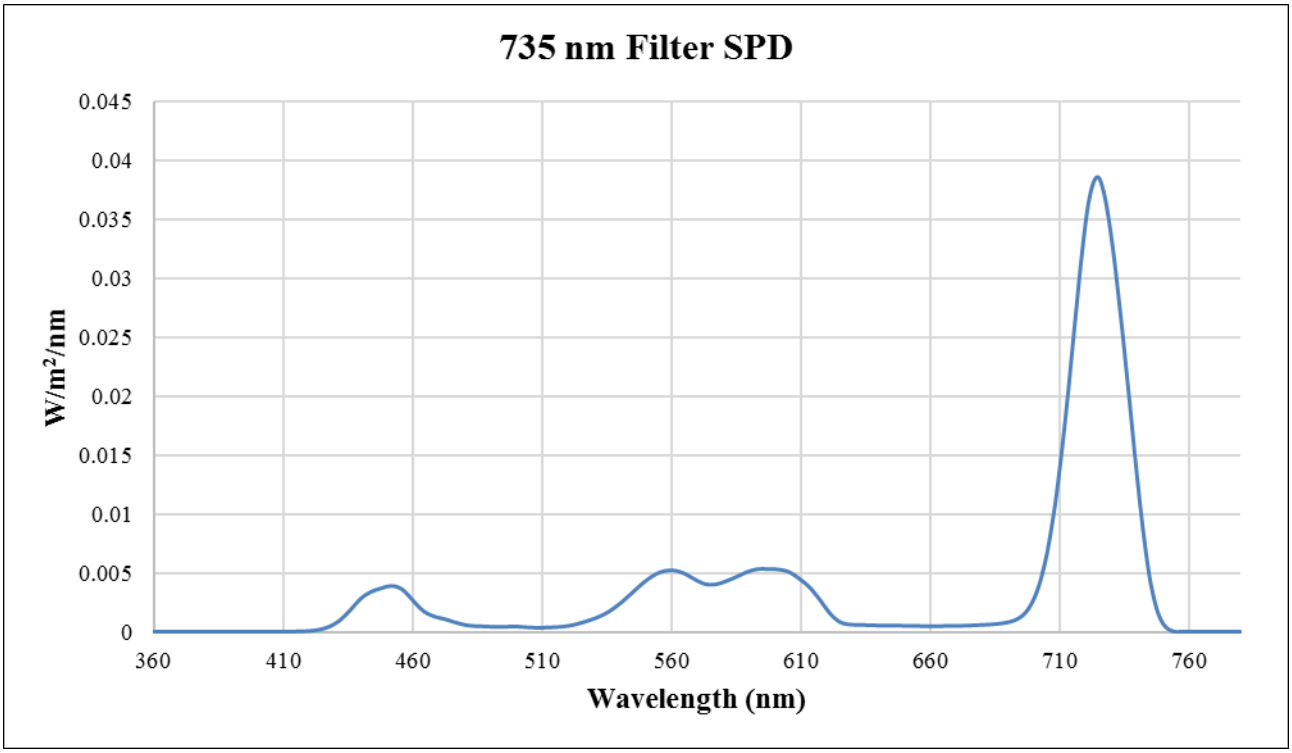
735 nm Filter SPD
0.045
0.04
0.035
0.03
0.025
0.02
0.015
0.01
0.005
0
W/m²/nm
360
410
460
510
560
610
660
710
760
Wavelength (nm)

Appendix B: Radiometric Versus Photometric Intensity

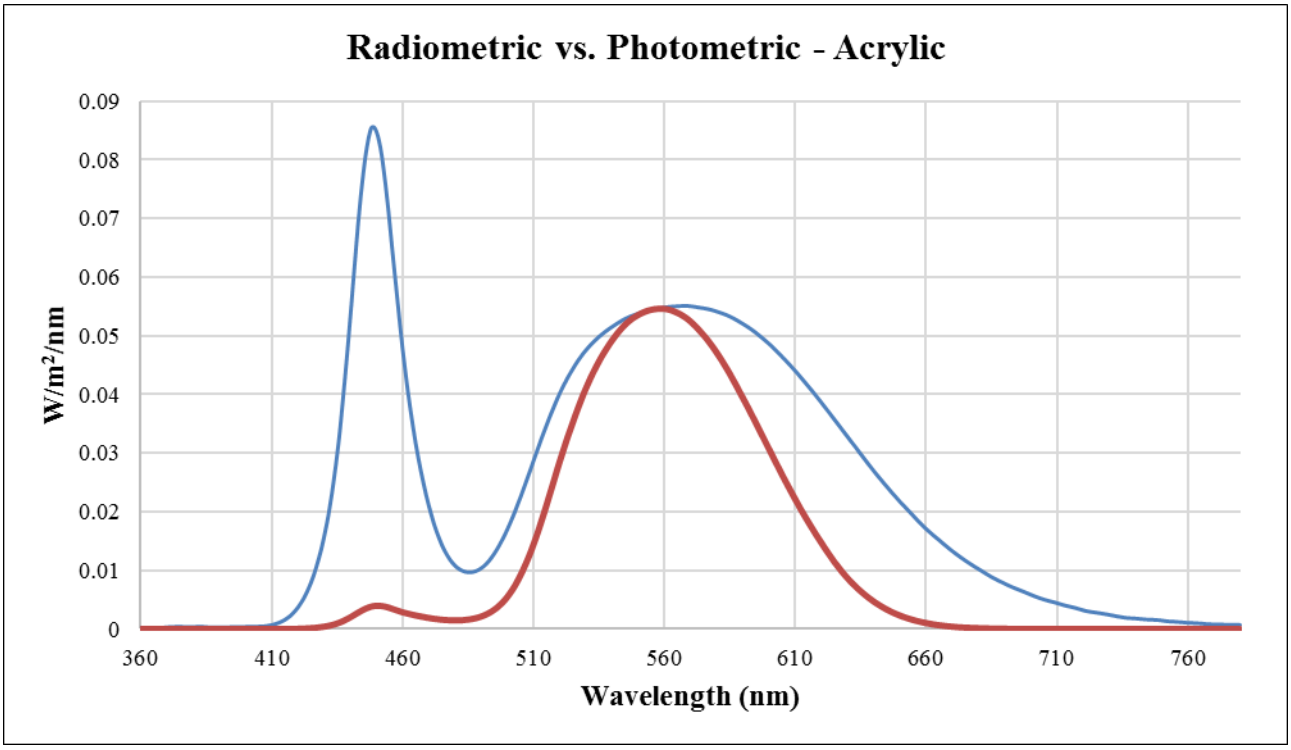

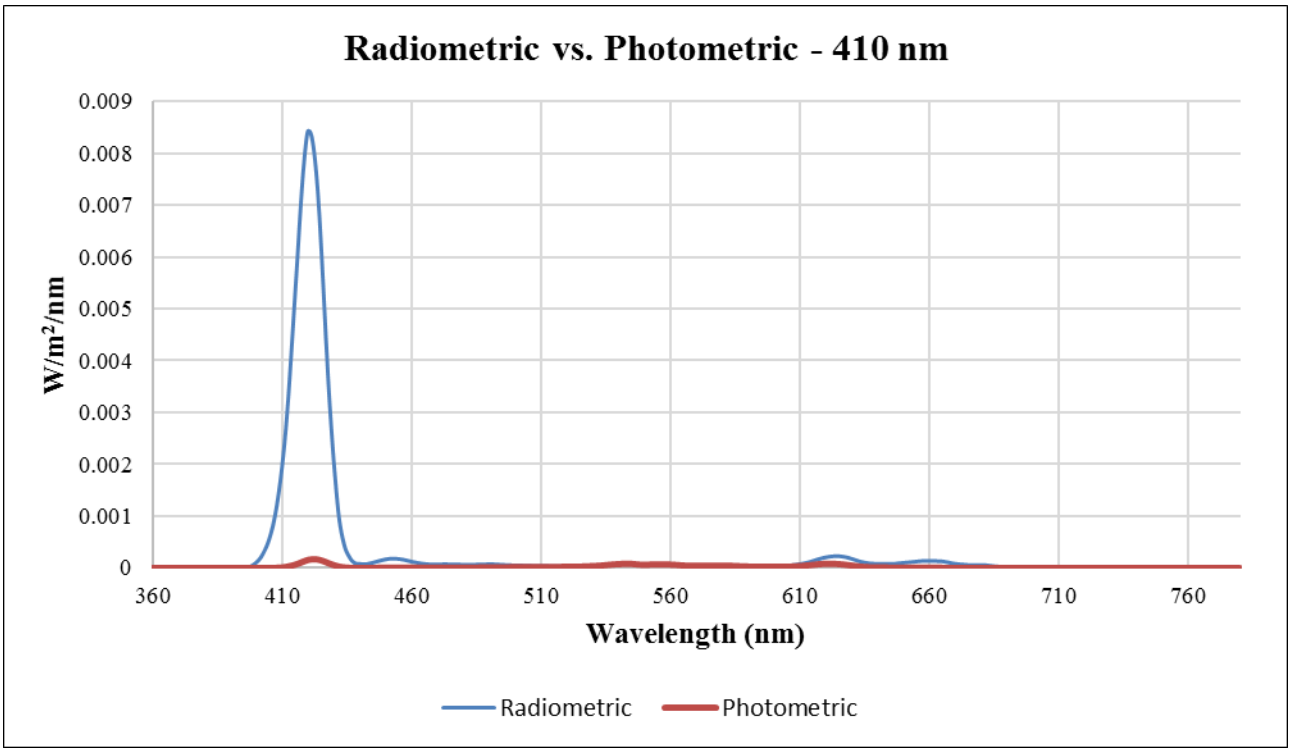

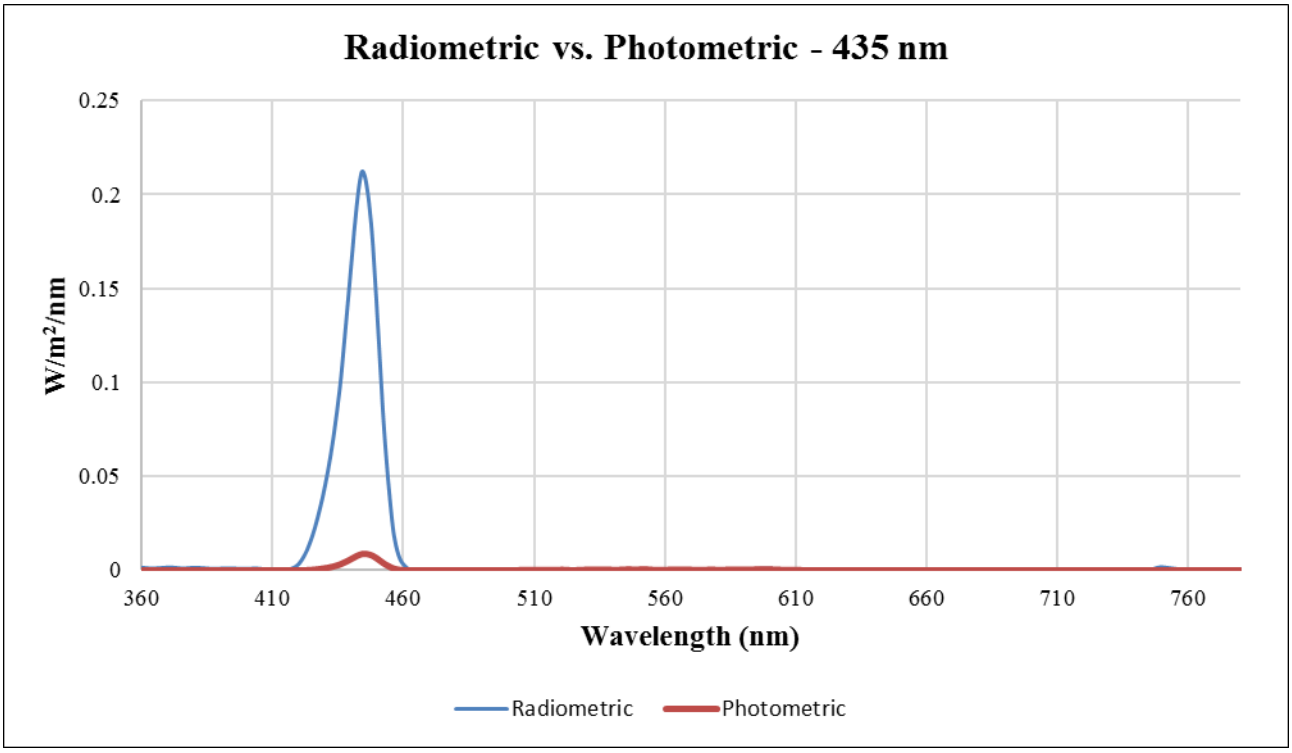
Radiometric vs. Photometric - 435 nm
0.25
0.2
0.15
0.1
0.05
0
W/m²/nm
360
410
460
510
560
610
660
710
760
Wavelength (nm)
Radiometric
Photometric

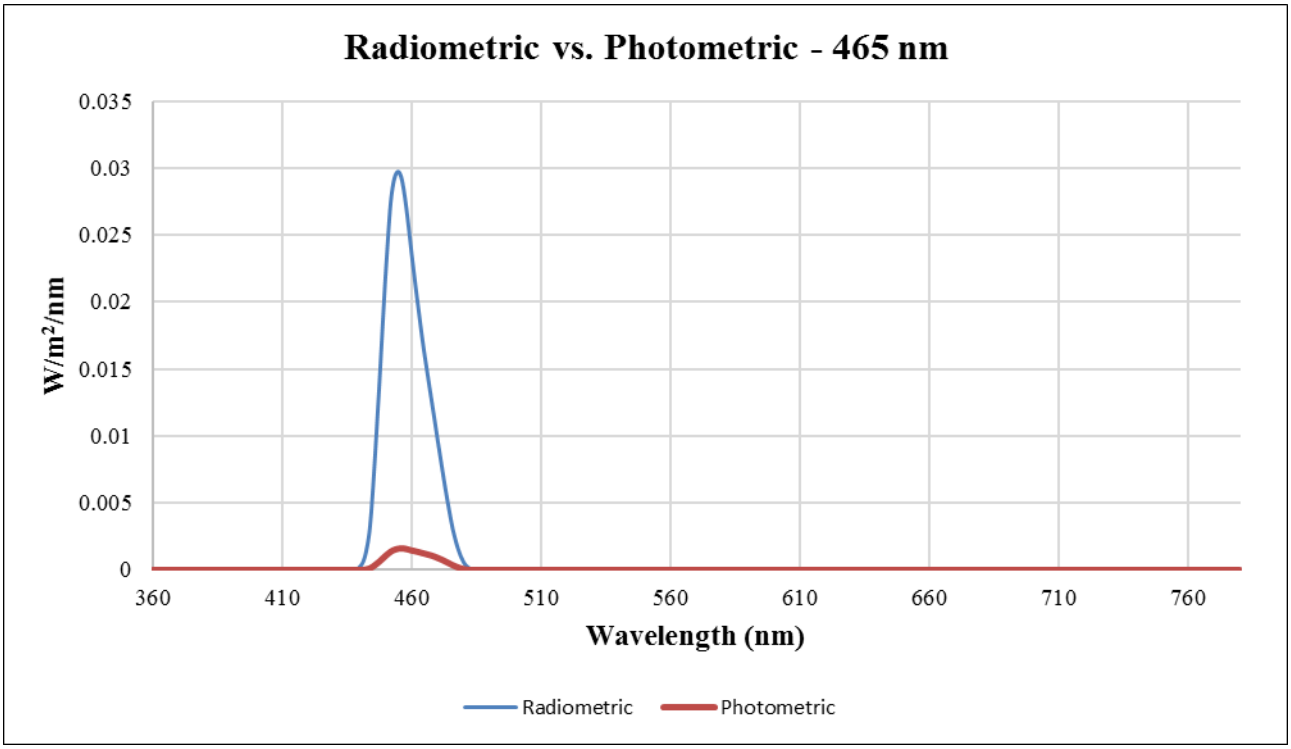
Radiometric vs. Photometric - 465 nm
0.035
0.03
0.025
0.02
0.015
0.01
0.005
0
W/m²/nm
360
410
460
510
560
610
660
710
760
Wavelength (nm)
Radiometric
Photometric

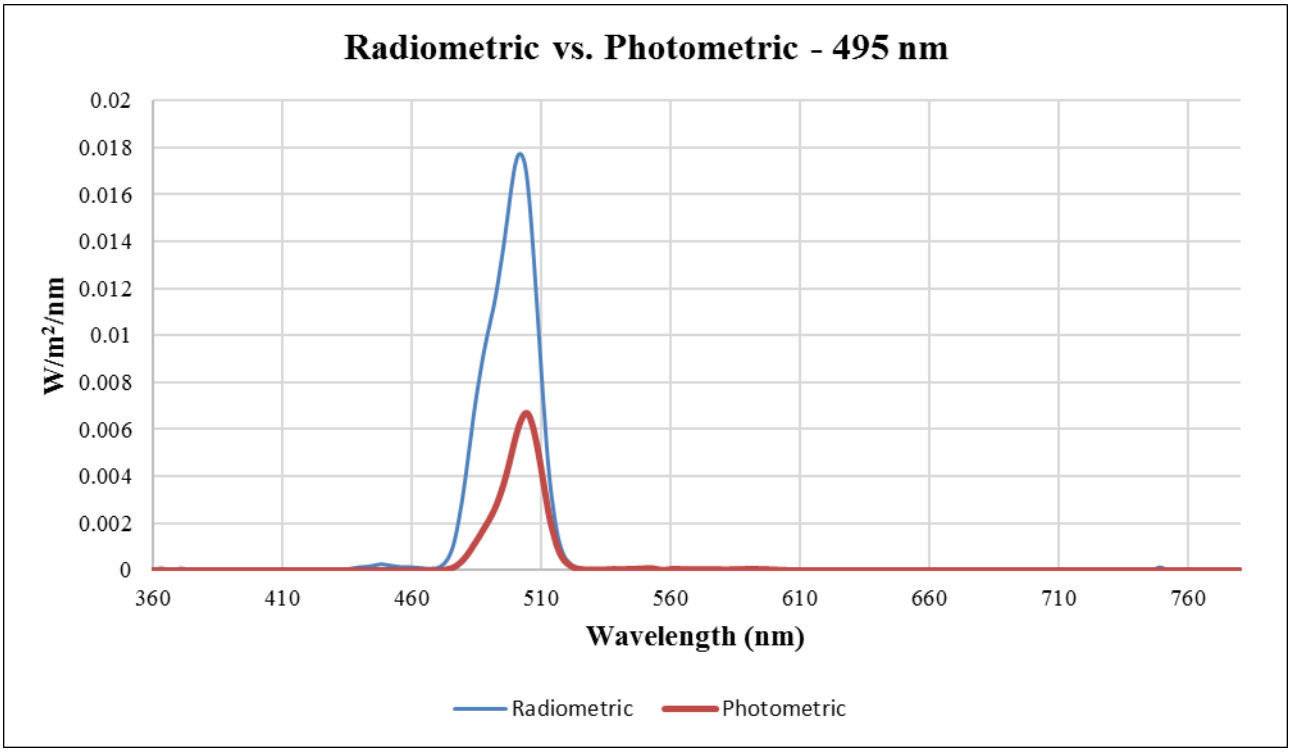
Radiometric vs. Photometric - 495 nm
0.02
0.018
0.016
0.014
0.012
0.01
0.008
0.006
0.004
0.002
0
W/m²/nm
360
410
460
510
560
610
660
710
760
Wavelength (nm)
Radiometric
Photometric

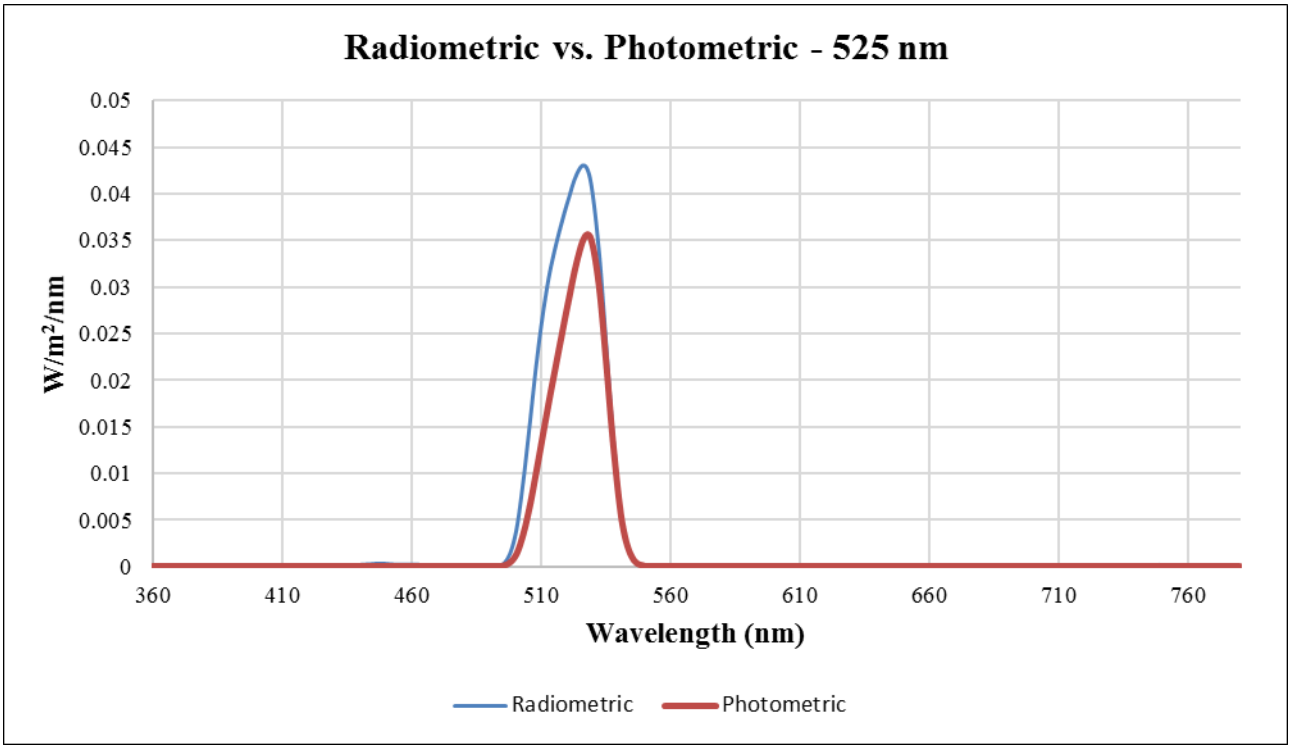
Radiometric vs. Photometric - 525 nm
0.05
0.045
0.04
0.035
0.03
0.025
0.02
0.015
0.01
0.005
0
W/m²/nm
360
410
460
510
560
610
660
710
760
Wavelength (nm)
Radiometric
Photometric

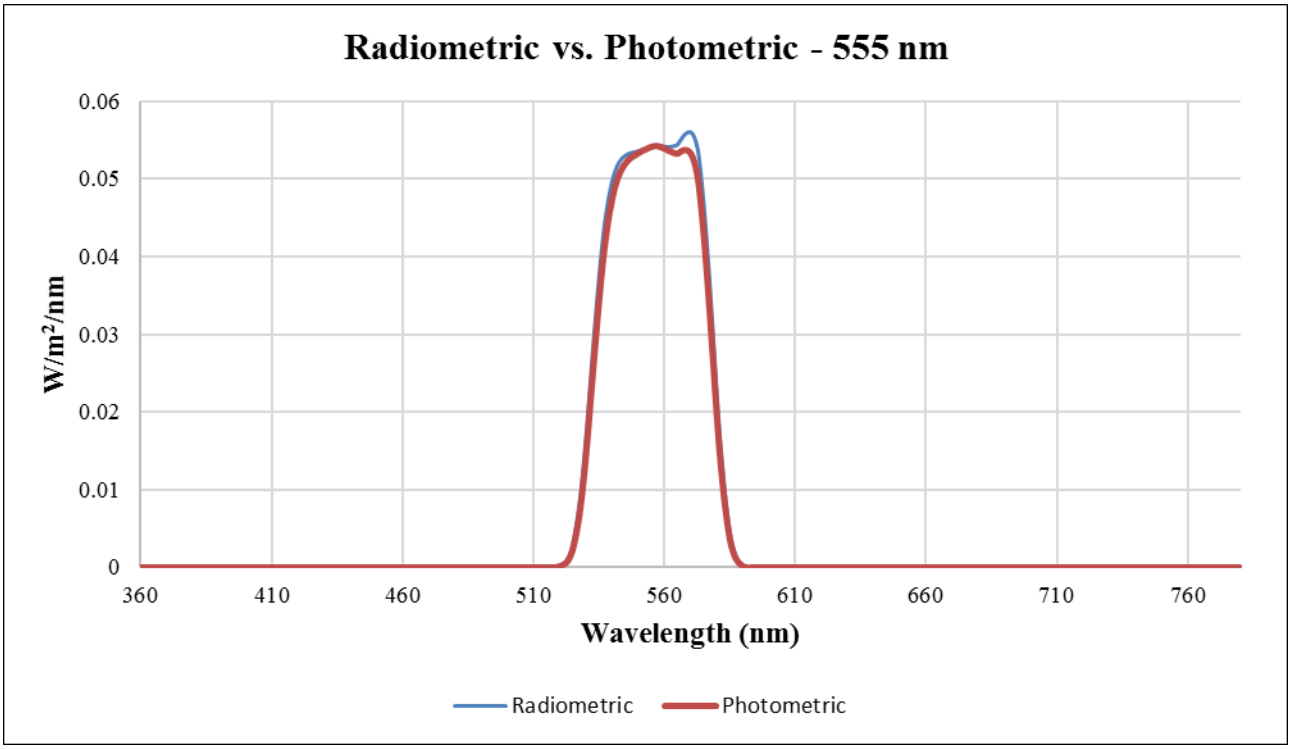
Radiometric vs. Photometric - 555 nm
0.06
0.05
0.04
0.03
0.02
0.01
0
W/m²/nm
360
410
460
510
560
610
660
710
760
Wavelength (nm)
Radiometric
Photometric

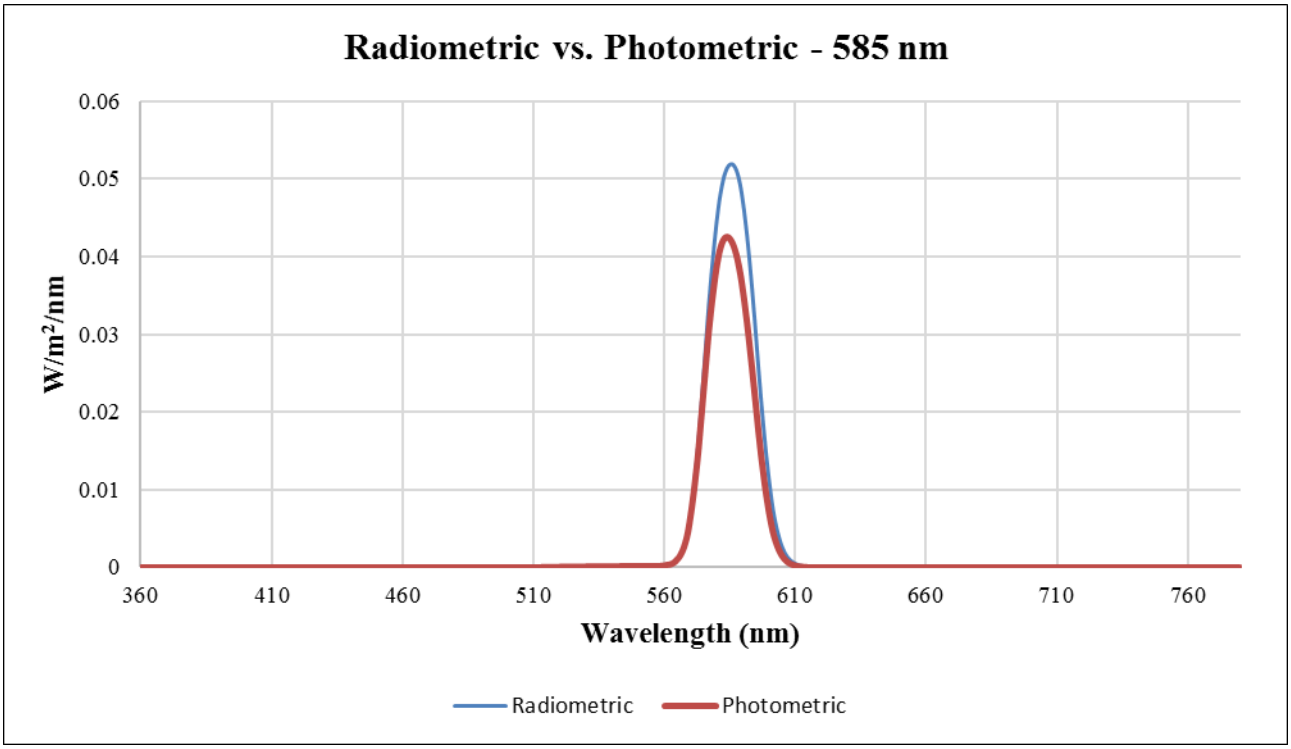
Radiometric vs. Photometric - 585 nm
0.06
0.05
0.04
0.03
0.02
0.01
0
W/m²/nm
360
410
460
510
560
610
660
710
760
Wavelength (nm)
Radiometric
Photometric

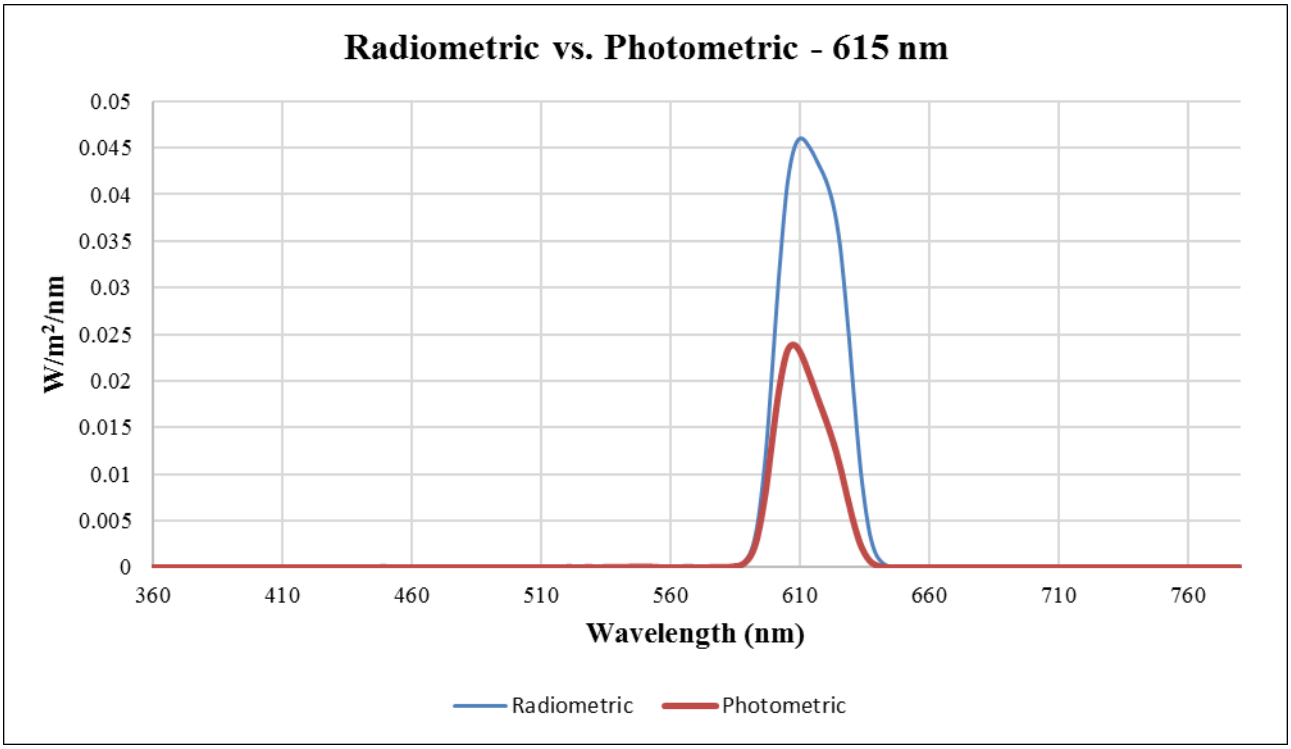
Radiometric vs. Photometric - 615 nm
0.05
0.045
0.04
0.035
0.03
0.025
0.02
0.015
0.01
0.005
0
W/m²/nm
360
410
460
510
560
610
660
710
760
Wavelength (nm)
Radiometric
Photometric

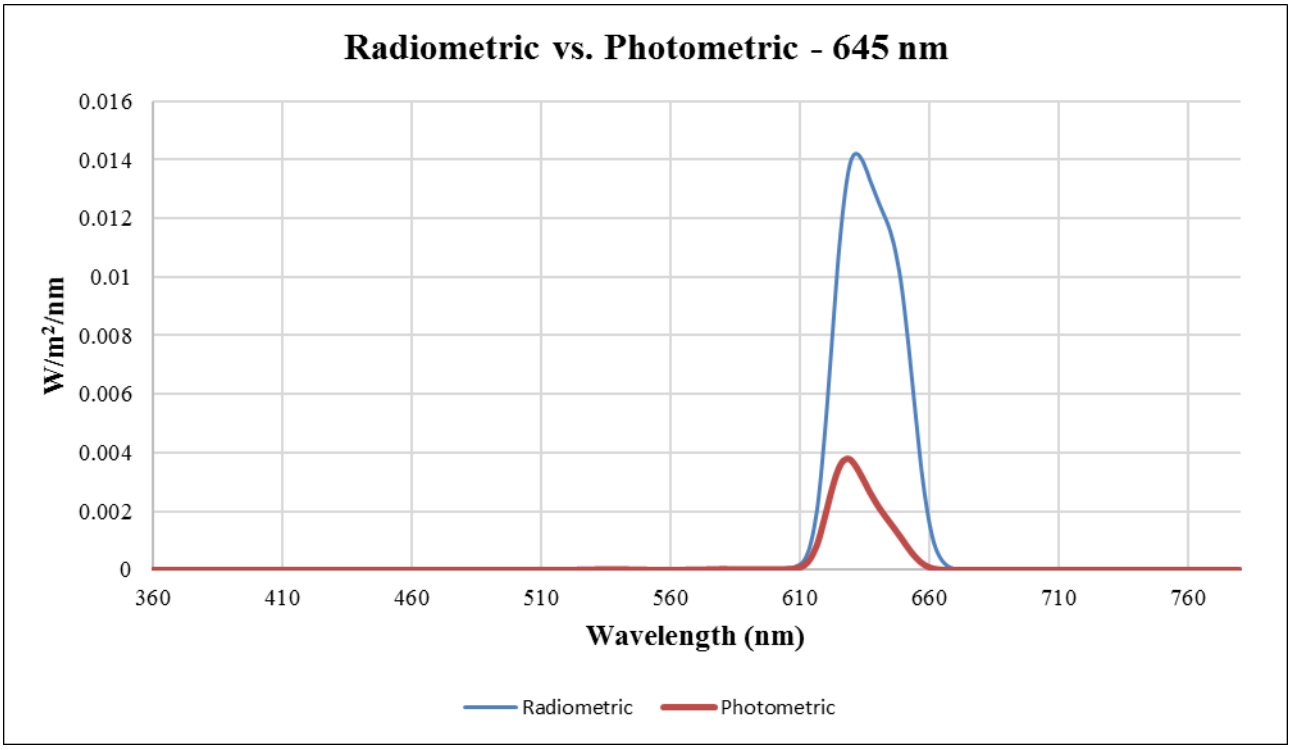
Radiometric vs. Photometric - 645 nm
0.016
0.014
0.012
0.01
0.008
0.006
0.004
0.002
0
W/m²/nm
360
410
460
510
560
610
660
710
760
Wavelength (nm)
Radiometric
Photometric

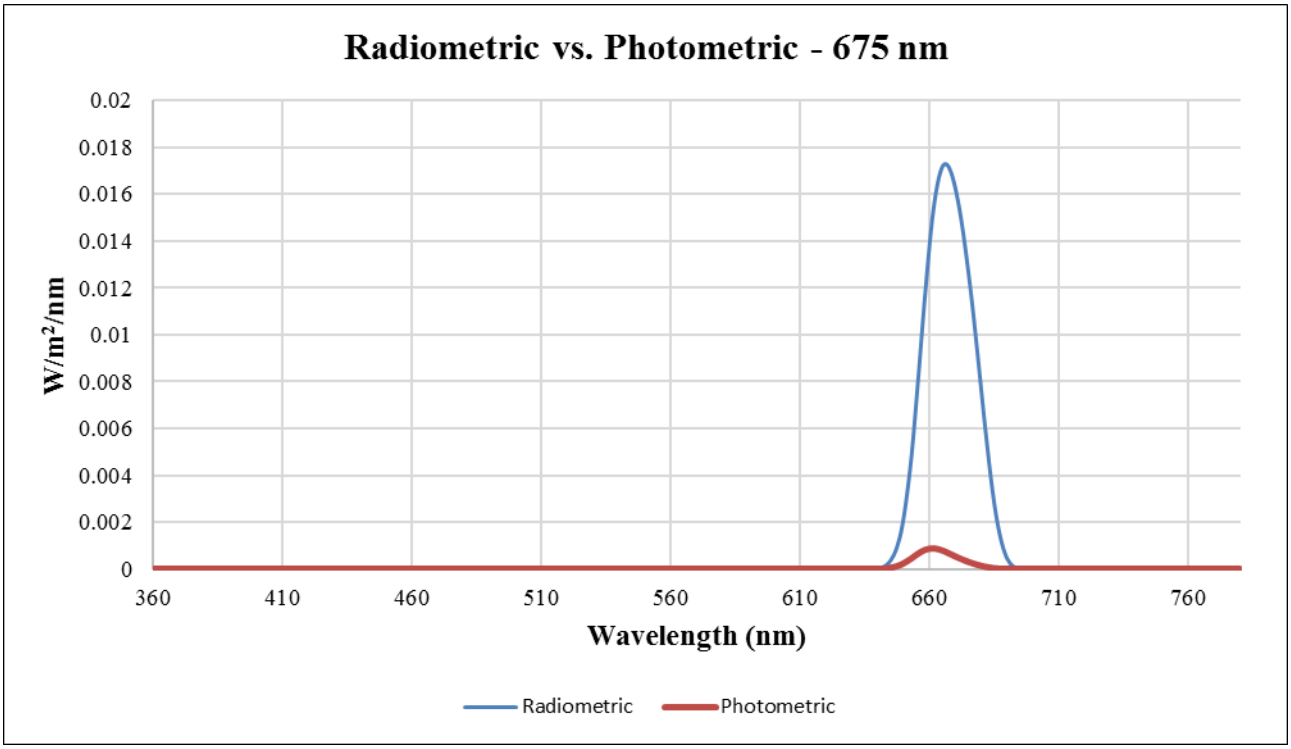
Radiometric vs. Photometric - 675 nm
0.02
0.018
0.016
0.014
0.012
0.01
0.008
0.006
0.004
0.002
0
W/m²/nm
360
410
460
510
560
610
660
710
760
Wavelength (nm)
Radiometric
Photometric

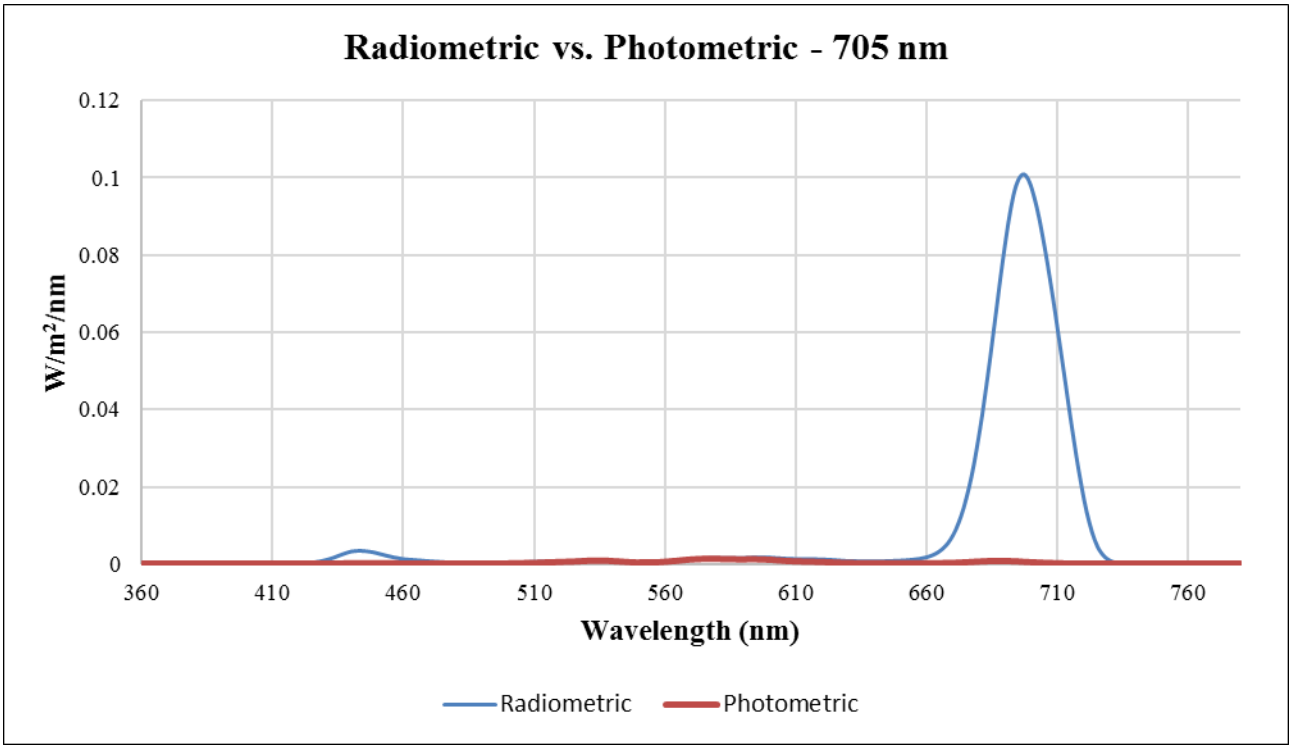
Radiometric vs. Photometric - 705 nm
0.12
0.1
0.08
0.06
0.04
0.02
0
W/m²/nm
360
410
460
510
560
610
660
710
760
Wavelength (nm)
Radiometric
Photometric

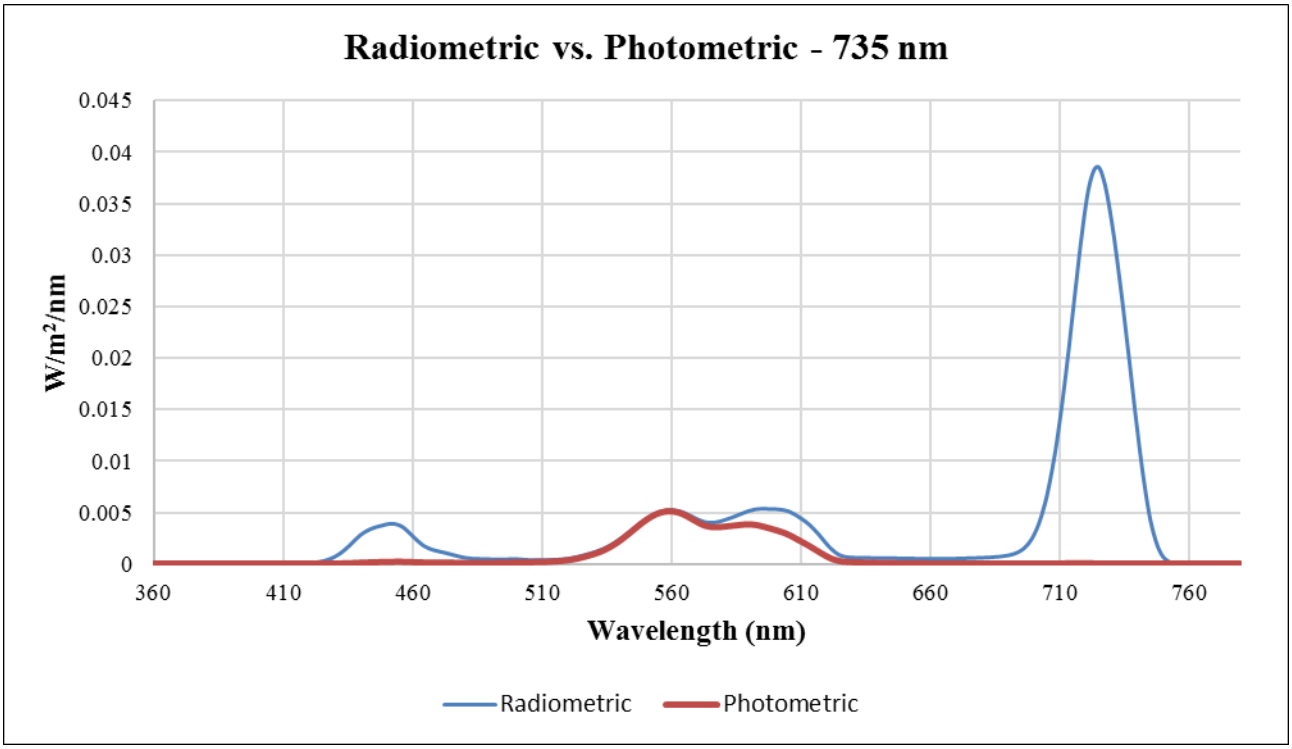
Radiometric vs. Photometric - 735 nm
0.045
0.04
0.035
0.03
0.025
0.02
0.015
0.01
0.005
0
W/m²/nm
360
410
460
510
560
610
660
710
760
Wavelength (nm)
Radiometric
Photometric

Appendix C: Filter Photometric Responses

*Photopic corrected spectrum only (multiplied by V(λ))

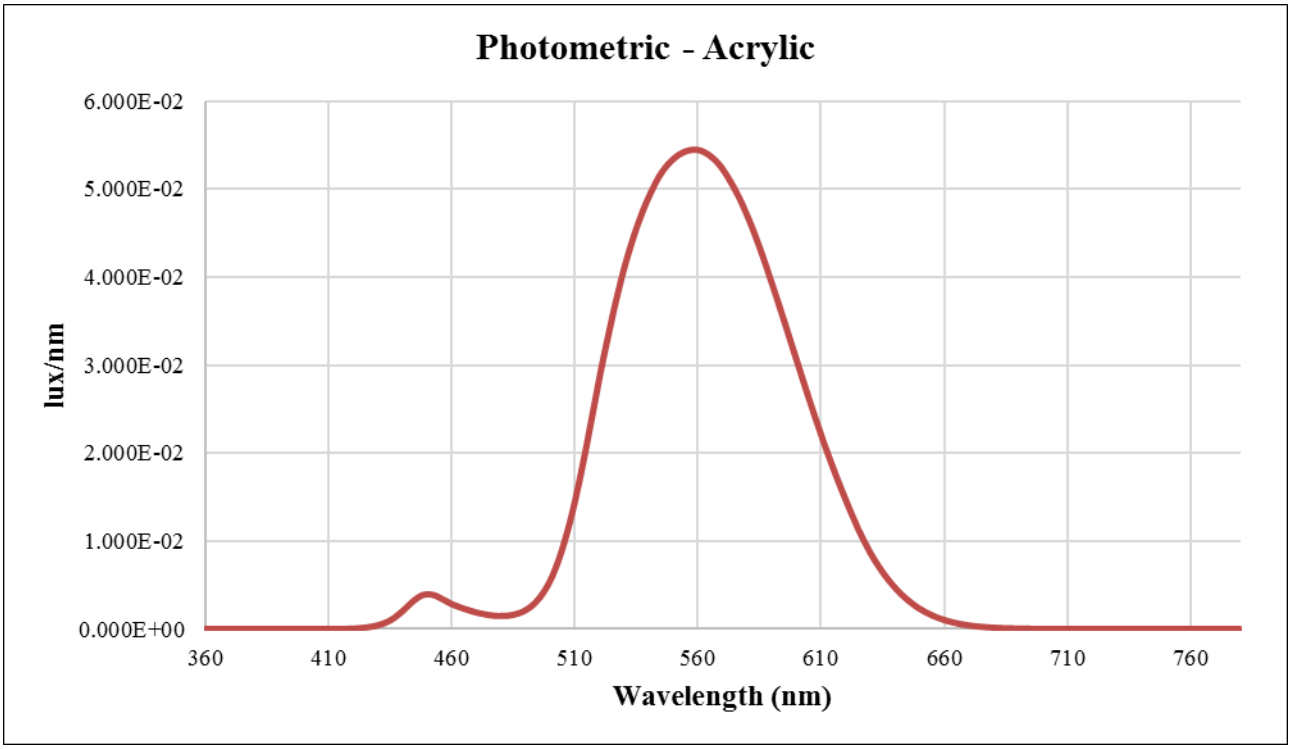

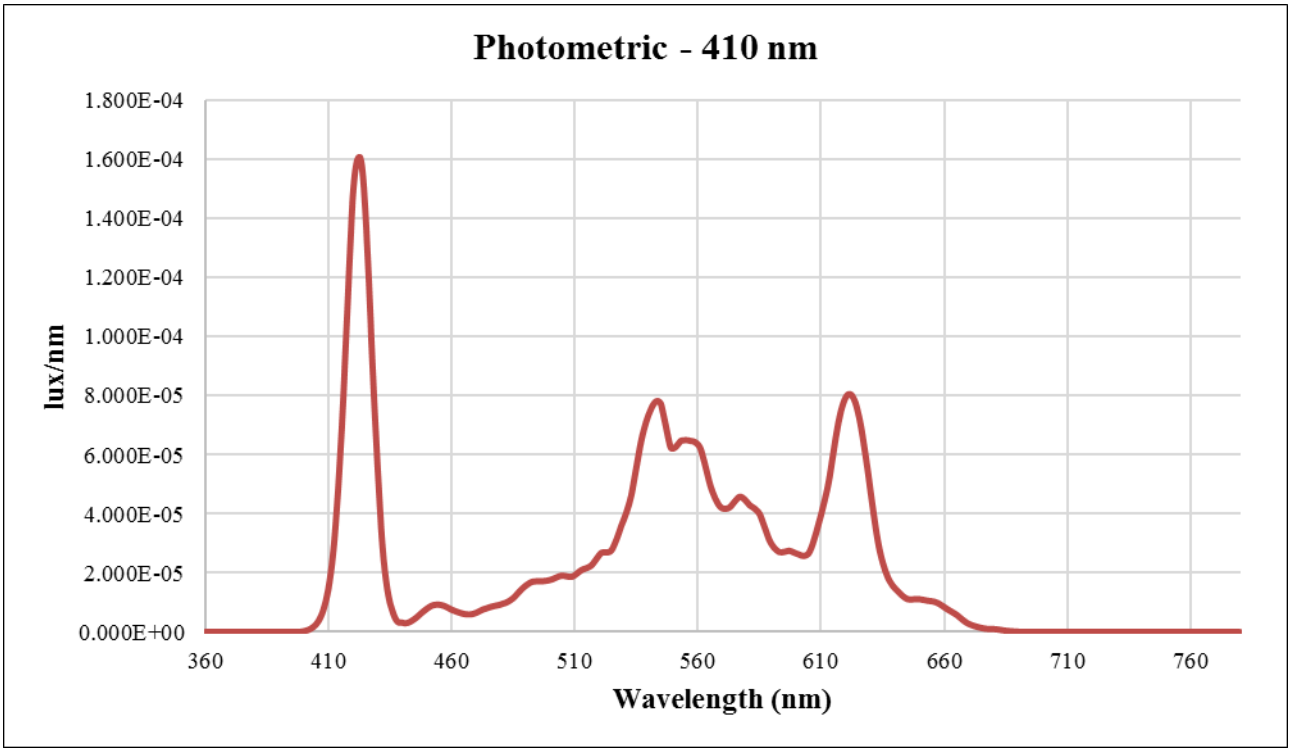

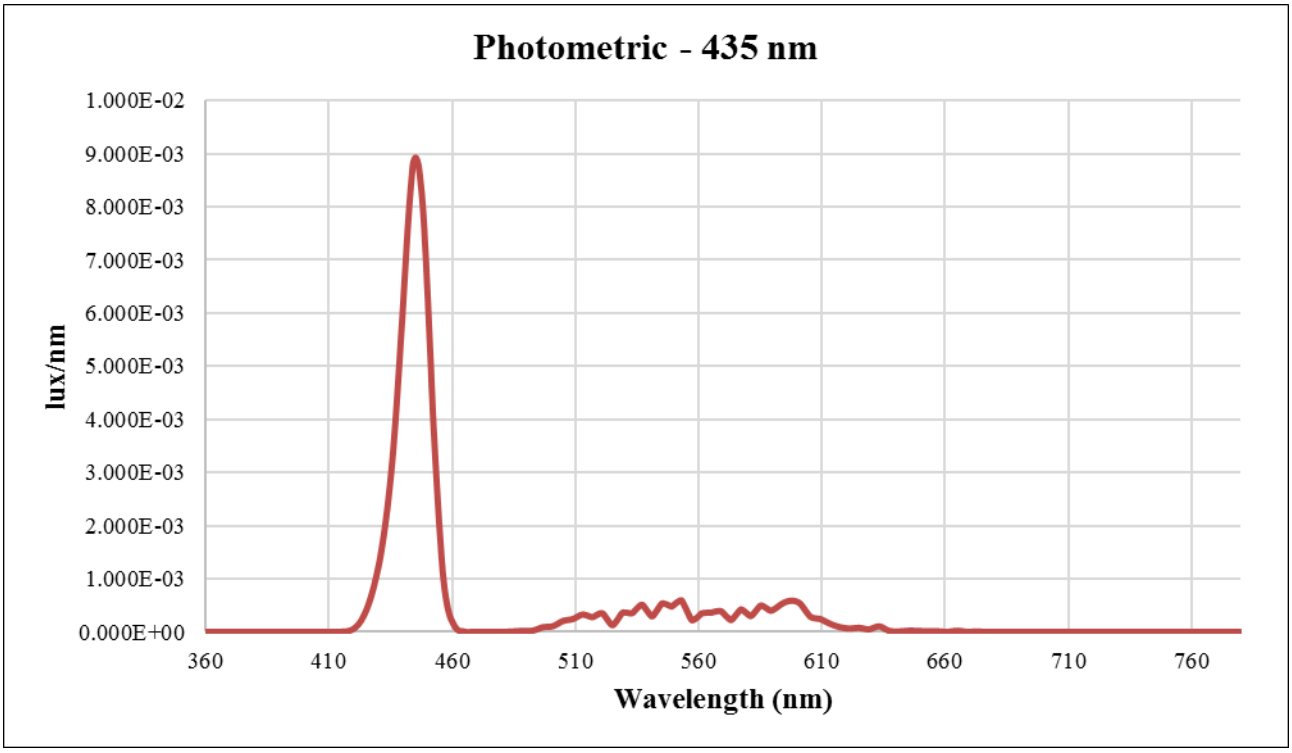
Photometric - 435 nm
1.000E-02
9.000E-03
8.000E-03
7.000E-03
6.000E-03
5.000E-03
4.000E-03
3.000E-03
2.000E-03
1.000E-03
0.000E+00
lux/nm
360
410
460
510
560
610
660
710
760
Wavelength (nm)

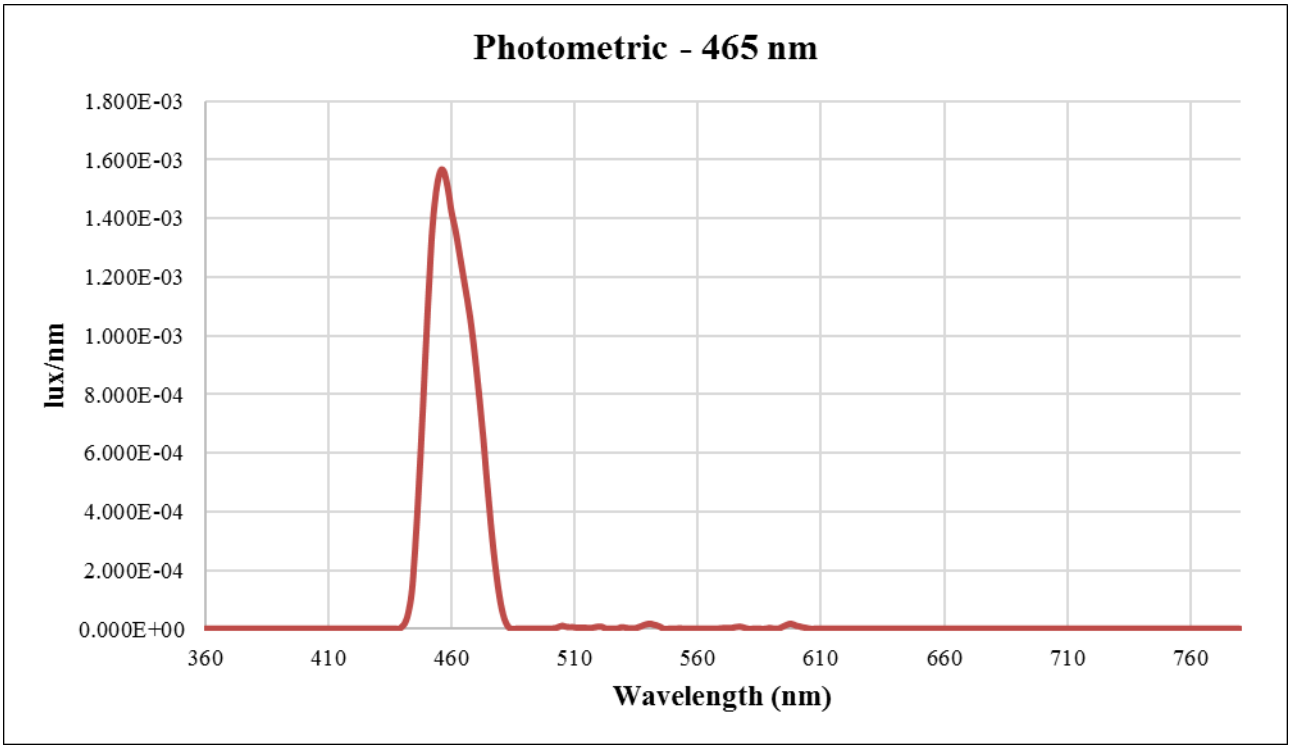
Photometric - 465 nm
1.800E-03
1.600E-03
1.400E-03
1.200E-03
1.000E-03
8.000E-04
6.000E-04
4.000E-04
2.000E-04
0.000E+00
lux/nm
360
410
460
510
560
610
660
710
760
Wavelength (nm)

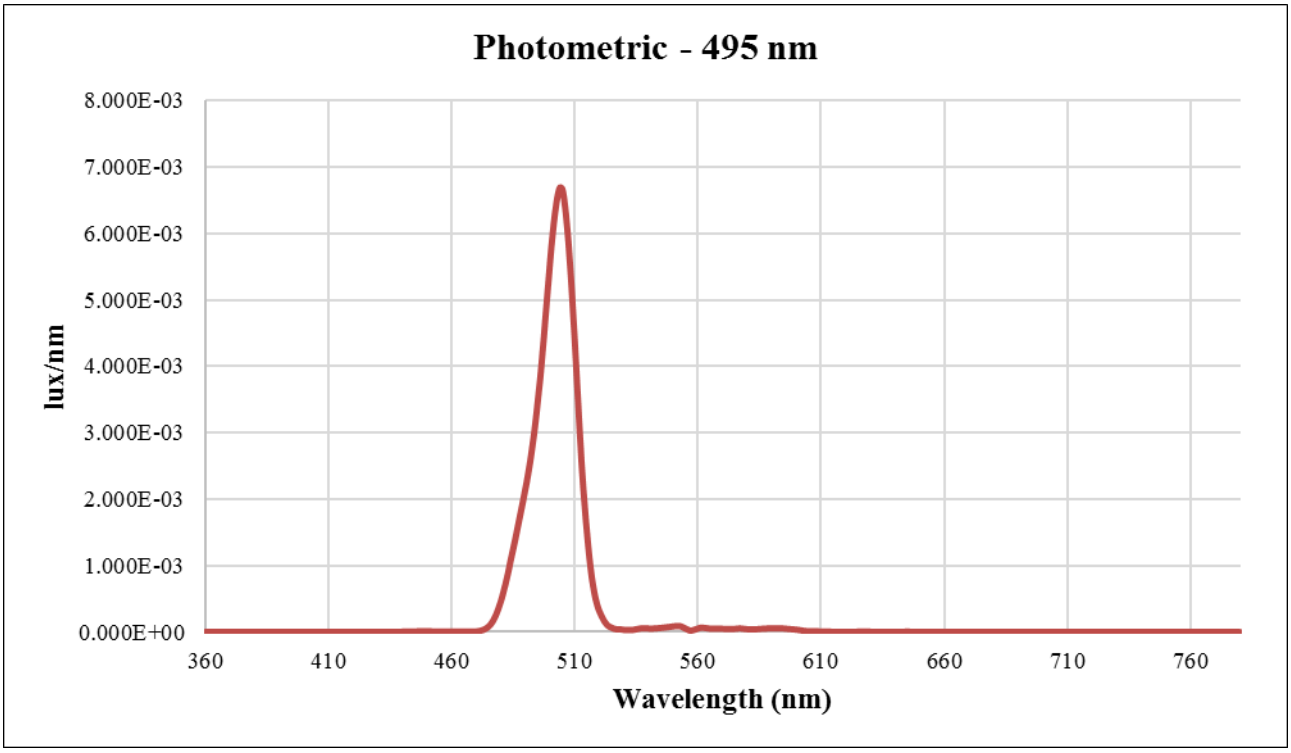
Photometric - 495 nm
8.000E-03
7.000E-03
6.000E-03
5.000E-03
4.000E-03
3.000E-03
2.000E-03
1.000E-03
0.000E+00
lux/nm
360
410
460
510
560
610
660
710
760
Wavelength (nm)

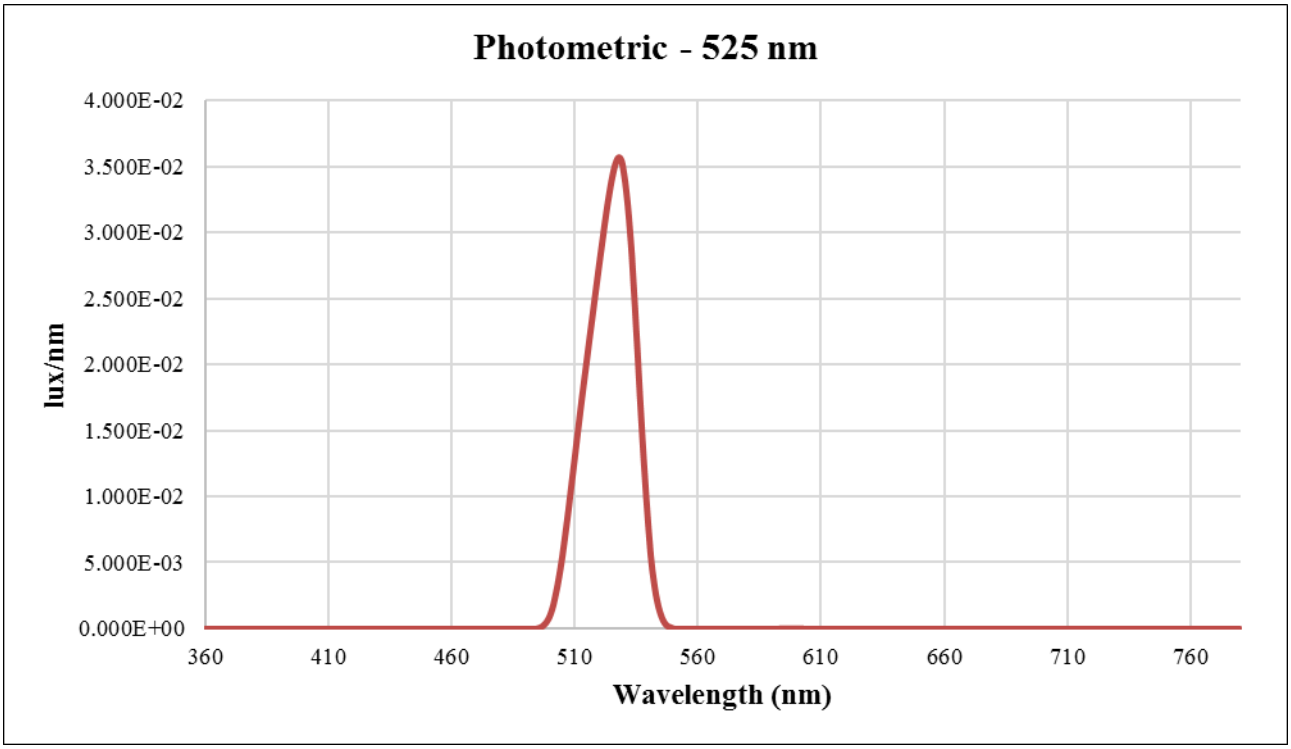
Photometric - 525 nm
4.000E-02
3.500E-02
3.000E-02
2.500E-02
2.000E-02
1.500E-02
1.000E-02
5.000E-03
0.000E+00
lux/nm
360
410
460
510
560
610
660
710
760
Wavelength (nm)

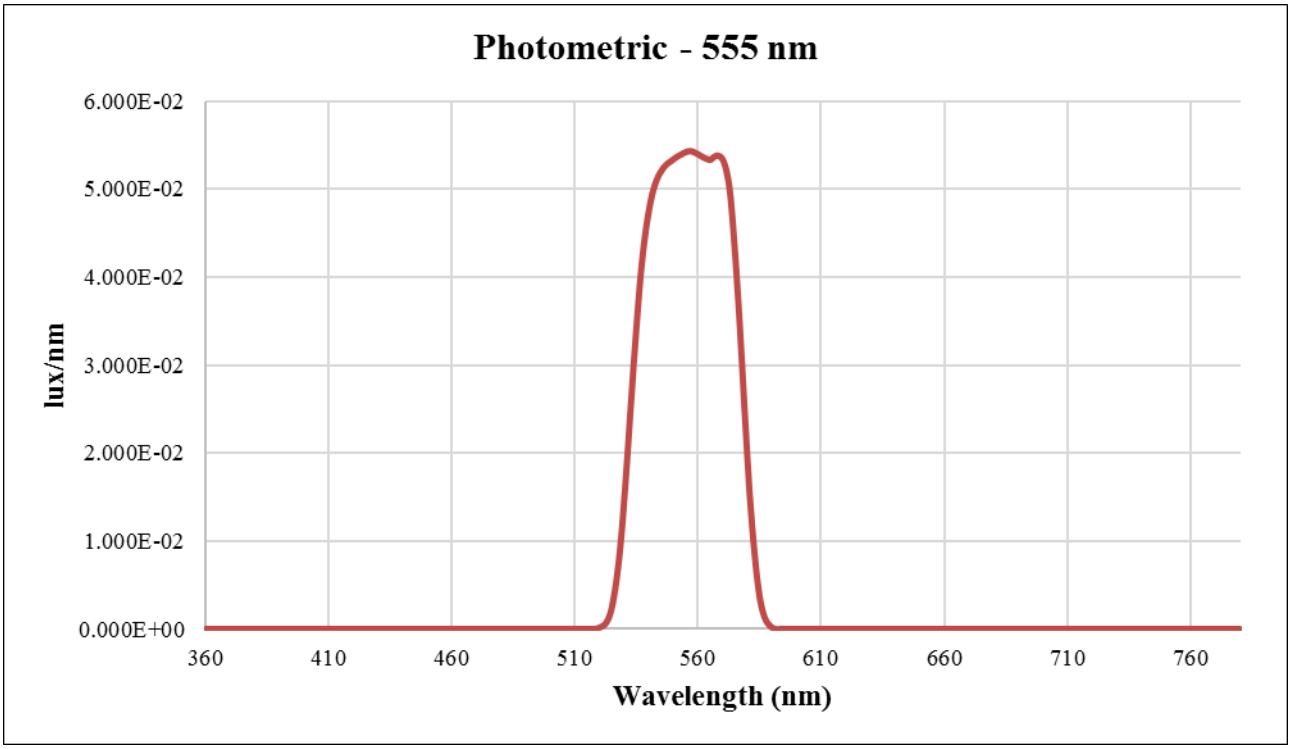
Photometric - 555 nm
6.000E-02
5.000E-02
4.000E-02
3.000E-02
2.000E-02
1.000E-02
0.000E+00
lux/nm
360
410
460
510
560
610
660
710
760
Wavelength (nm)

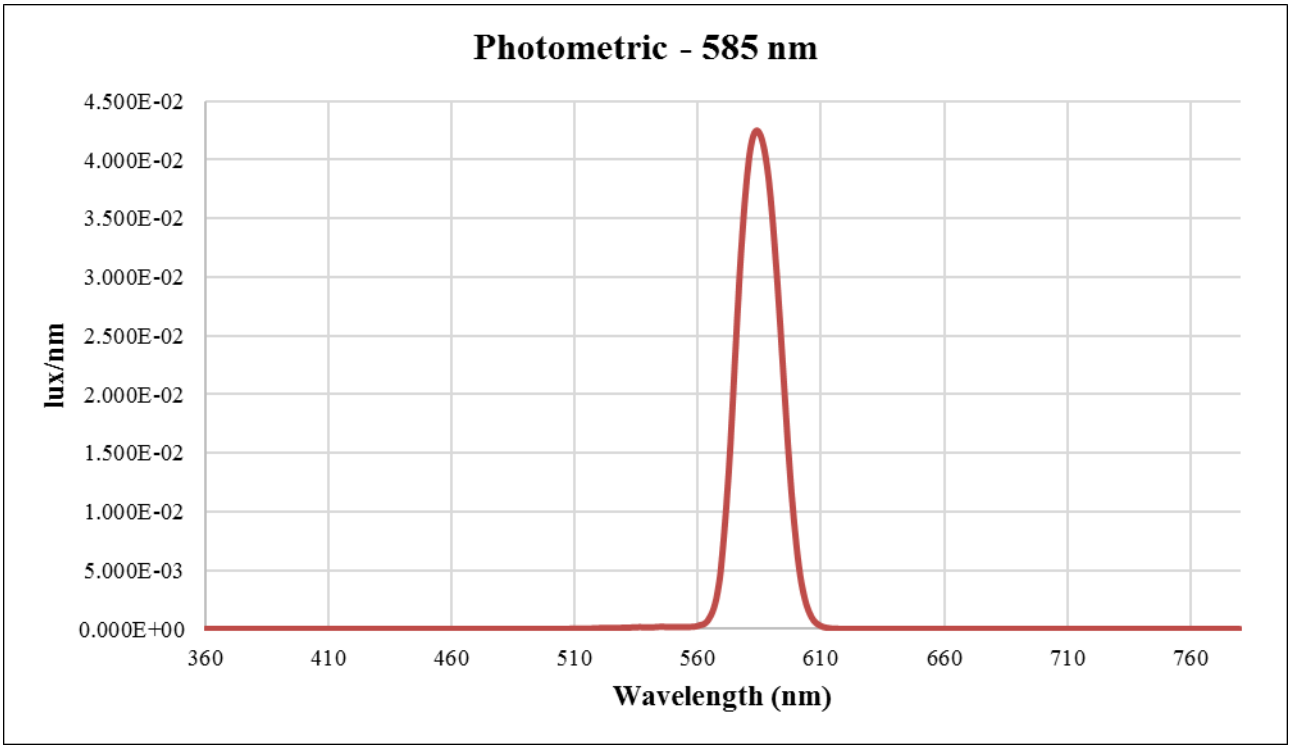
Photometric - 585 nm
4.500E-02
4.000E-02
3.500E-02
3.000E-02
2.500E-02
2.000E-02
1.500E-02
1.000E-02
5.000E-03
0.000E+00
lux/nm
360
410
460
510
560
610
660
710
760
Wavelength (nm)

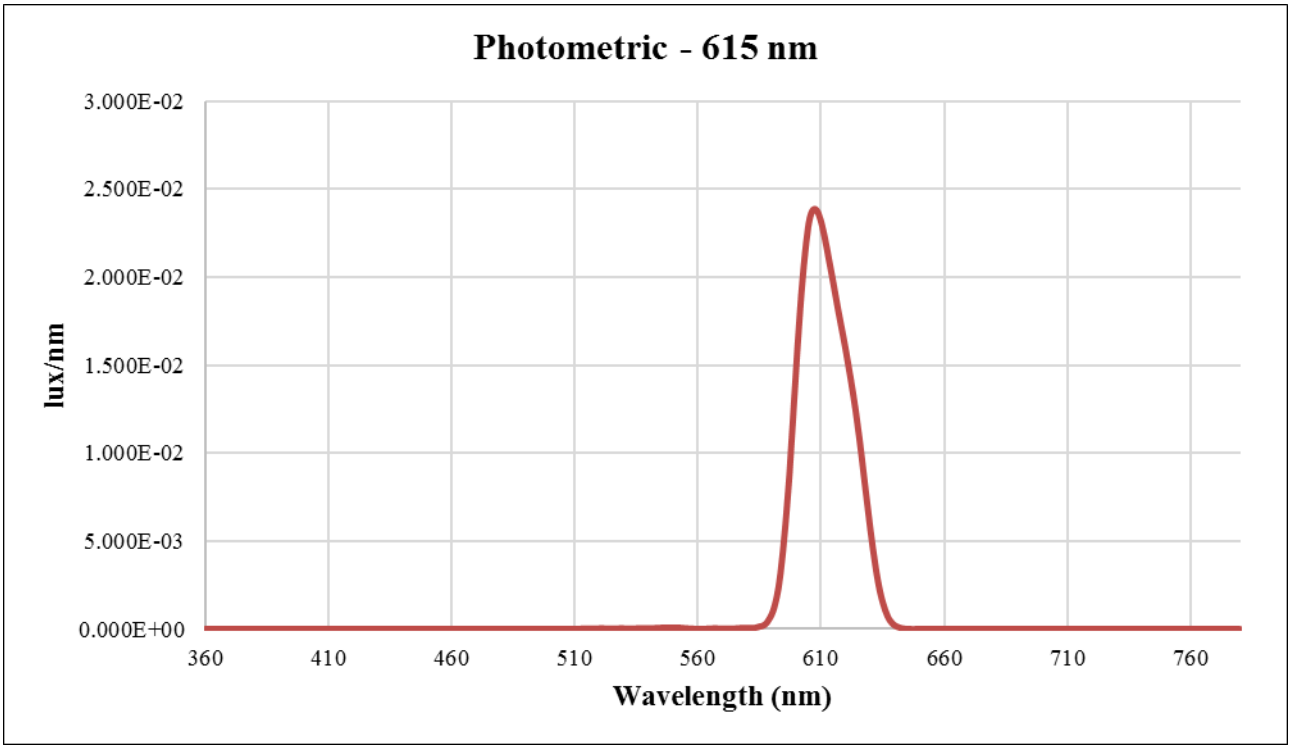
Photometric - 615 nm
3.000E-02
2.500E-02
2.000E-02
1.500E-02
1.000E-02
5.000E-03
0.000E+00
lux/nm
360
410
460
510
560
610
660
710
760
Wavelength (nm)

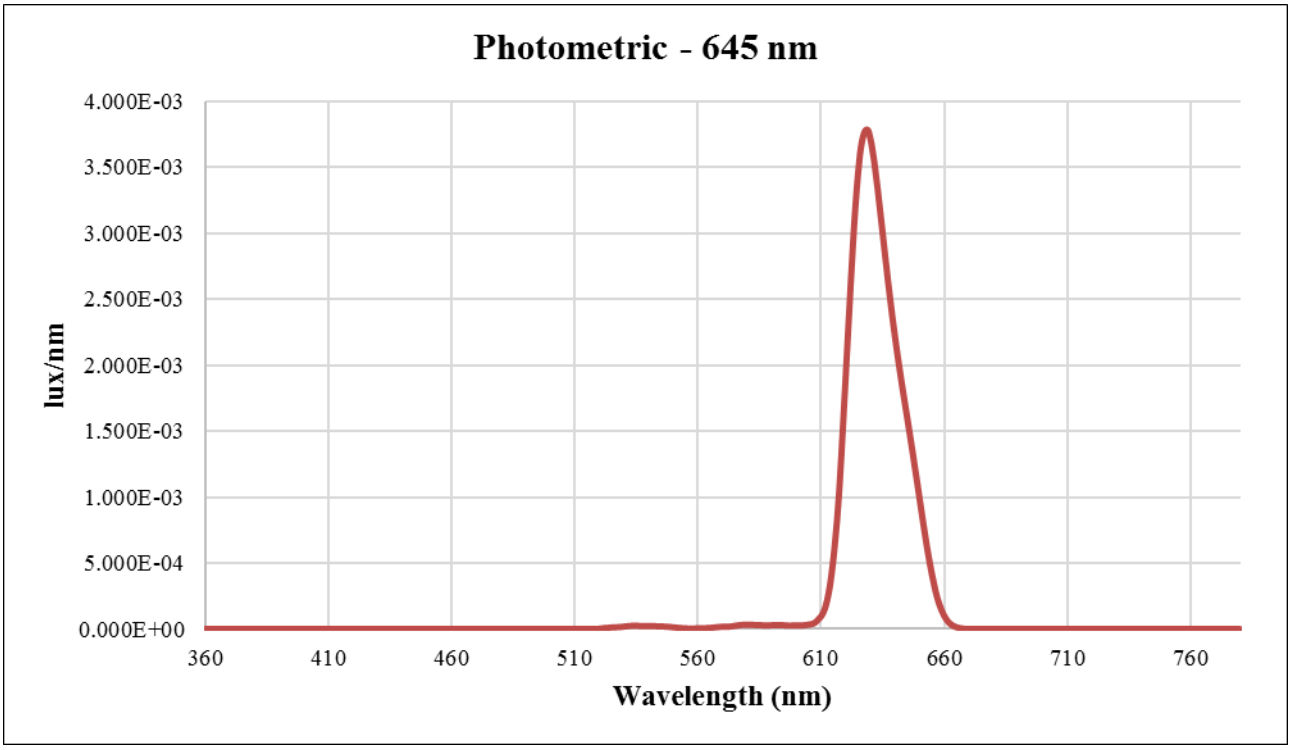
Photometric - 645 nm
4.000E-03
3.500E-03
3.000E-03
2.500E-03
2.000E-03
1.500E-03
1.000E-03
5.000E-04
0.000E+00
lux/nm
360
410
460
510
560
610
660
710
760
Wavelength (nm)

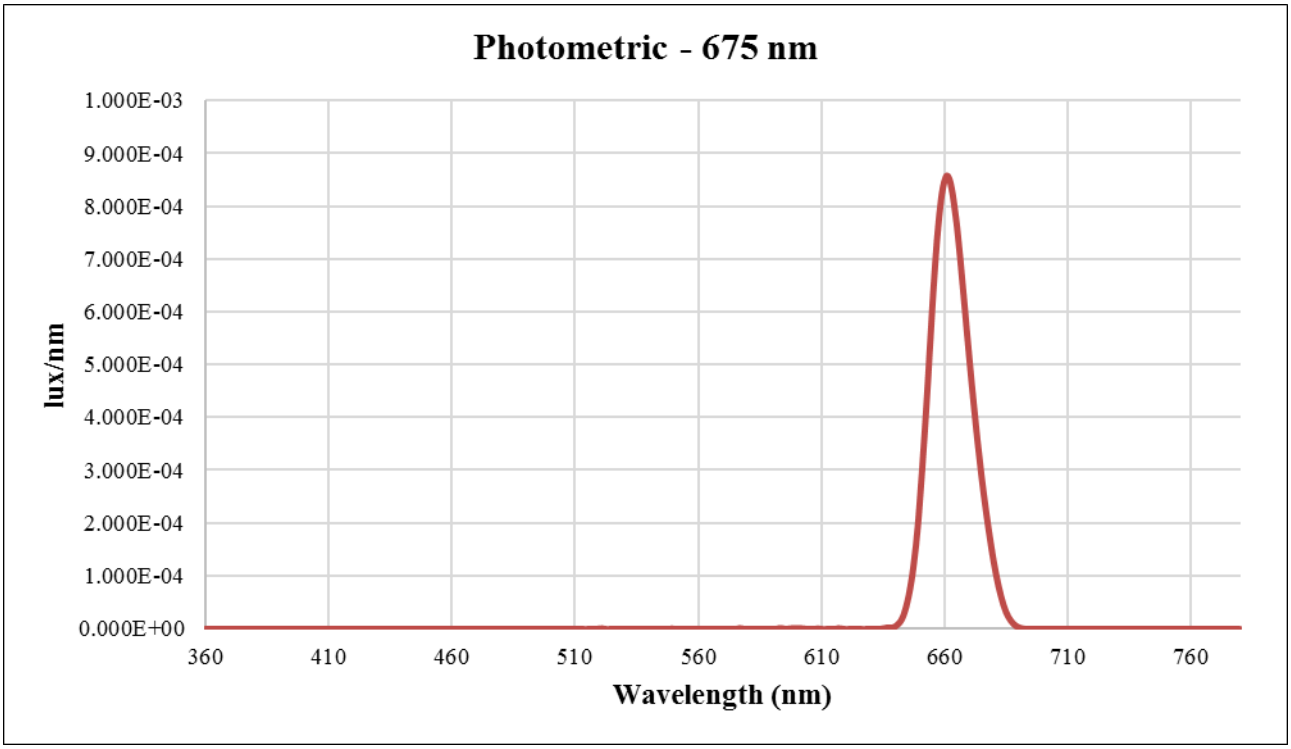
Photometric - 675 nm
1.000E-03
9.000E-04
8.000E-04
7.000E-04
6.000E-04
5.000E-04
4.000E-04
3.000E-04
2.000E-04
1.000E-04
0.000E+00
lux/nm
360
410
460
510
560
610
660
710
760
Wavelength (nm)

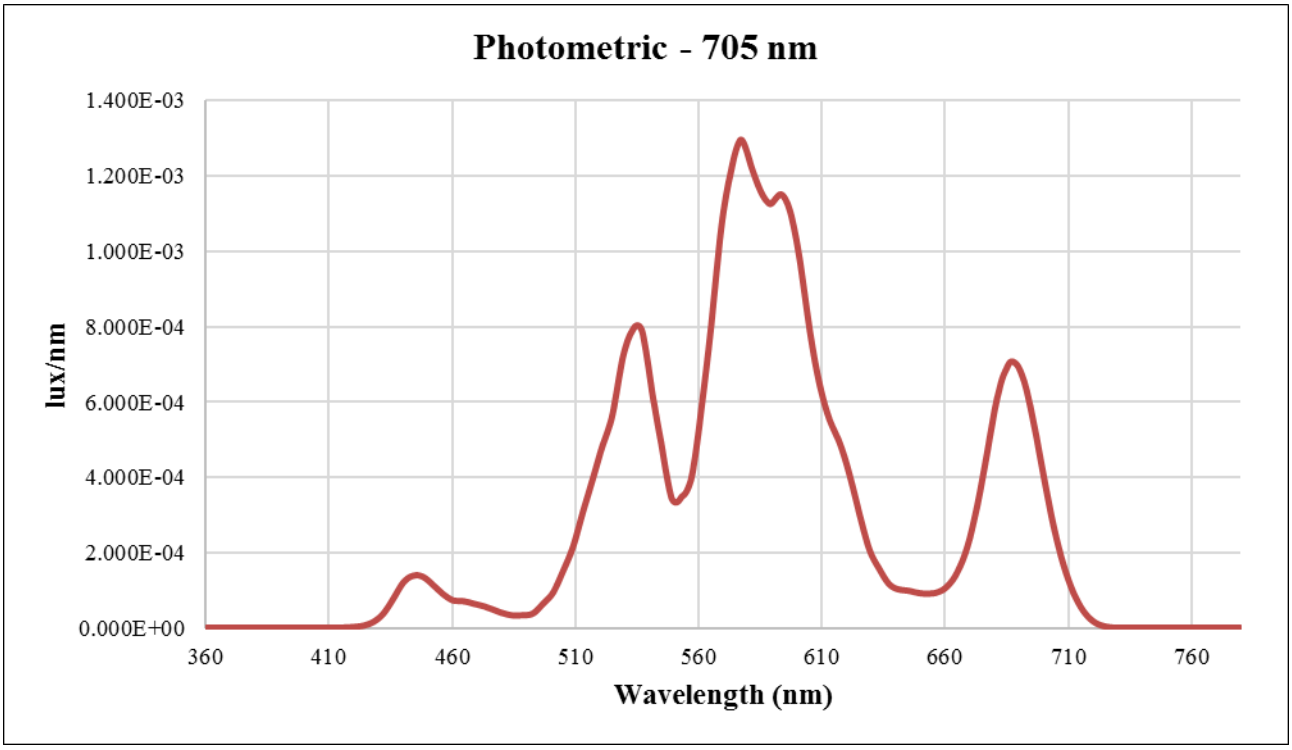
Photometric - 705 nm
1.400E-03
1.200E-03
1.000E-03
8.000E-04
6.000E-04
4.000E-04
2.000E-04
0.000E+00
lux/nm
360
410
460
510
560
610
660
710
760
Wavelength (nm)

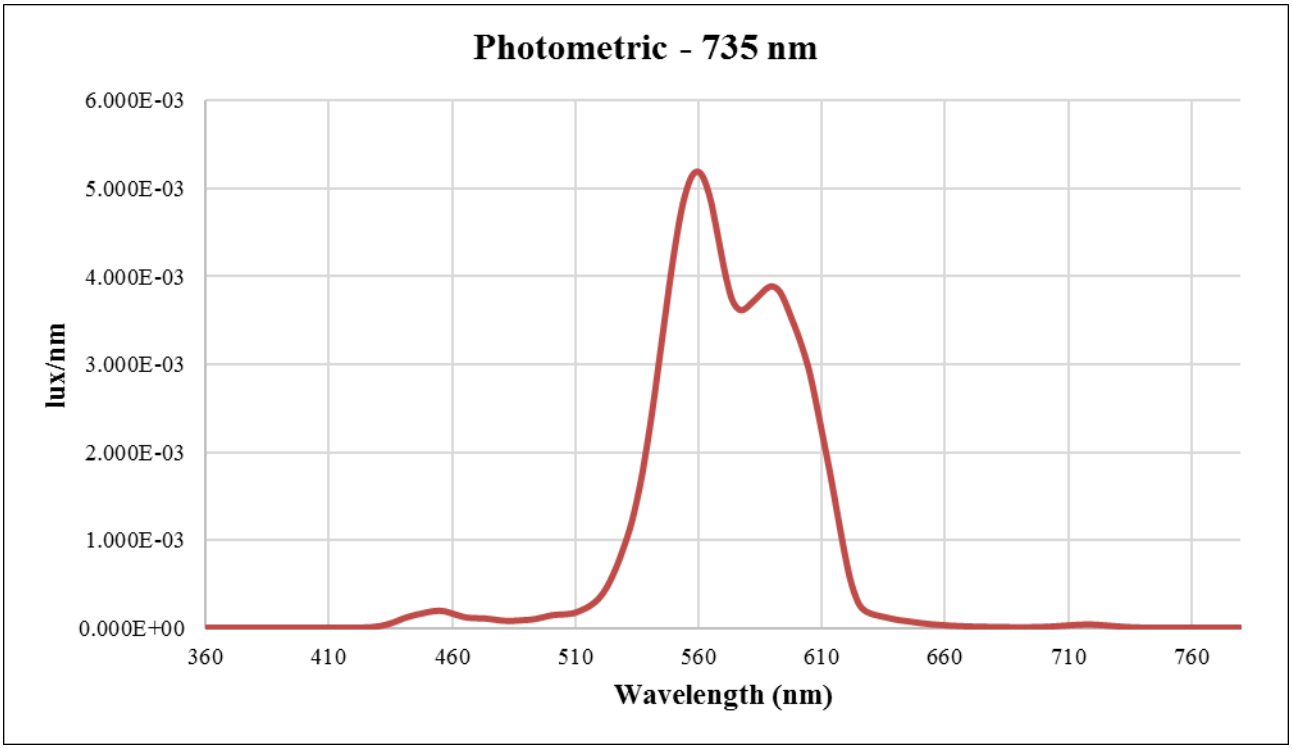
Photometric - 735 nm
6.000E-03
5.000E-03
4.000E-03
3.000E-03
2.000E-03
1.000E-03
0.000E+00
lux/nm
360
410
460
510
560
610
660
710
760
Wavelength (nm)

Appendix D: Illuminance and Distance Data

Filter	Filter Radius (m)	Trial	Before HDRI			After HDRI		
			Avg. E (lux)	Avg. D (m)	Calc. L (cd/m^2)	Avg. E (lux)	Avg. D (m)	Calc. L (cd/m^2)
Acrylic	0.01031	1	95712.2	0.0189	132760	96664.1	0.0212	161261
		2	70076.2	0.0263	167870	71070.8	0.0270	177745
		3	10007.7	0.0707	153097	9893.3	0.0712	153492
		4	3298.7	0.1204	144380	3352.8	0.1199	145541
		5	1597.0	0.1712	140620	1622.8	0.1703	141457
		6	1076.2	0.2079	139611	1080.9	0.2080	140375
		7	624.0	0.2733	139789	630.5	0.2728	140727
435nm	0.01031	1	525.4	0.0134	451.5	443.1	0.0136	386.9
		2	390.0	0.0191	552.3	333.4	0.0192	473.9
		3	163.3	0.0415	893.1	154.6	0.0402	797.3
		4	95.4	0.0639	1197.8	71.0	0.0636	883.5
		5	29.5	0.1130	1136.8	27.1	0.1133	1049.7
		6	15.0	0.1635	1206.4	13.1	0.1633	1049.8
		7	10.1	0.2007	1222.0	9.5	0.2011	1154.0
465nm	0.00400	1	187.4	0.0189	1395.4	202.1	0.0174	1288.9
		2	129.3	0.0229	1389.4	128.1	0.0222	1304.5
		3	32.4	0.0464	1400.6	54.0	0.0350	1338.4
		4	22.5	0.0555	1390.4	21.9	0.0563	1391.9
		5	14.9	0.0681	1382.1	14.0	0.0705	1391.7
		6	11.1	0.0798	1414.9	7.6	0.0950	1370.1
		7	7.3	0.0973	1380.7	6.6	0.1020	1371.9

Filter	Filter Radius (m)	Trial	Before HDRI			After HDRI		
			Avg. E (lux)	Avg. D (m)	Calc. L (cd/m^2)	Avg. E (lux)	Avg. D (m)	Calc. L (cd/m^2)
495nm	0.01031	1	1301.0	0.0143	1212.6	1518.1	0.0129	1239.3
		2	1078.5	0.0184	1435.2	1201.3	0.0177	1510.9
		3	247.8	0.0632	3039.6	244.9	0.0642	3100.3
		4	91.1	0.1125	3483.6	91.7	0.1122	3486.8
		5	43.5	0.1628	3467.0	45.1	0.1635	3624.7
		6	30.3	0.2007	3663.8	30.4	0.2003	3664.0
		7	17.9	0.2657	3789.3	17.6	0.2664	3746.8
525nm	0.01031	1	10325.8	0.0157	10891	9831.1	0.0152	9963.8
		2	7206.8	0.0224	13110	7806.7	0.0212	12959
		3	1577.5	0.0662	21199	1585.0	0.0657	20971
		4	571.9	0.1154	23003	559.0	0.1154	22471
		5	282.8	0.1655	23296	275.7	0.1658	22785
		6	187.9	0.2028	23208	183.5	0.2037	22861
		7	109.3	0.2682	23585	107.8	0.2685	23305
555nm	0.01031	1	38981.1	0.0145	37057	39710.1	0.0143	36792
		2	28170.6	0.0196	41529	28054.4	0.0198	41872
		3	4736.8	0.0642	59974	4814.1	0.0636	59847
		4	1658.9	0.1137	64801	1664.3	0.1130	64141
		5	819.4	0.1631	65511	817.1	0.1632	65427
		6	544.8	0.2009	66049	540.8	0.2015	65929
		7	319.2	0.2655	67491	317.5	0.2665	67638
585nm	0.01031	1	17050.7	0.0139	15358	17755.5	0.0140	16097
		2	11625.6	0.0195	16873	11509.1	0.0194	16610
		3	1779.7	0.0632	21858	1775.8	0.0630	21645
		4	608.9	0.1130	23465	605.9	0.1129	23327
		5	299.6	0.1632	23988	300.9	0.1627	23959
		6	198.4	0.2017	24234	200.6	0.2007	24257
		7	117.7	0.2655	24883	109.0	0.2662	23174

Filter	Filter Radius (m)	Trial	Before HDRI			After HDRI		
			Avg. E (lux)	Avg. D (m)	Calc. L (cd/m^2)	Avg. E (lux)	Avg. D (m)	Calc. L (cd/m^2)
615nm	0.01031	1	15615.7	0.0130	12924	15202.7	0.0135	13138
		2	10246.8	0.0180	13156	9155.8	0.0193	13161
		3	1258.4	0.0628	15270	1248.2	0.0631	15278
		4	417.4	0.1128	16034	417.9	0.1126	16001
		5	202.7	0.1633	16248	201.8	0.1637	16266
		6	134.2	0.2023	16500	136.5	0.2003	16450
		7	79.3	0.2652	16732	79.9	0.2655	16890
645nm	0.00438	1	756.6	0.0179	4267.8	940.1	0.0160	4289.0
		2	548.2	0.0211	4231.4	559.1	0.0211	4315.5
		3	167.6	0.0399	4493.9	139.6	0.0439	4521.6
		4	62.9	0.0656	4519.4	64.1	0.0659	4656.1
		5	38.9	0.0837	4542.3	37.3	0.0861	4608.2
		6	20.4	0.1155	4529.1	20.9	0.1157	4655.8
		7	12.7	0.1484	4657.4	13.0	0.1473	4696.2
675nm	0.00398	1	55.8	0.0177	369.9	73.5	0.0158	390.2
		2	33.1	0.0221	336.8	52.2	0.0185	375.5
		3	23.4	0.0251	305.0	41.8	0.0204	363.0
		4	11.9	0.0336	273.8	25.8	0.0251	335.8
		5	10.4	0.0359	272.7	19.4	0.0283	319.7
		6	10.0	0.0369	277.4	12.5	0.0349	309.5
		7	8.3	0.0402	272.7	9.1	0.0406	304.6

Appendix E: LS-110 Luminance Data

Filter	Metric (cd/m^2)	Trial 1	Trial 2	Trial 3	Trial 4	Trial 5	Trial 6	Avg.
Acrylic - Before	L	93290	90640	89290	92890	92050	87540	90950
	L, CCF	89100	87390	87230	88730	89020	91540	88835
435 nm	L	389.4	359.2	371.3	384.0	382.2	376.3	377.1
	L, CCF	450.5	430.2	436.5	412.5	420.2	422.5	428.7
465 nm	L	814.2	800.6	807	850.6	842.1	812.3	821.1
	L, CCF	837.6	908.3	887	908.5	920.2	931.3	898.8
495 nm	L	3508	3509	3499	3501	3507	3416	3490
	L, CCF	3830	3791	3792	3845	3878	3777	3819
525 nm	L	16820	16190	16350	16180	15850	15880	16212
	L, CCF	16420	16830	16700	15760	15760	15760	16205
555 nm	L	43310	41480	43740	43850	46120	46640	44190
	L, CCF	48350	47630	46210	47770	47840	45960	47293
585 nm	L	17830	17610	17820	17660	17770	17950	17773
	L, CCF	16170	16990	16930	17800	17550	18380	17303
615 nm	L	12350	12100	11560	12020	12920	12880	12305
	L, CCF	12210	11960	11630	12280	12680	12530	12215
645 nm	L	5497	5585	5363	5293	5480	5503	5454
	L, CCF	5456	5491	5584	5446	5535	5574	5514
675 nm	L	510.8	519.3	514.9	490.7	569.8	521.8	521.2
	L, CCF	514.1	592.0	510.9	555.9	566.6	585.0	554.1
Acrylic - After	L	84460	87100	87400	-	-	-	86320
	L, CCF	91260	88060	89500	-	-	-	89607

Appendix F: Error Propagation Results

Filter	Trial	% Error - Before HDRI	% Error - After HDRI	Avg. Uncertainty
Acrylic	1	3.3%	3.0%	0.62%
	2	2.7%	2.7%	
	3	2.0%	2.0%	
	4	2.0%	2.0%	
	5	1.9%	1.9%	
	6	1.9%	1.9%	
	7	1.9%	1.9%	
435nm	1	4.2%	4.1%	0.67%
	2	3.2%	3.2%	
	3	2.3%	2.3%	
	4	2.1%	2.1%	
	5	2.0%	2.0%	
	6	1.9%	1.9%	
	7	1.9%	1.9%	
465nm	1	3.3%	3.5%	0.67%
	2	2.9%	3.0%	
	3	2.2%	2.4%	
	4	2.1%	2.1%	
	5	2.1%	2.1%	
	6	2.0%	2.0%	
	7	2.0%	2.0%	
495nm	1	4.0%	4.3%	0.66%
	2	3.3%	3.4%	
	3	2.1%	2.1%	
	4	2.0%	2.0%	
	5	1.9%	1.9%	
	6	1.9%	1.9%	
	7	1.9%	1.9%	

Filter	Trial	% Error - Before HDRI	% Error - After HDRI	Avg. Uncertainty
525nm	1	3.7%	3.8%	0.63%
	2	2.9%	3.0%	
	3	2.1%	2.1%	
	4	2.0%	2.0%	
	5	1.9%	1.9%	
	6	1.9%	1.9%	
	7	1.9%	1.9%	
555nm	1	3.9%	4.0%	0.65%
	2	3.2%	3.2%	
	3	2.1%	2.1%	
	4	2.0%	2.0%	
	5	1.9%	1.9%	
	6	1.9%	1.9%	
	7	1.9%	1.9%	
585nm	1	4.1%	4.1%	0.65%
	2	3.2%	3.2%	
	3	2.1%	2.1%	
	4	2.0%	2.0%	
	5	1.9%	1.9%	
	6	1.9%	1.9%	
	7	1.9%	1.9%	
615nm	1	4.3%	4.2%	0.66%
	2	3.4%	3.2%	
	3	2.1%	2.1%	
	4	2.0%	2.0%	
	5	1.9%	1.9%	
	6	1.9%	1.9%	
	7	1.9%	1.9%	

Filter	Trial	% Error - Before HDRI	% Error - After HDRI	Avg. Uncertainty
645nm	1	3.4%	3.7%	0.64%
	2	3.1%	3.1%	
	3	2.3%	2.2%	
	4	2.1%	2.1%	
	5	2.0%	2.0%	
	6	2.0%	2.0%	
	7	2.0%	2.0%	
675nm	1	3.4%	3.7%	0.76%
	2	3.0%	3.3%	
	3	2.8%	3.1%	
	4	2.4%	2.8%	
	5	2.4%	2.6%	
	6	2.4%	2.4%	
	7	2.3%	2.3%	

*****_Trials in red were excluded because their luminance values were determined to be outliers through statistical analysis._

Appendix G: Luminance Versus Color-Corrected Luminance

The difference of the average LS-110 measured luminance with no correction compared to the average LS-110 color corrected luminance is shown in Figure G1 below.

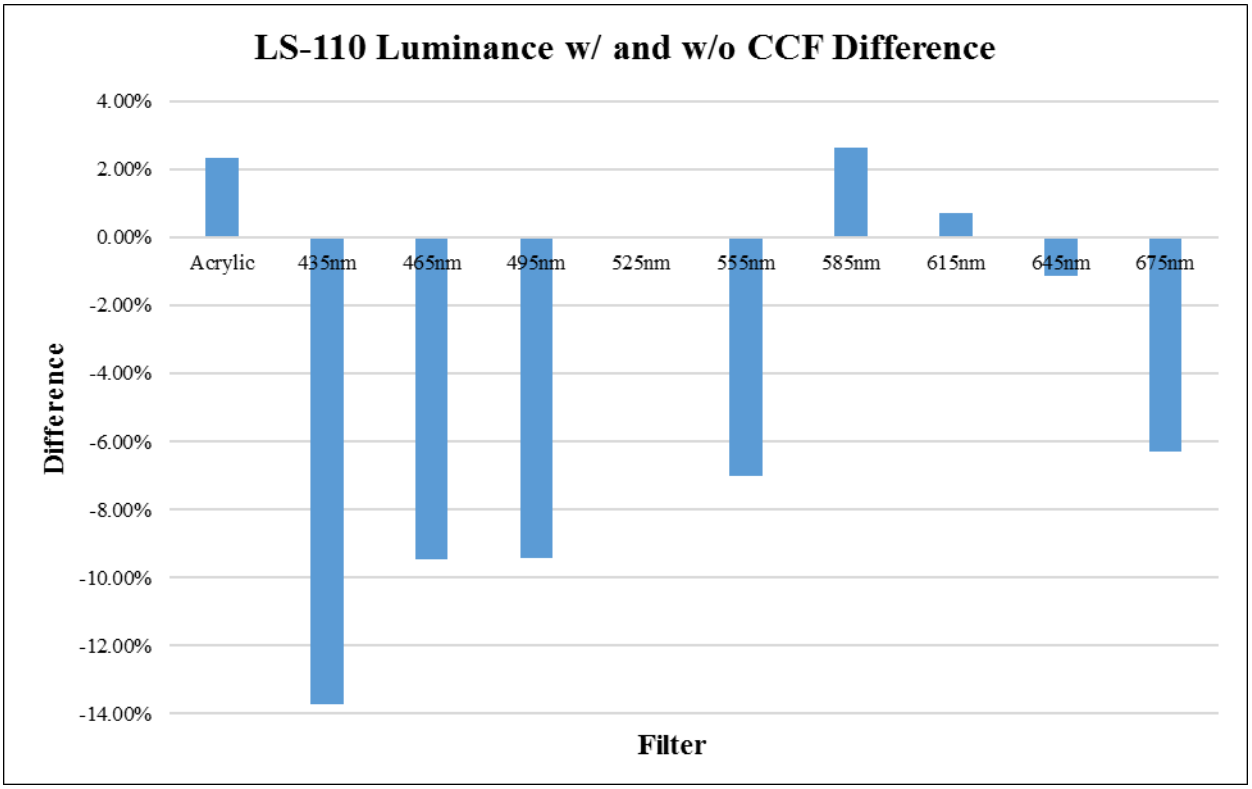

Figure G1: Comparison of CCF Luminance to Non-Color-Corrected Luminance

As shown above, half of the conditions resulted in a difference of less than 3% which is close to being within the measurement error of the instrument itself. These conditions are not particularly concerning in this case because the difference between measurements made with the CCF versus without it could simply be due to basic variance in the meter. Thus, the cases with glaring differences between the two styles of measurements will be focused on. Note that the largest difference between the two luminance measurements occurred for the 435 nm, 465 nm, and 495 nm filters, which all used the blue CCF. All of these percentages also were negative, which in this case means the luminance with CCF was greater than the luminance without a correction. Based on results presented in the

report, applying the CCF to meter measurements decreased the difference between the measured and calculated luminance values by 28% for the 435 nm filter, and 14% for the 465 nm. In this case it can be said that the accuracy of the LS-110 luminance measurements was improved by applying a CCF. Similarly, the change in calculated versus measured luminance value due to application of CCF is shown in Figure G2 for each of the test conditions. The accuracy of the 555 nm filter was also improved as indicated below by a positive change of 9%. The rest of the conditions caused either very minimal change or a negative effect to the accuracy of the LS-110 measurements when a CCF was utilized. This is likely due to the broad classification of a red, green, blue, or white source that CCFs were provided for.

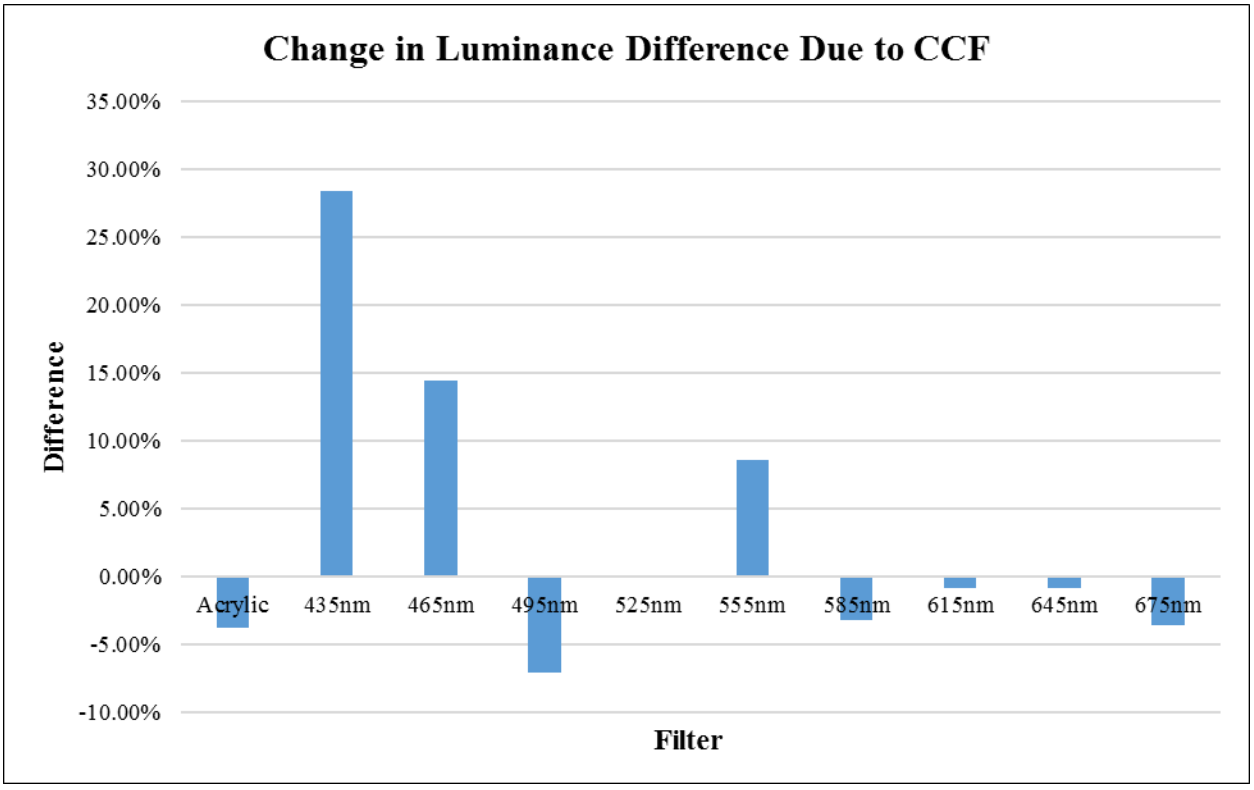

Figure G2: Effect on Calculated Versus Measured Luminance Difference by Applying CCF

A chart illustrating the difference in calculated luminance from the CL-500A results to luminance measurements from the LS-110 which used CCFs is shown in Figure

G3**Error! Reference source not found.**. These values may be compared to the similar chart which did not take into account color correction shown in Figure 48 of the report.

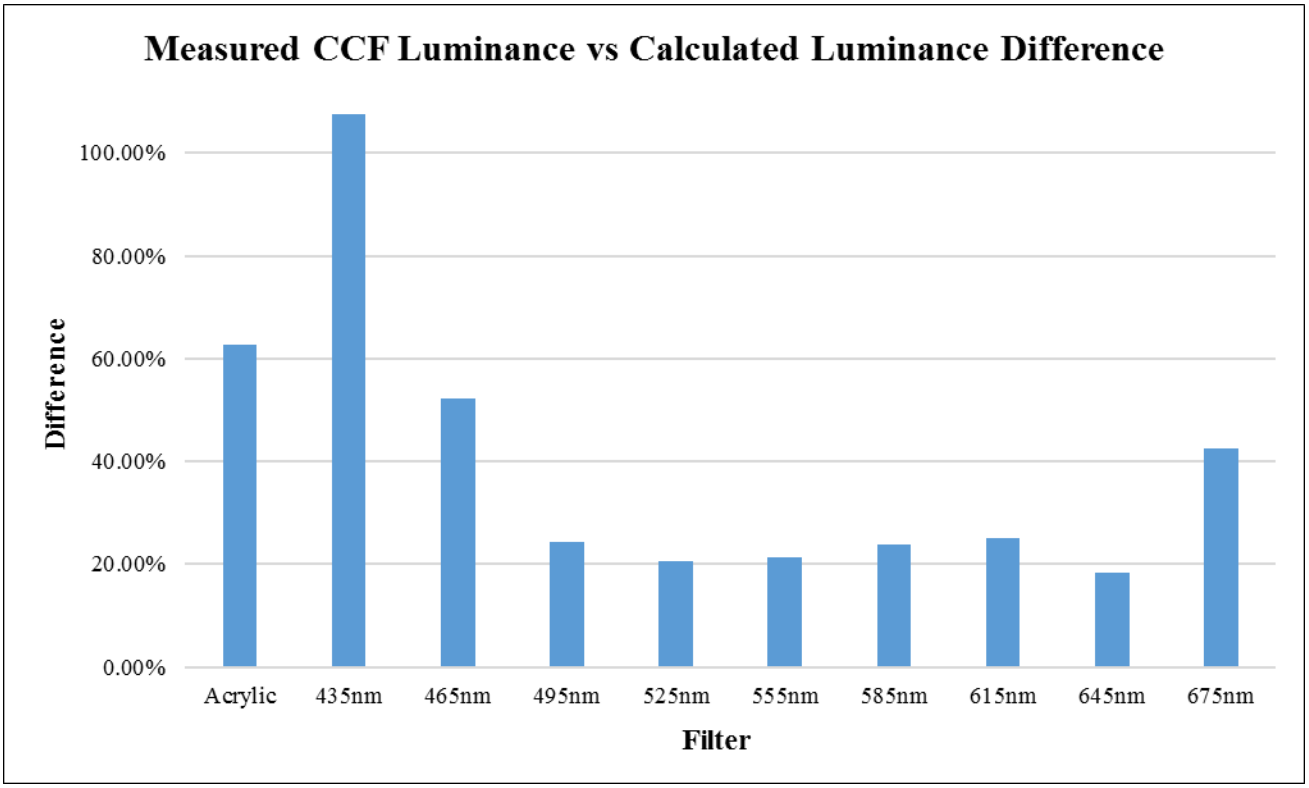

Figure G3: Absolute Difference Between Measured CCF Luminance with LS-110 and Calculated Luminance

Based on these results, it can be said that when measuring a source which is known to be on the blue end of the spectrum, applying the CCF will improve the accuracy of the results. Likewise, the accuracy of a true green source with output near 555 nm could also be improved by applying the appropriate CCF. On average, the color corrected luminance was greater than the regularly measured luminance by 10.86% for blue, 1.45% for green, and 2.23% for red, but less than the measured luminance by 2.33% for white.

No information was available from the manufacturer about which ranges of the visible spectrum qualified for the red, green, and blue CCFs, so the assignment of CCF to

particular filters was left up to the discretion of the researcher. This may be one reason for the decreased accuracy in using a CCF with some filters at various parts of the visible spectrum, since they might not have qualified as a true "red," "green," or "blue" source.

A comparison between standard luminance measurements taken with a CCF applied via the meter during the experiment, and luminance measurements which multiplied the CCF to the value during analysis was also evaluated. The average of luminance measurements taken without CCF was multiplied by the CCF corresponding to each condition to determine if calculating the CCF after, rather than applying it directly in the meter, would have any effect. The difference between the LS-110 luminance measurements with CCF applied later, and the average of CCF luminance measurements, were compared and is shown for each condition in Figure G4.

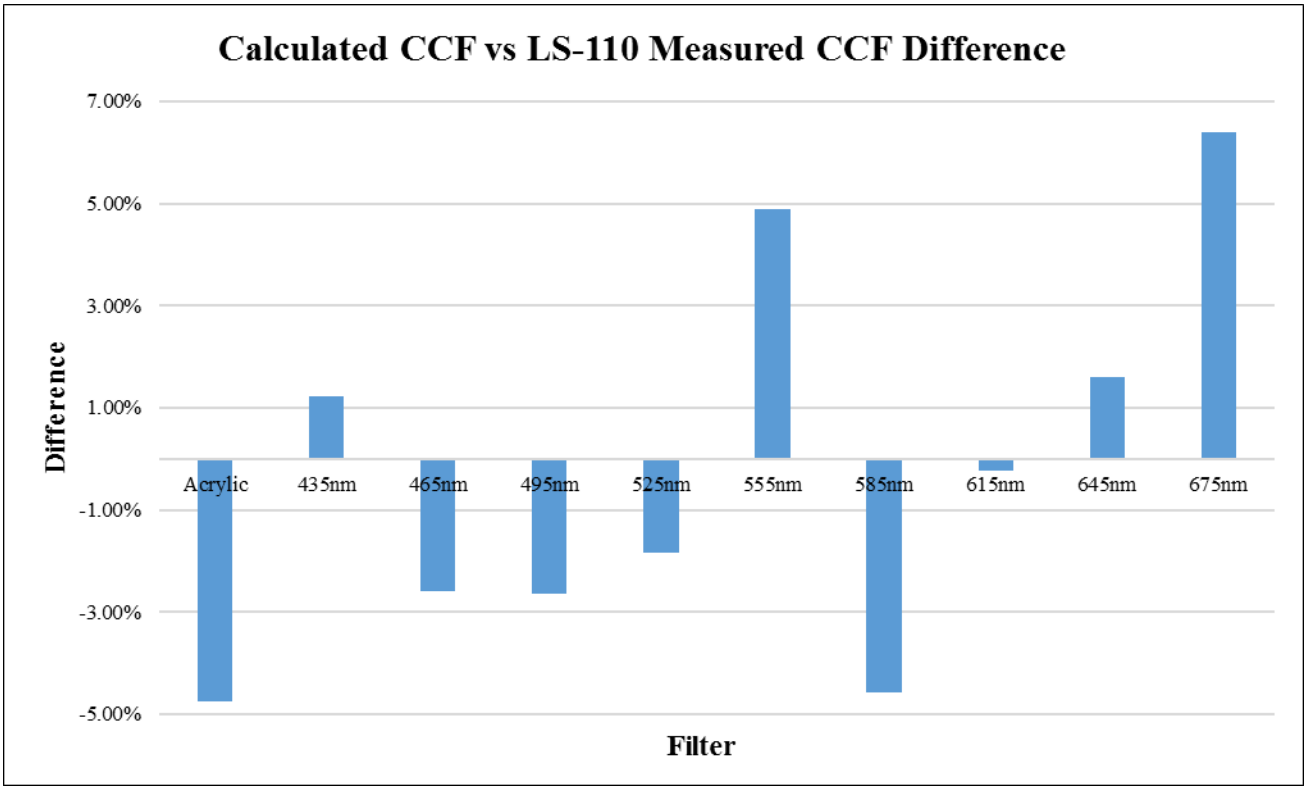

Figure G4: Comparison of CCF Luminance Measurement Methods

The difference between CCF programmed into the meter, versus that applied after the fact, does not seem to follow any particular pattern throughout the tested filters as shown above. All but one of the conditions was below a 5% difference. The small percentage differences and random pattern leads one to believe that applying the CCF during or after the measurement process would not make a significant difference in the results. Therefore, one final investigation involving different CCFs than were used in the experiment is justified. The acrylic condition which represents a white light source was assigned the "Color CRT – White" correction factor of 1.023 because it was the white option most similar to the provided RGB factors that were used. The LED in this experiment has a CCT of 5000 K, so other correction factors intended for similar CCT white sources were investigated. Table G1 lists some additional CCF options provided in the LS-110 manual for white sources.

Table G1: Additional White CCF Options

Illuminant	CCF	Avg. L w/ CCF	L Difference
Color CRT - white	1.023	93042	-55.2%
CIE Standard Illuminant B	1.007	91587	-57.7%
CIE Standard Illuminant C	1.010	91860	-57.2%
CIE Standard Illuminant D65	1.011	91950	-57.1%
Daylight fluorescent lamp (F5)	1.013	92132	-56.8%
White fluorescent lamp (F6)	1.008	91678	-57.5%

The CCF options above were multiplied by the average acrylic luminance from the LS-110 meter, and the difference was compared to the calculated luminance value. The 'L

Difference' column shows that the 'Color CRT – white' correction factor related most closely to the calculated luminance value out of the available CCF options. This CCF of 1.023 was used for all acrylic CCF analysis with this LED source. While the chosen CCF reduced the difference by more than its counterparts, the resulting difference was still greater than 50% which is concerning for a white LED light source.

Appendix H: Final HDRI

435 nm Filter Final HDRI

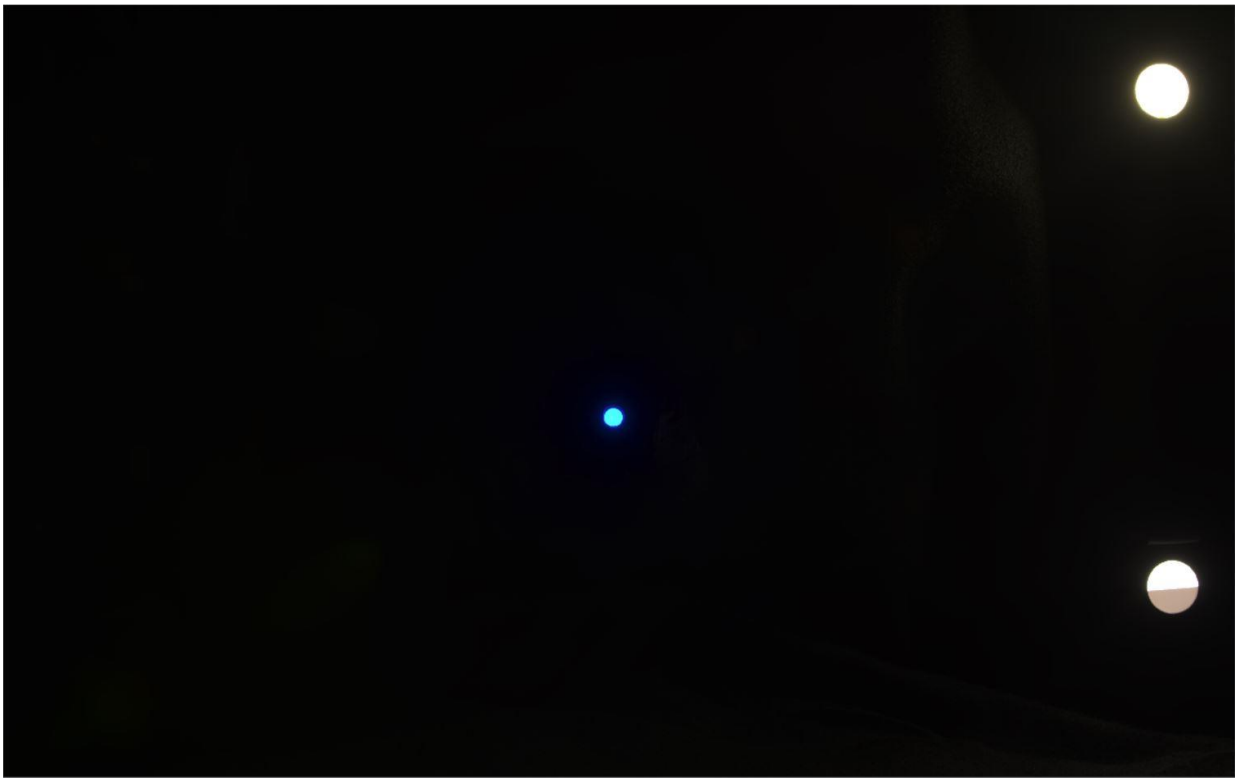

465 nm Filter Final HDRI

495 nm Filter Final HDRI

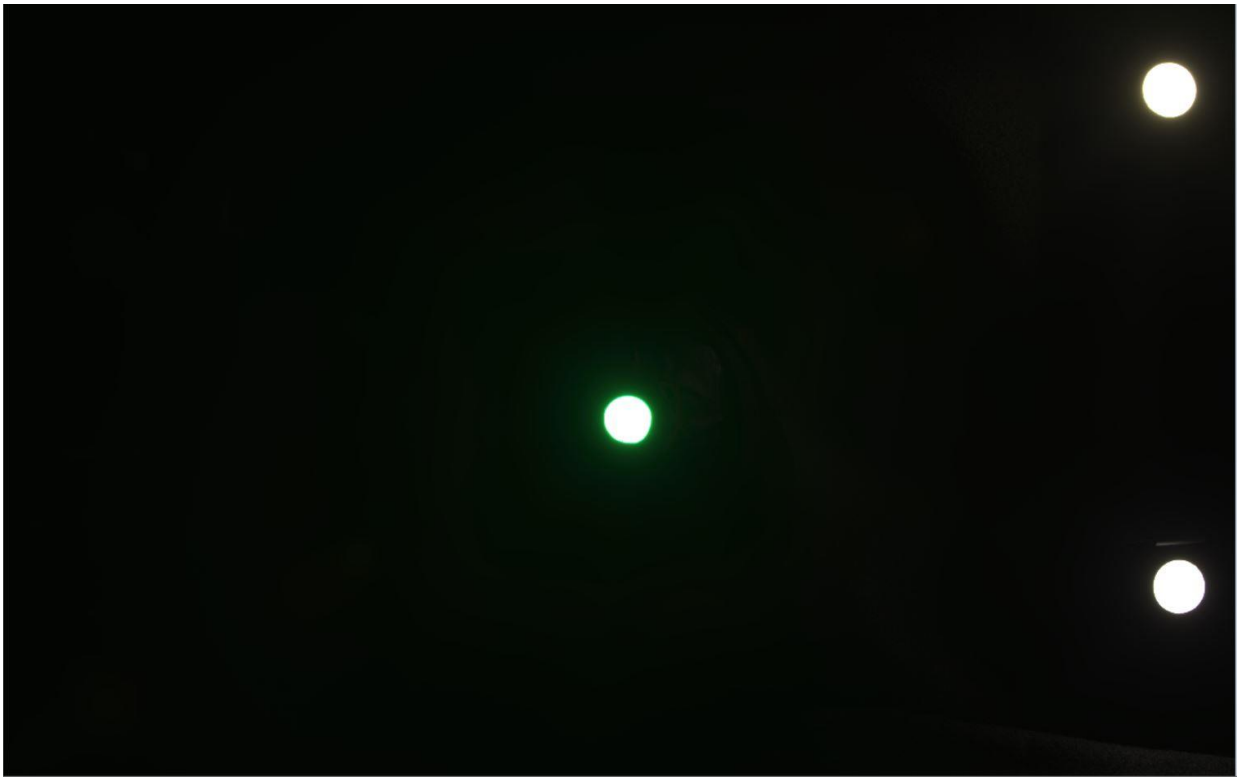

525 nm Filter Final HDRI

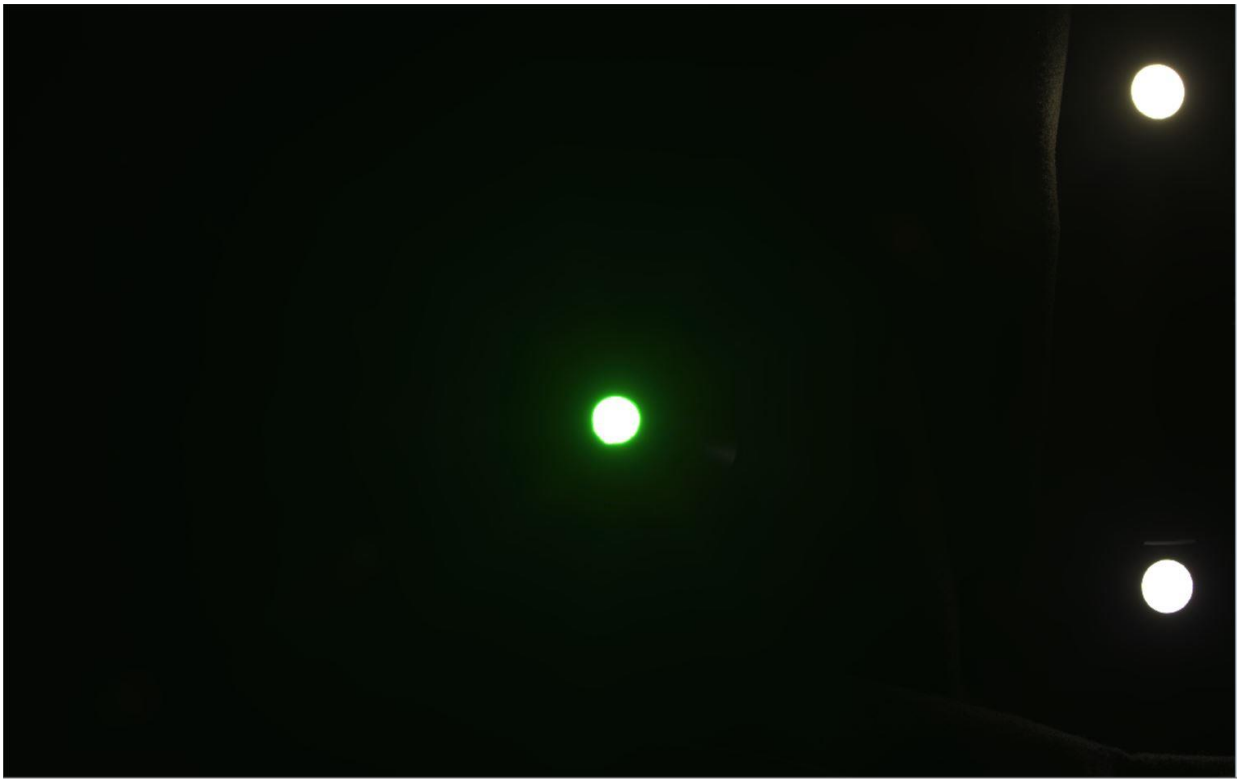

555 nm Filter Final HDRI

585 nm Filter Final HDRI

615 nm Filter Final HDRI

645 nm Filter Final HDRI

675 nm Filter Final HDRI